NASA Contractor Report 3861

A Feasibility Study on the Use of Wind Profilers To Support Space Shuttle Launches

R. B. Chadwich, A. S. Frisch,
and R. G. Strauch

DECEMBER 1984

NASA

NASA Contractor Report 3861

A Feasibility Study on the Use of Wind Profilers To Support Space Shuttle Launches

R. B. Chadwich, A. S. Frisch,
and R. G. Strauch
NOAA/ERL/Wave Propagation Laboratory
Boulder, Colorado

Prepared for
George C. Marshall Space Flight Center
under Purchase Order H-77152B

NASA
National Aeronautics
and Space Administration
Scientific and Technical
Information Branch

1984

CONTENTS

EXECUTIVE SUMMARY

A. Purpose

This report examines the feasibility of using a clear-air radar wind Profiler to support Space Shuttle launches by measuring prelaunch winds aloft at Kennedy Space Center (KSC), Florida and subsequently at the Vandenburg *AFB,* California. These winds currently are measured by Jimspheres (special balloons) tracked with a high resolution radar. This technique provides a single high resolution wind profile (surface to about 18 km) for each Jimsphere ascent (Johnson and Vaughan, 1978). Two operational disadvantages of the Jimsphere/radar tracking system are: it takes about 1 hour to measure a wind profile to the required 60,000 ft altitude; and the wind profile necessarily applies only to the path of the Jimsphere. In some cases it may be as much as 70 km from the actual trajectory of the Space Shuttle.

The radar wind Profiler automatically and nearly continuously measures the motion of natural tracers of the atmosphere rather than the trajectory displacement of an ascending balloon. This eliminates most of the two disadvantages of the Jimsphere, since the measurements can be made on a short time scale (a few minutes) in the region directly above the radar. The Profiler technology is described in terms of the experience gained from operating several clear-air radars at the NOAA Wave Propagation Laboratory. This is followed by an analysis of acquisition costs for systems with differing range and resolution characteristics.

Discussions with NASA Marshall Space Flight Center representatives lead to this "minimum" requirement for wind measurement to support Shuttle launch decision: The wind Profiler must be able to measure winds to 20 km with a resolution of 75 m and a 1 m/s or less vector error and give a new profile on the order of every 10-20 min. Although it would be even more desirable to be able to measure winds to 20 km with a resolution of 25 m and a 1 m/s or less vector error, the recommendations below are based on the 20 km range, 75 m resolution and a 1 m/s or less vector error "minimum" requirement.

B. Recommendations

1. NASA should strongly consider the use of a wind Profiler at KSC to support shuttle launch activites. Given appropriate funding support and bandwidth allocation, a wind Profiler can measure winds to heights exceeding 20 km with resolution less than 75 m.

2. Starting immediately, NASA should monitor the electromagnetic interference in the candidate radio frequency bands at the proposed wind Profiler sites.

3. NASA should prioritize high resolution and long maximum range. If maximum range exceeding 20 km is more important than resolution less than 75 m, the radar should be a large 50 MHz radar. If, however, resolution

less than 75 m is more important than ranges exceeding 20 km, better choices would be 225 MHz or 400 MHz radars because of the larger bandwidth available.

4. For any high resolution application at long ranges, it will be essential to use a high-duty-cycle transmitted signal with pulse compression, (One way of doing this is explained in Appendix B.)

5. If a 225 MHz radar is appropriate, then NASA should conduct some research to see if a colinear-coaxial phased array antenna would be applicable at 225 MHz. This could significantly reduce the cost of the radar.

6. If a 400 MHz radar is to be used to measure to 20 km, NASA should first determine how much of the time a 400 MHz radar will experience viscous cut-off at this altitude. This could probably be done using the extremely sensitive 400 MHz radar located at Arecibo, which, on occasions, has measured winds to as high as 31 km.

7. NASA should consider the possibility of a smaller high resolution radar to measure up to 10 km and a larger low resolution radar to measure to the maximum height. If this combination is judged to be acceptable for the shuttle launch problem, we would recommend a 400 or 900 MHz radar (similar to the WPL Profilers) for the high resolution radar, and a large 50 MHz radar for the low resolution radar.

8. If possible, NASA should operate portable clear-air wind Profilers at KSC and make an operation test evaluation before making final decisions.

C. Outline of Report

The first chapter of this report gives an introduction to the problem of measuring winds aloft to support Space Shuttle launches and a possible solution, The second chapter is an extensive description of the technology of wind profiling with clear-air radar. The third chapter discusses operations, performance, and limitations with the WPL VHF and UHF radars. The fourth chapter gives an analysis of the cost of various-sized radars at three different frequencies (50, 225, and 400 MHz). Given a height and resolution requirement, the results in this chapter will allow the radar cost to be estimated. The last chapter presents autocorrelation functions of wind as measured by a VHF wind Profiler in Colorado. The report concludes with six appen dixes of special interest to this radar problem and a seventh appendix that contains a large number of autocorrelation functions of the wind as measured with a 50 MHz wind Profiler.

CHAPTER 1

INTRODUCTION

During Space Shuttle ascents small scale wind fluctuations cause added mechanical stress to structural members and control systems. The goal of maximizing payload results in lighter structural members; therefore, it is vital to ensure that the wind profile structure does not cause element structural loads beyond those established as allowable for launch. Because wind profiles are variable in time and space, they must be measured as close to the launch time and trajectory as is practically possible with the required accuracy and resolution needed to meet pre-launch wind loads simulation requirements.

One method of making these measurements is by releasing a balloon, tracking it, and determining the wind profile. Conventional rawinsondes do not have sufficient height resolution to adequately measure the wind profile for this application. Currently at Kennedy Space Center (KSC), special balloons called Jimspheres are released and tracked with high resolution radar. The radar information can then be processed to yield very accurate high resolution wind profiles. If a precision tracking radar such as an FPS-16 is used, the resulting wind profiles extend to 18 km height with an accuracy of about 1 m/s and a resolution of 50 m (Johnson and Vaughan, 1978). The technique is fully developed, and the launch personnel have faith in the profiles; however, they realize that there are two disadvantages. First, it takes a significant time (about 1 hr) for the Jimsphere to ascend through the heights of interest so that the profiles are not in real time and cannot be updated rapidly (this takes about 1.5 to 2.0 hrs for update). Second, the profile only applies to the Jimsphere path which at altitude, may be removed by some distance from the actual trajectory of the Space Shuttle. These time and space differences are currently accounted for by making a reduction of the loads allowable from the Space Shuttle prelaunch loads simulation.

This report covers another wind measuring technique, clear-air radar, that eliminates most of the two disadvantages. Such radars are called wind Profilers and they have been used in atmospheric research for the past decade. Some wind Profilers will cover the same height interval as the Jimsphere system, but always with reduced resolution. Range resolutions of 1500 m are not uncommon for large wind Profilers, but given the necessary resources, the resolution could be made to approach that of a Jimsphere wind system.

The radar technology used in a wind Profiler is similar to that used in conventional Doppler radar systems except the frequency is generally lower. The Wave Propagation Laboratory (WPL) has built six wind profilers over the past few years. One of these, a 915 MHz radar located at Stapleton Airport, uses state-of-the-art technology (solid-state power transmitter and offset paraboloid antenna) whereas the remainder use less advanced technology (vacuum tube power transmitters and array antennas). The lower technology was used to reduce costs. Descriptions of all these radars and our experience with them are given in Chapters 2 and 3. A

method for estimating acquisition cost of radars similar to our "low technology" models is given in Chapter 4.

Conventional weather radars use hydrometeors as tracers of atmospheric motion and are therefore not all-weather devices. Clear-air radar uses naturally occurring small-scale turbulent eddies as tracers of larger scale atmospheric flow. The turbulent eddies with scale sizes near one-half a radar wavelength cause fluctuations in radio refractive index that result in Bragg backscatter. The backscattered signal is weak, but is always present in a turbulent atmosphere. The scattering phenomenon is not highly frequency dependent in the lower atmosphere but does experience a "cut-off" at higher frequencies in the upper atmosphere. Because of viscosity, turbulent eddies are constantly being converted to heat and thus are no longer available to scatter the radar signal. This happens at the inner scale of turbulence, and if the half-wavelength of the radar is smaller than the inner scale of turbulence, the radar will experience viscous cut-off. The inner scale of turbulence increases with altitude. So, to make measurements at higher altitudes longer wavelengths (lower frequencies) are required.

Another factor in frequency selection is the radio interference caused by other people using the same or nearby frequencies. For conventional weather radars this is rarely a problem because they are generally operated at centimeter wavelengths where there is less frequency congestion and where practical antennas are more directive. Because of the inner scale problem alluded to above, wind Profiler radars generally operate at frequencies less than 1 GHz. In these frequency bands there are many users, including commercial broadcasting and mobile radio, who use significant amounts of bandwidth and would cause devastating interference for a sensitive profiling radar.

Yet another facet of the frequency selection problem is the extreme range resolution needed to characterize the wind for Shuttle launches. The range resolution is inversely related to the signal bandwidth, and hence small range resolution cells require large bandwidths. For example, to achieve a 25 m range cell requires 6 MHz of bandwidth, exclusive of guard bands, to avoid interference with other users. It will be impossible to obtain this amount of bandwidth at 50 MHz, but it may be possible at 225 or 400 MHz.

CHAPTER 2

PROFILER EQUIPMENT

A. Precipitation Considerations

A wind Profiler must operate in the cloud-free atmosphere, in non-precipitating clouds, and in precipitation. Clear-air operation restricts the choice of radar wavelengths, and it establishes the sensitivity that the radar must have. Atmospheric scattering from refractive turbulence in the clear air is very weak; scattering from hydrometeors can he significantly stronger than the clear air signal, especially at shorter wavelengths. When this occurs, the Doppler velocity measured by the radar will be that of the particles rather than the wind. At radar wavelengths suitable for wind profiling, the signal from water droplets will dominate that from refractive turbulence for light-to-moderate (and greater) rainfall rates. Thus, to measure the true horizontal wind a correction must he made for the fall speed of particles by using at least three antenna pointing positions.

Figure 2-1 shows the radar reflectivity of refractive turbulence and precipitation for wavelengths suitable for wind Profilers (0.7 to 7 m). Radar reflectivity for refractive turbulence at wavelengths longer than the inner scale is given by

$$\eta = 0.38 \; C_n^2 \; \lambda^{-1/3} \qquad (1)$$

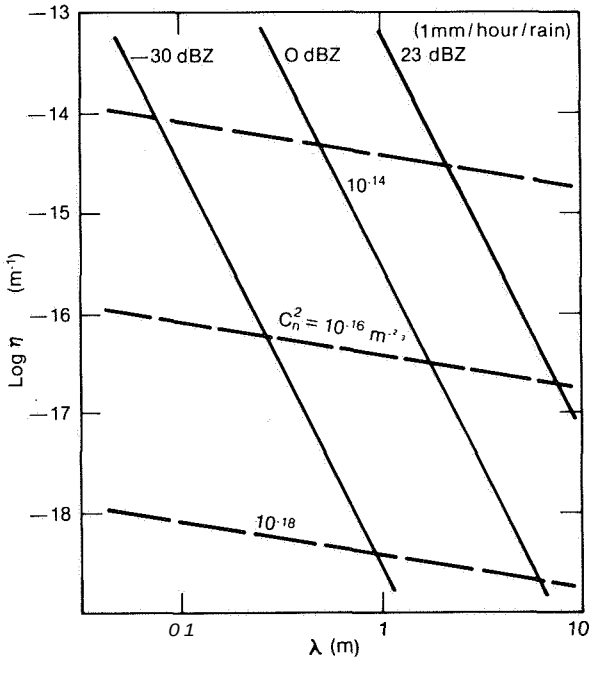

Figure 2–1. Radar reflectivity of hydrometeors and refractive turbulence.

(Ottersten, 1968) where η is the radar reflectivity (m^{-1}), C_n^2 is the refractive turbulence structure constant ($m^{-2/3}$), and X is the radar wavelength (m). Radar reflectivity for scattering by hydrometeors is given by

$$\eta = \frac{\pi^5}{\lambda^4} |K|^2 \frac{\Sigma D^6}{V} \qquad (2)$$

(Batten, 1973) where

$$K = \frac{m^2 - 1}{m^2 + 2},$$

m is the complex refractive index of the hydrometeors, D is the diameter of the drops and the summation is over the radar resolution volume V. The hydrometeors are assumed to be

spheres with diameter much less than the radar wave length, a condition well-satisfied with clear air radars. The crossing of solid and dashed lines in Fig. 2-1 indicates equal scattering from these two mechanisms, and provides an example of when the wind profiles will have confusing signals and may not be able to measure winds. This condition will only occur for a very special case of rainfall rate or particle size distribution, If the particles are small, their fall speed is low so the Doppler spectrum will not separate the two scattering mechanisms. For the long wavelength radars used in wind profiling, the equal-scattering condition will usually occur with large particles and the Doppler spectrum should sort the two mechanisms (for antenna elevation angles used for wind profiling). The probability of equal or near-equal signal strengths from refractive turbulence and raindrops is very low, and moreover, could be treated in most cases.

A more common situation where the single Doppler radar cannot be expected to measure vertical profiles of horizontal (and vertical) wind is in convective storms. During the past decade, research with multi-Doppler radar networks have shown the complex nature, during convective storms, of the horizontal and vertical velocity fields and their rapid change in time and space. Particle size distributions (fall speeds) are also highly variable in time and space. Clear-air Doppler radars with large antenna apertures and limited scanning observe radial velocity profiles in several different volumes of space at each height, but the assumptions that must he used to calculate wind profiles are not valid when the winds and particle fall speeds are changing rapidly in time or space.

One must always be aware of the meteorological assumptions that are made when measuring winds with radar. These assumptions differ for various antenna pointing strategies. Additional pointing directions (more than three) are desirable because they can be used to observe more complex wind fields or validate assumptions; however, they are not without cost. If the antenna beams are simultaneous, then the cost is that of more transmitters and antennas. If the antenna beams are sequential, then the cost is for a more powerful single transmitter that can acquire the data more rapidly, and for a more complicated and costly antenna.

B. Wavelengths for Radar Wind Profilers

The range of radar wavelengths appropriate for wind profiling Doppler radars to operate throughout the troposphere is about 0.7 to 7 m or frequencies of about *40* MHz to *400* MHz. The long wavelength limit is governed by practical considerations such as antenna aperture needed to define the beamwidth, the percent bandwidth needed to define the range or height resolution, and radio interference problems with other communications equipment. The radio interference problem may actually dictate the radar frequency in some locations. The bandwidth required depends on the range resolution needed; this in turn depends on the required height resolution and antenna elevation angle, Range and height resolution are usually about the same because antenna elevation angles are 60° or greater. Therefore, a bandwidth of 2 MHz plus guard bands is required for 75 m height resolution.

The short wavelength limit for radar wind profiling is determined by the scattering mechanism. The radar samples the spectrum of refractive turbulence at scale sizes of $\lambda/2$. If $\lambda/2$ scale sizes are in the inertial subrange of turbulence, then the clear-air radar reflectivity is given by Eq. (1), but if the $\lambda/2$ scale sizes are damped by viscosity, then radar reflectivity decreases abruptly as shown by Hill (1978). Longer wavelength radars are needed to probe to higher altitudes because the viscous cutoff of radar reflectivity occurs at longer wavelengths with increasing altitude (lower density). Figure 2-2 shows how the cutoff wavelength varies with altitude for various levels of mechanical turbulence. These theoretical relationships have not been tested adequately to specify a precise upper frequency limit for a radar that can measure winds throughout the troposphere, Atmospheric turbulence (eddy dissipation rate) is highly variable, and recent work by Gossard et al. (1984) using tower data suggests that this cutoff problem may limit radar coverage of 10 cm wavelength radars even in the boundary layer. For years it has been observed that sensitive 10 cm clear-air radars measure a sharp decrease in radar reflectivity above the boundary layer. These radars detect elevated layers on occasion and sometimes detect a layer of high reflectivity at the tropopause. Figure 2-2 suggests the reason why 10 cm Doppler radars can measure low level winds but are not suitable for routine clear-air wind profiling above about 5 km altitude. Results obtained with WPL's 33 cm radar indicate that this radar, although not as sensitive as some 10 cm radars, routinely measures wind profiles well above the heights that 10 cm radars observe scattering. There is evidence (see Chapter 3) that the 33 cm radar reflectivity also often decreases abruptly above about 8 km MSL; the particular height of abrupt decrease varies with the type of air mass.

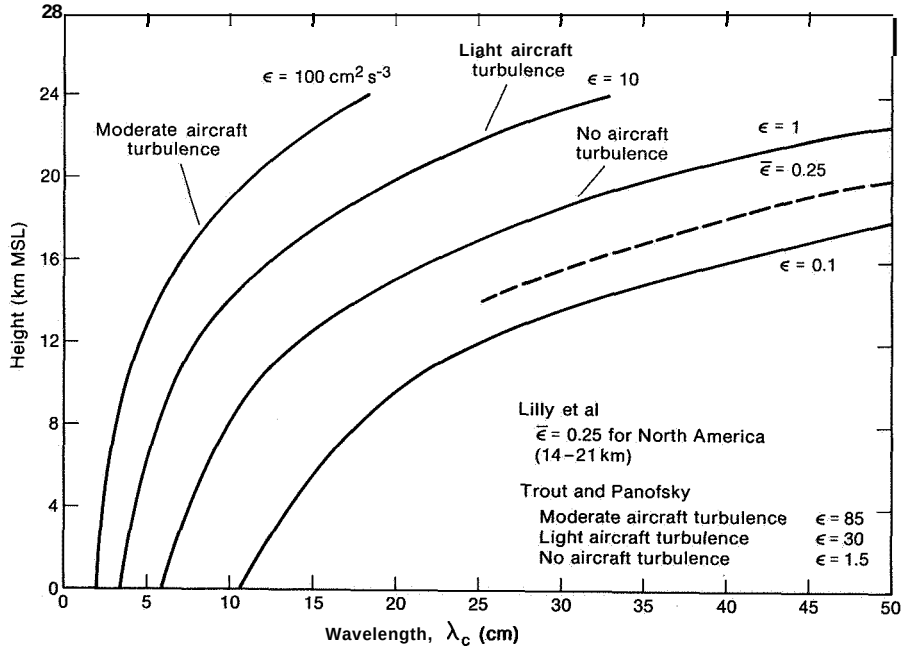

Figure 2-2. Cutoff wavelength (λ_c) vs. height for various levels of mechanical turbulence (ε). Routine clear-air wind profiling should be possible with radar wavelengths greater than λ_c, i.e., to the right of the curves.

Therefore, the prudent designer of a clear air wind Profiler would select radar wavelengths considerably longer than 33 cm. WPL is presently testing a 74 cm radar; because of the variability of clear air radar performance with the type of air mass it will require some months of evaluation to determine if this wavelength is suitable for tropospheric wind profiling. A general wavelength recommendation for a clear air radar that should operate to 16-18 km MSL with 75 m height resolution is to select the longest wavelength that allows the necessary bandwidth. The present state of knowledge with regard to viscous cutoff is that 6 m (50 MHz) radars do not experience cutoff, but that 33 cm (900 MHz) radars suffer cutoff for heights above 8-12 km.

The approximate frequency range of about 40 MHz to 400 MHz noted above may seem large, but practical considerations of frequency assignments shrink it considerably. There are very few bands between 40 MHz and 225 MHz where a quiet 2 MHz band could be used for an operational clear-air radar. These types of radars must detect extremely weak signals, so interference levels that would not affect most applications, e.g., communications or broadcasting, would be devastating to the operation of a clear-air radar. To operate a clear-air radar in the 40-225 MHz band near populated areas would require (1) considerable influence with frequency assignment authorities; (2) cooperation with users on nearby frequencies; or (3) antennas with very low sidelobes. Operation in the 225 MHz to 400 MHz region would be easier because this band is mainly used by the government (DOD and FAA) and hence is not as crowded. Interagency cooperation would be essential. In summary, the optimum frequency for a tropospheric wind profiler with a resolution less than 75 m will probably lie in the range of about 225 MHz to 400 MHz (wavelengths of 1.3 to 0.7 m).

C. Transmitter

The radar sensitivity required for a 50 MHz wind Profiler can be estimated from theoretical considerations and from results obtained with WPL radars.

Theoretical calculations are based on Eq. (1) which relates η and C_n^2 and on the radar equation for the minimum detectable radar reflectivity (Strauch, 1976):

$$\eta_{min} = \frac{128\, R^2\, k\, T_{op}\, W\, L_F\, L_T\, L_R}{\sqrt{\pi\, P_t\, A_e\, AR\, \sqrt{\lambda_o\, AV\, T_o}}} \qquad (3)$$

This form of the radar equation includes gain from signal processing. In Eq. (3)

R is the range to the scattering volume (m)

k is the Boltzman constant

T_{op} is the system noise temperature given by

$$T_{op} = \frac{T_{ANT}}{L_R} + (1 - 1/L_R)T_{LR} + T_R$$

T_{ANT} = antenna temperature (K)

L_R = RF loss in the receiver path

T_{LR} = temperature of the loss in the receiver path (K)

T_R = receiver noise temperature (K)

W is the width of the Doppler spectrum (m/s)

L_F is the loss in the receiver filter

L_T is the RF loss in the transmitter path

$\overline{P_t}$ is the average transmitted power (W)

A_e is the effective aperture of the antenna (m^2)

AR is the range resolution (m)

λ_o is the radar wavelength (m)

AV is the velocity resolution of the Doppler analyzer (m/s)

T_o is the total observation time (s).

We assume the following parameters:

T_{op} = *4835* K for 6 m wavelength radar

T_{ANT} = 100 $\lambda^{2.4}$, background noise for VHF wavelengths (Hogg, and Mumford, 1960)
= 7371 K for 6 m wavelength radar

L_R = 1.6, feedline losses and T/R switch losses

T_{LR} = 290 K

T_R = 120 K, 1.5 dB noise figure

W = 1 m/s, typical for clear-air radar scattering

L_F = 1.7, 2.3 dB matched filter loss (Doviak and Zrnic, 1979)

L_T = 1.6, feedline losses and T/R switch losses

AR = 75 m

λ = 6 m

ΔV = 0.5 m/s, typical for clear air radars (64-point power spectra and ±16 m/s Nyquist velocity)

T_o = 100 s, typical of total observation time used to estimate a single radial profile

Thus,

$$\eta_{min} = (1.61 \times 10^{-19}) \frac{R^2}{\overline{P_t} A_e}$$

Using (1), this equation can be written in terms of a minimum detectable C_n^2 as

$$\overline{P_t} A_e = 7.7 \times 10^{-20} R^2/(C_n^2)_{min} \quad . \qquad (4)$$

Range and height are approximately the same because the elevation angle must be high so that the radar observes as close to a vertical profile as possible. For 18 km range,

$$\overline{P_t} A_e \sim 2.5 \times 10^{-11} (C_n^2)_{min}.$$

Original design of WPL radars was based on expected C_n^2 values of 10^{-18} to 10^{-19} $m^{-2/3}$ in the lower stratosphere. Using these values, we project that an average transmitted power-antenna aperture of 2.5 x 10^7 to 2.5 x 10^8 W-m^2 is needed for this radar. The antenna aperture should be at least 100 m × 100 m for a 50 MHz radar (antenna beamwidth ~4.1').

The proposed first-cut design for this radar is for a 100 m x 100 m antenna with 10 kW of average transmitted power, as in Table 2.1. A modular concept for both transmitter and antenna would allow increased sensitivity to be added to a first construction.

To achieve the required average power, given the desired height resolution and range requirements, two operating modes are proposed. The "LOW" mode will be used to measure profiles to 6-8 km altitude starting at about 1 km (perhaps somewhat less) above ground. The **"HIGH"** mode uses all of the transmitted power available to achieve maximum height coverage. In this example the range resolution has been increased to about 100 m to approximate the known bandwidth capability of an existing transmitter module (Appendix A) ▪

The proposed operating modes are not rigid; the radar should be capable of a wide variety of operating parameters. The **HIGH** mode uses pulse compression to take advantage of solid state modular transmitters that operate with relatively high duty cycle and relatively low peak power. A brief paper by Farley (Appendix D) describes the commonly used pulse codes. The pulse repetition period is low so the unambiguous range

Table 2.1.--Preliminary Design of Wind Profiler

	Low Mode	High Mode
1. Radar		
Frequency	46–50 MHz	46–50 MHz
Bandwidth	1.6 MHz	1.6 MHz
Peak power	200 kW	200 kW
Pulse width	2/3 microsecond	10 microseconds
Pulse repetition	100 microseconds	200 microseconds
Pulse compression	---	16
Average power	1332 Watts	10 kW
2. Antenna		
Antenna type -- phased array of YAGI elements		
Antenna aperture - 100 m x 100 m		
Antenna beamwidth - 4.1 degrees		
Antenna pointing - 9 positions; N/S/E/W at 12.8 degrees off–zenith, NE/SE/SW/NW at 18.3 degrees off zenith and zenith		
3. Data processing		
Time domain averages	2000	1000
Spectral averages	8	32
Maximum radial velocity	+15 m/s	±15 m/s
Maximum horizontal velocity		
12.8° pointing	±67.7 m/s	±67.7 m/s
18.3° pointing	±47.8 m/s	±47.8 m/s
Dwell time per profile	51.2 sec	204.8 s
First height	1 km	6.4 km
Number of heights	256	256
Height spacing	50 m	50 m

is only 30 km; however, signals that are range aliased can be eliminated as shown in Appendix C.

The transmitter proposed here would use 144 modules similar to the type described in Appendix A (2350 W peak output power, 5% duty cycle). The peak power output for each of the 144 modules proposed would be 1400 W. Note that reliable higher power modules are produced commercially.

D. Antenna

The WPL radar wind Profilers use two or three beam pointing directions. Their primary function is to measure hourly–averaged vertical pro-

files of horizontal wind. A radar for obtaining wind measurements on shorter time scales and a radar to obtain additional wind information (not just mean wind) will need more pointing directions. The WPL radars point toward north and east at 75° elevation angle. The measurement volumes are displaced by 0.27 H from above the radar (also from a zenith observation volume), where H is the measurement height. The horizontal observation volumes are displaced by 0.38 H from each other. When measurements from these two volumes are combined to form a wind vector with a very short time average, horizontal homogeneity must be assumed. For applications such as shuttle launch support this assumption may be too restrictive and other antenna pointing strategies might be needed. If required, the measurement volumes can be moved closer together by (1) increasing the elevation angle or (2) not having orthogonal pointing directions. The elevation angle is a compromise of many factors as discussed in Appendix D. Similar compromises arise if the azimuth pointing angles are separated by less than 90°; if the pointing directions are too close together accuracy of one wind component will degrade.

The antenna concept outlined below combines features from a number of research radar systems to arrive at a modular design that allows nine beam pointing directions. Main features of this antenna are given in Table 2.2. It uses 576 Yagi-Uda elements in 16 identical subarrays of 36 elements. Each element is driven by a solid-state transmitter module; corresponding elements in the other subarrays have the same phase and therefore can be driven by the same module (no high-power phasing is used). The number of modules needed is therefore 36 or 72 or 144 or 288 or 576, depending on the power output of each module. If there are 576 modules (as used by the MUR, Appendix A), then there is total flexibility in beam steering and the subarray concept can be ignored. The identical subarrays simplify the phasing and steering and lead to a modular concept. As shown in Figs. 2-3 and 2-4, the antenna as proposed with four groups of 36 transmitters yields four identical antennas, each with the same steering capability as the entire array. Each element has six selectable phases, differing by $\lambda/6$. The beam pointing directions are given by

$$\text{arc sin}\left(\frac{\text{element phase difference}}{\text{element spacing}}\right) .$$

Table 2.2.--Antenna Feed and Positioning

Antenna pointing - 9 positions: N/S/E/W at 12.8 degrees off-zenith NE/SE/NW/SW at 18.3 degrees off-zenith Antenna elements - 576 YAGI elements Element spacing - $3\lambda/4$ Aperture - 103.5 m × 103.5 m Element phasing - 0, 60, 120, 180, 240, or 300 deg 4 YAGI elements fed from a solid state transmit/receive module 16 identical sub-arrays of 36 elements

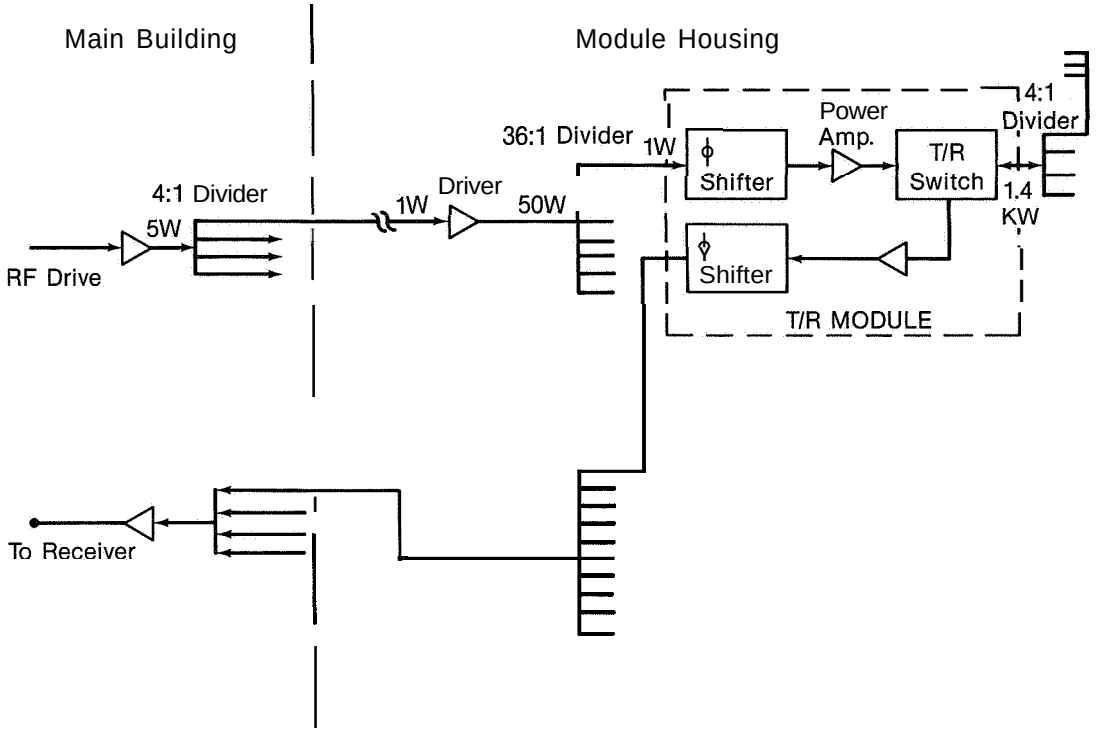

Figure 2-3. RF power distribution.

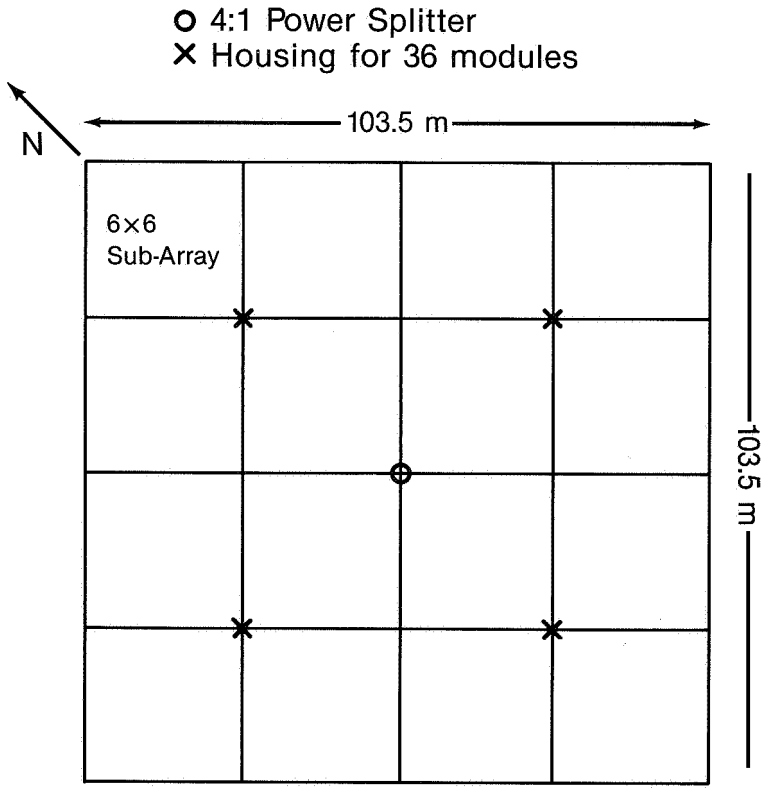

Figure *2-4.* **Antenna concept.**

In the NE, SE, SW, and NW directions this is

$$\text{arc sin}\left(\frac{\lambda/6}{3\lambda/4}\right) = 12.8^\circ \ .$$

In the N, S, E, and W directions the pointing is

$$\text{arc sin}\left(\frac{\lambda/6}{3/2\ \lambda/4}\right) = 18.3^\circ \ .$$

Table 2.3 shows the phasing required for each element in the sub-array. Many other beam-pointing directions are also possible with this configuration, but these nine positions (zenith is generated by feeding all elements in-phase) are the primary ones for wind profiling. Theoretical antenna patterns have not been calculated; however, the concept of beam steering by phasing Yagi-Uda elements has been implemented in the MUR and SOUSY radar systems at 50 MHz and in the WPL system at 400 MHz. The MUR and SOUSY radars use similar element spacing (2/3 X and $\lambda/\sqrt{2}$) as opposed to 3 $\lambda/4$ proposed here, whereas the WPL system uses many fewer elements (spacing = 1.1 λ) but with degraded antenna performance. This antenna proposal would have to be studied by computer simulation to see if illumination tapering is required and to determine the quality of the antenna patterns. This antenna would be scaled for higher frequency radars. At 225 MHz the antenna would be about 20 m x 20 m. Appendix E describes a proposed 225 MHz wind profiling radar for White Sands Missile Range. The White Sands radar should measure wind profiles throughout the troposphere but not with the height resolution of the 50 MHz radar proposed here.

E. Signal Processing

Most radars used for wind profiling use a data-processing scheme similar to that illustrated in Fig. 2-5. This processing method uses spectral analysis and assumes a pulse Doppler radar. The WPL pulse Doppler radars operating at 6, 0.74, and 0.33 m wavelength (50, 405, 915 MHz) all use this processing scheme. Spectral analysis yields the complete Doppler velocity spectrum; other processing methods such as autocovariance ("pulse-pair") analysis can be performed with less computation power, but analyzing the Doppler spectrum facilitates treating unwanted signals such as ground clutter and narrowband interference. Radial profiles of the first three moments of the Doppler spectra are estimated: signal power P, mean radial velocity V_r, and spectrum width W. The input signal is the backscattered signal for each radar resolution cell after translation to a convenient frequency. The receiver limits the bandwidth with a filter that is (usually) matched to the transmitted pulse. Complex video is obtained by baseband mixing with a reference voltage. Samples of video are generated for each pulse repetition period T and for each range resolution cell centered along the antenna axis; these voltage samples represent the composite amplitude and phase of the scattering process in the resolution volume.

Part of the processing for the WPL radars is performed in a special purpose radar controller (designed and built in-house). The remainder of

Table 2.3.--Required Phasing for Eight Reams Using 60° Phase Increments. Diagram is Basic 6 × 6 Element Sub-array.

NE ↑

300	300	240	300	180	300	120	300	60	300	0	300
0	0	60	60	120	120	180	180	240	240	300	300
60	0	120	0	L80	0	240	0	300	0	0	0
0	300	300	240	240	180	180	120	120	60	60	0
240	240	180	240	120	240	60	240	0	240	300	240
300	0	0	60	60	120	120	180	180	240	240	300
120	60	180	60	240	60	300	60	0	60	60	60
60	300	0	240	300	180	240	120	180	60	120	0
180	180	120	180	60	180	0	180	300	180	240	180
240	0	300	60	0	120	60	180	120	240	180	300
180	120	240	120	300	120	0	120	60	120	120	120
120	300	60	240	0	180	300	120	240	60	180	0
120	120	60	120	0	120	300	120	240	120	180	120
180	0	240	60	300	120	0	180	60	240	120	300
240	180	300	180	0	180	60	180	120	180	180	180
180	300	120	240	60	180	0	120	300	60	240	0
60	60	0	60	300	60	240	60	180	60	120	60
120	0	180	60	240	120	300	180	0	240	60	300
300	240	0	240	60	240	120	240	180	240	240	240
240	300	180	240	120	180	60	120	0	60	300	0
0	*0*	300	0	240	0	180	0	120	0	60	0
60	0	120	60	180	120	240	180	300	240	0	300
0	300	60	300	120	300	180	300	240	300	300	300
300	300	240	240	180	180	120	120	60	60	0	0

NW ← → SE

↓ SW

ϕN	ϕNE
ϕE	ϕSE
ϕS	ϕSW
ϕW	ϕNW

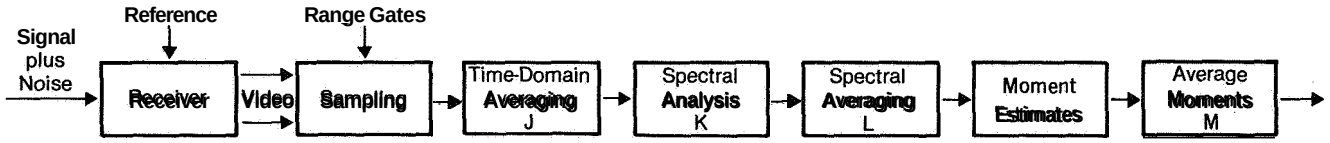

Figure 2–5. Data processing steps for wind profiling Doppler radars.

the processing is implemented in software on a standard minicomputer (Fig. 2-5). The radar controller generates all of the timing signals, performs the analog–to–digital conversions (sampling) of the video signals, does the time–domain integration, and provides the radar/computer interface that enables the radar to be controlled by the computer in all its functions. The same radar controller and software are used for all the radars. The various stages of data processing, the averaging that occurs at each stage, and the improvement in sensitivity in each stage of processing are examined below.

Sampling of the complex analog video signals is performed by analog–to–digital (A/D) converters. Dynamic range is usually not a consideration because, except for the lowest few kilometers of height, the signal levels are equal to or below the receiver noise level. Therefore, 8–bit A/D converters can be used and low cost A/D converters that operate at a conversion rate 2/3 μs or less are available. In the lowest few kilometers the signals and ground clutter can be much greater than the receiver noise level, particularly with high peak power transmitters. In this case a sensitivity time control (STC) can be used to reduce the receiver gain at short range so an 8–bit A/D is still satisfactory. All of the WPL wind Profiler radars use 8–bit A/D converters without STC.

The signal–to–noise ratio (SNR) can be improved for wind profiling radars by summing the complex video samples from a number J of consecutive received pulses. Since the noise bandwidth is determined by the radar pulse width, noise samples taken at the pulse repetition period will be uncorrelated; therefore, the noise power increases linearly with the number of samples added. The signal, however, remains well correlated for approximately 0.2 λ/W seconds (Nathanson, 1969), where λ is the radar wavelength. Typically W is ~1 m/s, so the correlation time is milliseconds with microwave radars and seconds with VHF radars. If, in addition to being correlated, the phase of the signal samples changes very little between samples, then signal samples can be added so that signal power increases with the square of the number of samples added. This occurs for radars whose unambiguous velocity λ/(4T) is much greater than the radial velocity of the scatterers. The SNR improves by the number J of samples averaged, and the unambiguous velocity decreases to λ/(4JT).

Three points should be noted in regard to time–domain signal averaging. (1) It is not necessary to use time–domain averaging to improve detection. The SNR improvement can be obtained in later processing, but time–domain averaging minimizes the calculation burden in succeeding processing stages without sacrificing sensitivity, and it redu-

ces the data rate throughout the signal processor. (2) Time-domain averaging filters the input signal so that signal components with velocity greater than $\lambda/(4JT)$ will be aliased and attenuated (Schmidt et al., 1979). Without time-domain averaging, when signal components are aliased they are not attenuated. (3) It is possible to select J and T (and an appropriate window) so that interference at particular frequencies is virtually eliminated. For the 6 m wavelength radars we select J and T so that 60 Hz is rejected as shown in Fig. 2-6. We select J as large as possible such that $\lambda/(4JT)$ is greater than the maximum expected mean radial velocity and such that the signal is correlated for much longer than JT.

Time-domain integration of the sampled video is best accomplished in special purpose hardware rather than software because this function must be performed for all ranges (heights) during the pulse repetition interval. If this averaging is implemented in the computer, the spacing of the range samples and the total number of range samples will be restricted by the transfer time to the computer and the speed of the computer. The time-domain integration for the WPL radars is a simple summing of samples from J consecutive radar pulses. If this integration is a weighted sum, then with proper choice of weighting, the filter response shown in Fig. 2.6 can be modified so that response is more uniform in the desired frequency band (0 to the Nyquist frequency) and so that response at higher frequencies (filter sidelobes) is reduced. This filter shaping can be useful in rejecting interference from the carrier frequency of stable transmitters.

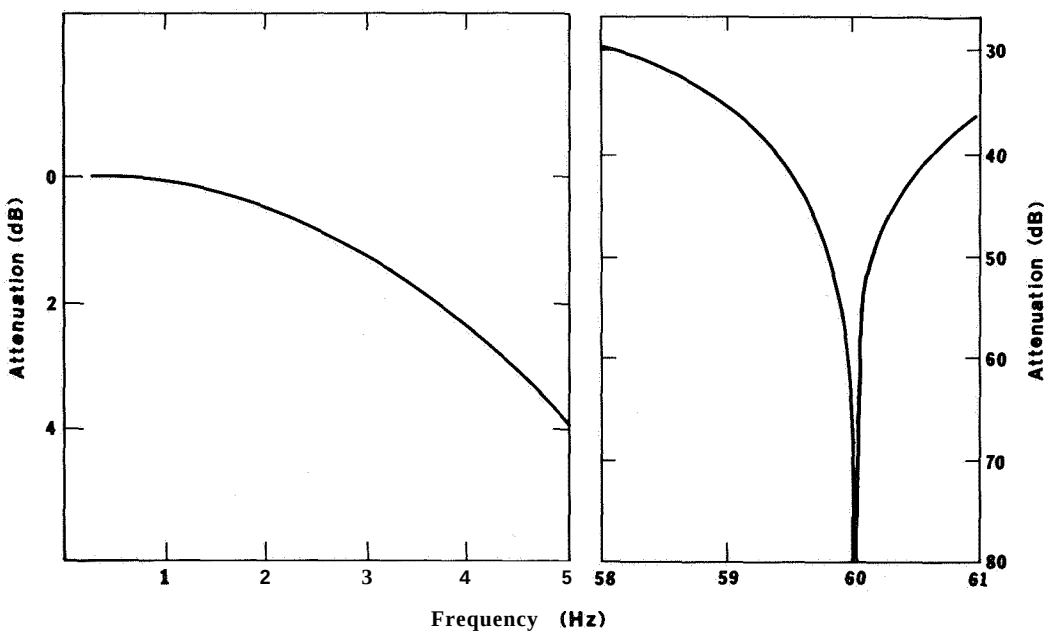

Figure 2-6. Filter response for time-domain integration of video samples. The Nyquist frequency is 5 Hz. Pulse repetition period and the number of time domain averages are selected to attenuate 60 Hz.

The next step in signal processing is to compute the power spectrum of K (averaged) signal samples, We select K such that the achievable coherent integration is realized. If K is too small, sensitivity is reduced; if K is too large, the calculation burden is increased without improving sensitivity or retrieving additional information. Figure 2-7 shows how the SNR in the spectral domain improves as dwell time T_D = JKT increases. (Spectral domain SNR is the peak signal level divided by the rms noise fluctuations.) The improvement factor is given by

$$K \operatorname{erf} (\Delta V/2\sqrt{2W}) ,$$

where AV is the velocity resolution of the spectral processor $\lambda/(2T_D)$. For small K the improvement factor increases linearly with K; spectral resolution is so poor that all the signal power remains in one velocity resolution element. As observation time increases, the noise power in each velocity resolution element decreases, while signal power remains constant. When the dwell time is increased to the extent that signal power starts to occupy more than one spectral point, SNR improvement no longer increases linearly with dwell time. When the dwell time is $\lambda/(2W)$ ($K = \lambda(2JTW)$), 95% of the available coherent integration is achieved. Longer dwell times yield little SNR improvement because both noise power and signal power decrease in the velocity resolution element that contains maximum signal. Note, however, that for large K, spectral points can be averaged and the spectrum will still be resolved. If this is done, SNR improves as $T_D^{1/2}$, as expected for incoherent integration. Thus, to minimize calculations we choose $K = \lambda(2JTW)$ and use any additional observation time to measure new spectra. Spectral processing can be implemented in special-purpose hardware such as array processors, or it can be done in software. The WPL radars use software fast Fourier transform (FFT) spectral analysis. Software FFT is satisfactory for the VHF (6 m wavelength) radars but not for the shorter wavelength radars. The computation time is small relative to the data acquisition time for VHF radars, but the acquisition time is less with UHF radars, so the computation time significantly reduces the time used to observe the signal. The acquisition time JKT is directly proportional to radar wavelength because the unambiguous velocity $\pm\lambda/(4JT)$ is the same for all wavelengths.

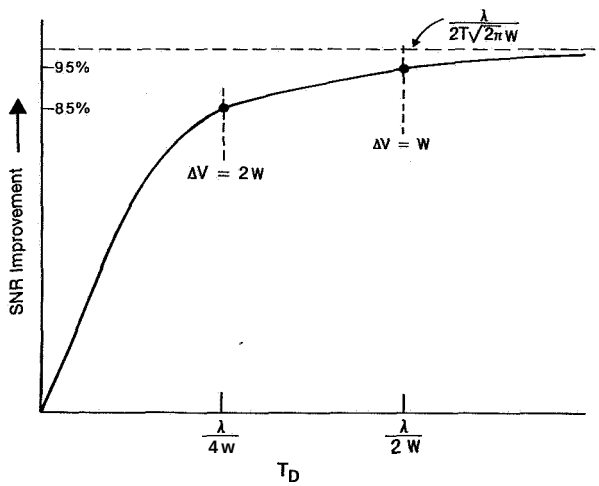

Figure 2-7. Signal-to-ratio improvement from spectral processing. Coherent integration achieved with spectral processing is limited by the coherence time of the scattering process. The limiting value, $\lambda/(2T\sqrt{2\pi}\ W)$, can be obtained by spectral processing alone or by a combination of time domain integration and spectral processing,

The next processing step is the averaging of L spectra, each obtained from JK radar pulses. The L power spectral density estimates for each frequency or velocity will be exponentially distributed with a standard deviation equal to the mean (Hildebrand and Sekhon, 1974). We expect averaging to improve the spectral domain SNR by $\sqrt{L}$; however, this improvement will occur only if the mean wind is the same for each dwell time. If the mean wind is not the same, then the width of the averaged spectrum increases during the averaging time so that spectral domain SNR improvement will be less than $\sqrt{L}$. It is readily seen that if the mean wind changes abruptly by more than W, then the SNR can actually decrease with averaging time. The dependence of spectral width on averaging distance was studied by Frisch and Clifford (1974) and Labitt (1981). They derive the relationship $W \alpha d^{1/3}$, where d is the maximum dimension of the observation volume (beamwidth or range resolution, whichever is greater) and d is less than the outer scale of turbulence L_o. If we average for time T_o such that $d < \bar{v}T_o < L_o$, then, using Taylor's hypothesis, $W \alpha (vT_o)^{1/3}$ where $\bar{v}$ is the mean wind speed. Therefore, if the averaging time is less than $d/\bar{v}$, then the width of the averaged spectrum is about the same as the width of the individual spectra; for greater averaging time, the width of the averaged spectrum increases as $T_o^{1/3}$. To take full advantage of $\sqrt{L}$ improvement in SNR by averaging spectra, L should be limited to about $d/(JK\bar{T}\bar{v})$.

At this point in the processing we have an averaged Doppler spectrum for each radar resolution cell as illustrated in Fig. 2-8. Note that with signal and noise powers defined as in Fig. 2-8, the signal-to-noise ratio (S/N) is J times the SNR of the input video. Spectral analysis and averaging of spectra do not increase S/N; however both these processing steps improve the signal detectability or spectral domain SNR. Spectral analysis spreads the noise uniformly over the Nyquist interval and concentrates the signal power in a narrower band while spectral averaging reduces the fluctuations of the noise thereby making a given signal easier to detect. If the signal power is all contained in one spectral point, then the rms noise fluctuations will be equal to the signal power (spectral domain SNR equal unity) for an input SNR of $-10 \log_{10}[JK\sqrt{L}]$ dB. Actual radar signals of spectral width W require an input signal-to-noise of about $-10 \log_{10}[\lambda \sqrt{L}/(2T \sqrt{2}\, \pi W)]$ dB for a spectral domain SNR of unity. This result is the product of the time-domain integration J, the limiting value of improvement by spectral processing $[\lambda/(2JT \sqrt{2}\, A\, w)]$, and incoherent averaging of L power spectra. Note the result is independent of time-domain integration, illustrating that

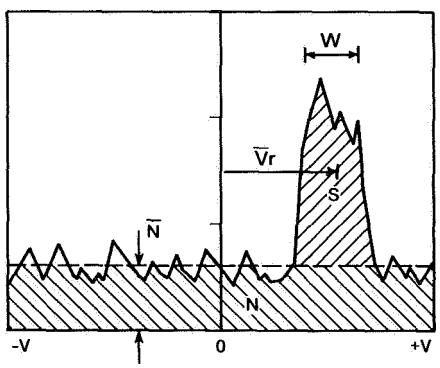

Figure 2-8. Derivation of spectral moments from Doppler spectra. $\bar{N}$ is the noise level, N the total noise power, S the signal power, V_r the mean radial velocity and W the width of the spectrum.

time–domain integration is not essential for optimizing detection.

As an example of the processing gain used in clear air radars, typical values for a 6 m wavelength radar are J = 100, K = 64, L = 16, and T = 500 μs. The processing system can detect a sinusoid with input SNR of –44 dB. Actual radar signals occupy a bandwidth of about 8 of the 64 spectral points, so the input SNR needed to detect actual signals is about –35 dB. The spectral domain S/N needed for detection is 20 dB greater than the input SNR.

The next data processing step is the estimation of the important spectral moments (S, W, V_r) from the averaged Doppler velocity spectrum. The signal spectrum must be isolated from the measured signal–plus–noise spectrum before the moments can be found. The methods used to do this (and to remove undesired spectral components such as ground clutter near zero velocity) are usually empirical. The average value of the complex time series is usually removed prior to calculating the power spectrum. Noise rejection is accomplished by applying a threshold, either a specified amount above the mean noise level or below the peak level. Another method to locate the signal is to find the maximum power in a velocity window of width equal to the expected signal width. The method used with the **WPL** wind Profilers is as follows (Carter, 1982):

> First, the average value of the complex time series is removed prior to calculating the power spectrum to eliminate any fixed clutter or DC offsets in the signal channel. Next, the mean noise level is found by applying an objective technique (Hildebrand and Sekhon, 1974) for each spectrum. A fixed noise level cannot be assumed for the 6 m wavelength radars because the noise is governed by cosmic background. The signal spectrum is isolated by locating the peak value of the averaged spectrum and including all those contiguous spectral points that exceed the noise level, The classical definition of the moments is then applied to the isolated signal spectrum after subtracting the mean noise level from each of the selected spectral points. In very weak signals, or if the input consists of noise only, the algorithm selects the peak and a few adjacent spectral points; it therefore becomes a maximum likelihood estimator of the mean velocity (Whalen, 1971). It is an unbiased estimator of the mean velocity [in noise it selects a random value between $(\pm\lambda/(4JT)]$. Since it selects that portion of the noise in the isolated spectral points that exceeds the mean noise as "signal," both power and width estimates are biased by the noise. This method appears to work well for a wide variety of conditions.

Special features are available for modifying the measured Doppler spectrum; these include a ground clutter rejection method for selected heights and suppression of interference at particular frequencies.

Finally, estimates of spectral moments can be averaged. The averaging time depends on the type of information sought and the temporal evolution of the scattering phenomena and meteorology. For example, the WPL 6 m

wavelength radars are used to obtain hourly estimates of mean tropospheric winds; during 1 hour, M radial velocity profiles of mean velocity are measured for each orthogonal wind component. At the upper heights the mean velocities are sometimes random because of low SNR. Some of the profiles are also contaminated by interference from other transmitters or by scattering from aircraft. In the WPL wind Profilers the radial velocity profiles are averaged by applying a simple version of random sample consensus (Fischler and Bolles, 1981).

The set of M radial velocity data points at each measurement height is examined to find the largest subset of points within X spectral points of each other. If this subset includes fewer than Y data points, the data are rejected for that height; otherwise the subset is averaged to obtain the mean radial wind. In practice the averaging is as follows. The number of observations (M) for each height is 12. The radial velocities are examined to find the largest subset whose mean radial velocities are within two (X = 2) spectral points of each other. The total number of spectral points K in the Doppler velocity spectrum is 64; the window of acceptable data is, therefore, 1/16 of the total radial velocity interval. If the largest subset is four or more (Y = 4), the average of this subset is taken as the mean radial velocity during the observation period. If the largest subset is less than four, the data are discarded and no wind component is computed for that height. If there is more than one subset with the same (largest) number of data points, then the subset containing measurements closest to the end of the data acquisition period is accepted. This algorithm has proved effective for rejecting data contaminated by aircraft and for rejecting data when the signal-to-noise ratio is so low that the set of twelve estimates of radial velocity are essentially uniformly distributed over the Nyquist velocity interval.

To see how this algorithm functions in the case of no atmospheric signal, and because an analytic solution for the probability of occurrence of the largest subset was not obvious, the performance was simulated. The probability p that exactly k values will be in the data window is the following:

k	p (largest subset = k)
0	0
1	0.007
2	0.413
3	0.463
4	0.104
5	0.013
6	0.001
7	0.001

The probability is zero that the largest subset is zero because the algorithm centers the window on each measured data point to count the subset. The probability that the largest subset is greater than seven is too low to measure by simulation. If the input is noise, the probability that the largest subset is four or more is 0.119. When the radar attempts to measure winds at heights where the atmospheric signal is too weak to

detect, the largest subset is usually two or three; this indicates that the radial velocity estimates are uniformly distributed, as they must be for this algorithm to function properly.

The radar measures a mean radial veloctiy profile for each antenna pointing angle. The observation time used for each radial profile is one to 2 min for the VHF radars and 10 s to 1 min for the UHF radars. The antenna pointing angles are fixed to observe orthogonal wind components (two-beam systems) or orthogonal wind components and the vertical wind (three-beam system). In the two-beam systems the vertical motion is assumed to be negligible when measurements are averaged over periods of about an hour.

In the two-beam systems the wind components are

$$u = V_E/\cos\ \Theta_e \text{ and } v = V_N/\cos\ \Theta_e$$

when V_E and V_N are the measured radial velocities (assumed to be toward east and north) and Θ_e is the antenna elevation angle. For three-beam systems,

$$u = V_E/\cos\ \Theta_e - V_Z \tan\ \Theta_e$$

$$v = V_N/\cos\ \Theta_e - V_Z \tan\ \Theta_e$$

where V_Z is the measured vertical velocity.

A worst-case accuracy of the measured u and v wind components can be found by examining the data processing algorithm. If there are just $Y = 4$ data points in the subset of averaged data, and these data points are uniformly distributed over the velocity window, then the variance of the consensus averaged u or v will be $\Delta^2/48$ where Δ^2 is the velocity window. Here, A is 1/16 of the Nyquist velocity interval analyzed by the data system, typically A = 2 m/s. Thus the variance of radial velocity is at most 1/12 m^2/s^2. In general the variance of u and v will be much less than this because there are usually more than four estimates in the average and they are not uniformly distributed in the window. The spatial and temporal consistency of the wind profiles indicate that the variance of the estimates of hourly averaged winds is much less than 1 m^2/s^2.

Both wind components must be available to measure wind speed and direction; therefore, although each component has a probability of 0.119 that the processing will yield an estimate if the input is noise, the probability of obtaining an estimate of wind speed and direction is only 0.014 for noise input.

Conclusions and recommendations for data processing are the following.

1. Spectral processing should be used for VHF and UHF wind Profilers because it offers flexibility in treating ground clutter and interfering signals. There do not seem to be (at this time) reasons for using

spectral processing methods other than FFT of the input time series (such as maximum entropy). However, there should be sufficient computer power available so that other methods could be implemented if improved processing algorithms are developed. This is particularly true for a sensitive radar system with costly antenna and transmitter--the computer and data processing are equally important components of a radar system.

2. If there are a large number of height increments or if a UHF radar is used, the data system should include a hardware FFT processor or array processor; an array processor as an integral part of the computer is recommended because these processors have been fully developed with supporting software and they are now cost effective.

3. Time-domain integration may also be possible in an array processor; however, this component can be built following existing special-purpose processors designed specifically for wind profiling radars. Thus it is a no-risk and low-cost development. The special purpose processor solves the sampling and data transfer problem by reducing the data rate at the input.

4. The data system should be able to store several hours or more of radial velocity profiles or averaged radial velocity profiles. The data system should be able to calculate wind averages with any specified averaging time and with more than one averaging time.

5. Wind profiles should be stored for the immediate past (say about twelve profiles with each averaging period) because these past profiles can be used to obtain the maximum amount of valid data from the presently measured profiles using temporal and spatial continuity algorithms. Algorithms for this processing are now being developed.

6. A measured vertical velocity profile is essential for measuring horizontal winds with short (1 to 10) min averaging times; a vertically-pointing beam should be included. The vertical beam provides a direct measurement of whether the horizontal wind measurements may be in error because some of the radial motion will be from vertical motion. Direct measure of vertical motion also tells what averaging time is needed to ignore vertical motions. In some cases it may be possible to use the measured vertical motion to correct the measured horizontal winds.

CHAPTER 3

PAST PROFILER OPERATIONS

The Wave Propagation Laboratory (WPL) has operated a network of radar wind Profilers in Colorado for more than 1 year. The network consists of four VHF (50 MHz) radars and a UHF (915 MHz) radar, located as shown in Fig. 3-1. The Platteville VHF radar was developed by the Aeronomy Laboratory (AL) and has been operated jointly by WPL and AL for several years. The other radars were installed between February and May 1983. The Platteville radar uses older hardware and will not be described here. The other radars use similar data systems and software; their method of operation and our experience with them is described below.

A. VHF Radar Operations

The VHF radars near Sterling (Fleming), Craig (Lay Creek), and Cortez (Cahone) were placed in operation in March, April, and May 1983. Table 3.1 lists the radar characteristics. These radars transmit simultaneously in two pointing directions and have 50 m × 50 m coaxial-colinear array antennas. Computers and data systems perform the complete data analysis at the radar site. Wind profiles are sent by telephone once per hour to the Denver computer. Two resolution modes are used: a 3 μs pulse width for low and middle levels, and a 9 us pulse width to extend the height coverage as high as possible.

The radar signals are digitized with 2 and 6 μs sample spacing for the two modes. In the usual sequence of operation, 12 profiles are measured for each pulse width and averaged to produce hourly wind profiles. The radars alternate pulse widths and finish the hourly data acquisition cycle in about 45 min. The last 15 min are idle to allow the telephone communication system to poll all the outlying sites and to allow the radar operator to access the station to make changes or obtain diagnostic outputs. Figure 3-2a shows how the time is shared between the two modes of operation. Figure 3-2b shows the details of how the time is spent during each mode. The telephone transmission from each site takes about 40 s.

Figure 3-3 shows a sample of the hourly data transmission from one of the VHF radars to the central hub computer located in Denver-Boulder area. The data format shown in Fig, 3-3 has remained unchanged since the radars were placed in operation. It includes the wind speed (m/s) in Column 2, wind direction (degrees) in Column 3, and the height (km above mean sea level) in Column 4. Columns 5 and 6 list the number of profiles in the consensus average as explained in the data processing section. The signal power (not range corrected) is in Column 7. The width of the Doppler spectra is also calculated but is not being transmitted.

Table 3.1--New **VHF** radar characteristics and operating parameters

Radar characteristics		
Frequency	49.8 MHz	
Authorized bandwidth	*0.4* MHz	
Peak power	30 kW (maximum ≈60 kW)	
Average power	400 W (maximum ≈1 kW)	
Pulse width	3, 9 µs	
Pulse repetition period	238.67, 672 µs	
Antenna aperture	50 m x 50 m	
Antenna pointing	15° off-zenith to north and east (2 antennas)	
Antenna type	fixed phased array of colinear-coaxial dipoles	
Two-way beamwidth	5°	
Operating parameters		
Mode	1	2
Data processing	**3-ps** pulse	9-ps pulse
Time domain averaging	419 pulses	124 pulses
Spectral averages	8	16
Maximum radial velocity	±15.7 m/s	±19.6 m/s
Spectral resolution (64 points)	0.49 m/s	0.31 m/s
Height sampling		
First height	0.6 km	3.0 km
Height spacing	290 m	870 m
Number of heights	22	18

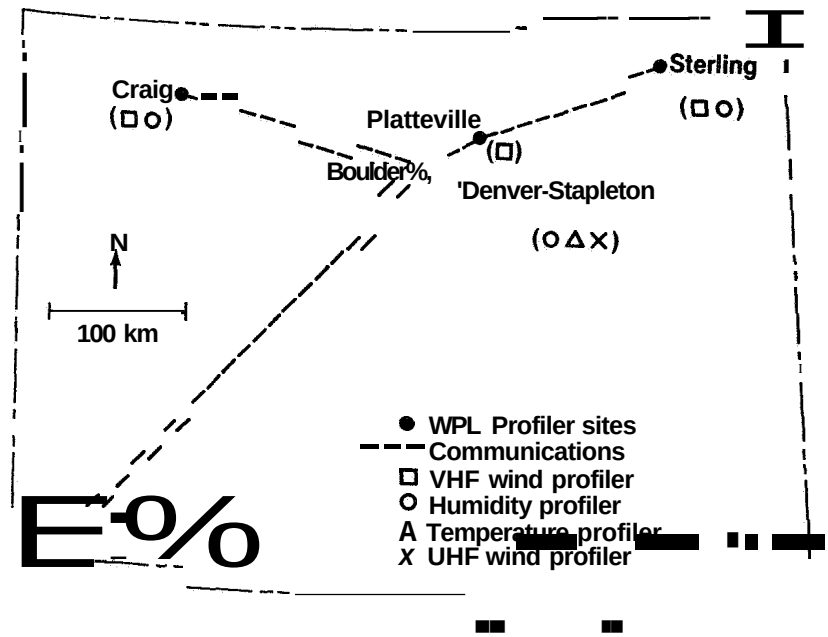

Figure 3-1. Wind profiling radar sites in Colorado. Temperature and humidity profilers are currently installed at Denver-Stapleton.

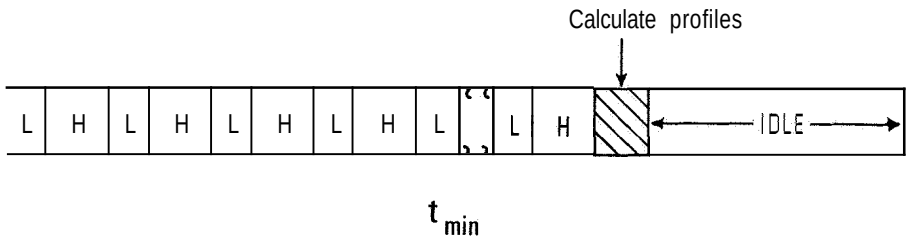

Figure 3-2a. Hourly sequence of wind observations with 3-μs pulses (L) and 9-μs pulses (H). The idle period is for network communications.

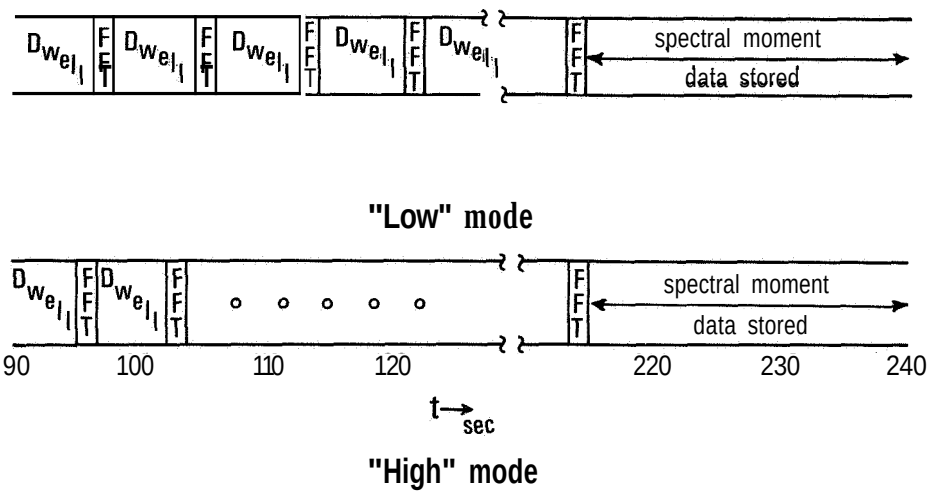

Figure 3-2b. Details of temporal averaging during the 3-μs ("LOW") mode and 9-μs ("HIGH") mode of operation.

```
SITE: FLEMING
DRTE:  5  7 83
TIME: 12  0  a
NPRO:  11  NTDR:  413  NOSP:   8  PULW:   3.67  PRPR:  238.67
UNRXH:  58.147
FIRS] HEIGHT (KM,AGL):   1.40
# OF HEIGHTS:   22
DELTR HEIGHT (KM):  .23
RFLC ANT:  ]
HT#   WS     WD      HT     #E     #N    RFLC
 1    1.1   255.7    2.7    11     11    56.4
 2    1.2   232.0    3.0    11     11    43.7
 3    2.8   261.5    3.5    11     11    52.3
 4    2.8   285.0    3.6    11     11    53.6
 5    5.0   330.1    3.9    11     10    53.1
 6    3.7   347.3    4.2    11     11    54.0
 7   10.5   355.1    4.5    11     11    52.2
 8   10.7     4.2    4.8    11     11    50.2
 9   10.5     5.4    5.1    11     11    43.8
10   10.1   358.1    5.3    11     11    50.3
11    9.8   347.0    5.6    11     11    47.7
12    8.8   335.3    5.9    11     11    46.2
13    9.2   331.4    6.2    11     11    41.2
14    6.7   313.7    6.5    11     11    30.8
15    7.5   330.9    E.a    11     11    32.1
16    6.0   323.4    7.1    11     11    31.5
17    3.3   340.4    7.4    10     11    28.4
18    2.3    30.6    7.7     9     11    27.2
19    2.4      .8    8.0     8     10    21.8
20    4.0   315.5    8.2    11     11    32.2
21    6.6   321.4    8.5    11     11    34.3
22    7.0   313.6    8.8    11     11    31.3

SITE: FLEMING
DATE:  5  7 83
TIME: 12  1 33
NPRO:  11  NTDA:  124  NOSP:  16  PULW:   9.67  PHPR:  672.00
VMAXH:  68.782
FIRST HEIGHT (KM,AGL):   2.90
# OF HEIGHTS:   18
DELTA HEIGHT (KM):  .87
RFLC ANT:  1
HT#   WS     WD      HT     #E     #N    RFLC
 1   10.1   351.7    4.2    11     11    54.7
 2   10.2   357.9    5.1    11     11    53.5
 3    9.3   344.3    6.0    11     11    43.3
 4    7.5   333.8    6.8    11     11    39.3
 5    4.2   332.5    7.7    11     11    34.5
 6    6.9   324.6    8.6    11     11    38.2
 7   13.4   324.9    9.4    11     11    37.2
 8   20.6   320.7   10.3    11     10    35.8
 9   23.5   314.5   11.2    10      3    33.6
10   25.1   298.0   12.1    10      3    23.1
11   23.9   288.7   12.9     9     10    27.6
12   21.8   288.7   13.8    10     10    25.6
13   20.9   283.2   14.7    10      9    25.4
14   20.9   283.4   15.5     8     10    24.8
15   14.0   239.5   16.4     8      6    24.8
16   14.4   244.2   17.3     7      5    22.3
17 -999.0 -999.0   18.1     1      4  -393.0
18    8.9   227.7   19.0     5      5    19.4
```

Figure 3-3. Sample computer printout for the Colorado Network.

A. VHF Radar Performance

The Colorado Network radars have demonstrated that continuous hourly averaged wind profiles are feasible with automated and unattended systems. Figure *3-4* shows a sample of the hourly averaged winds measured by the VHF radar at Fleming (near Sterling). (Some of the problems that are apparent with the data from 0600 to 1200 GMT on February *24,* 1984, are discussed in Section C of this chapter.) The details that can be observed during events such as frontal passages give a temporal and spatial picture of the flow fields that are not available from other sounding systems.

An important question in the design of a tropospheric wind Profiler is that of sensitivity: given a desired height resolution, an averaging time for the wind data, the maximum height desired, and the fraction of time the winds must be measured, how sensitive must the radar be? For **VHF** radars the answer to this question determines the average transmitted

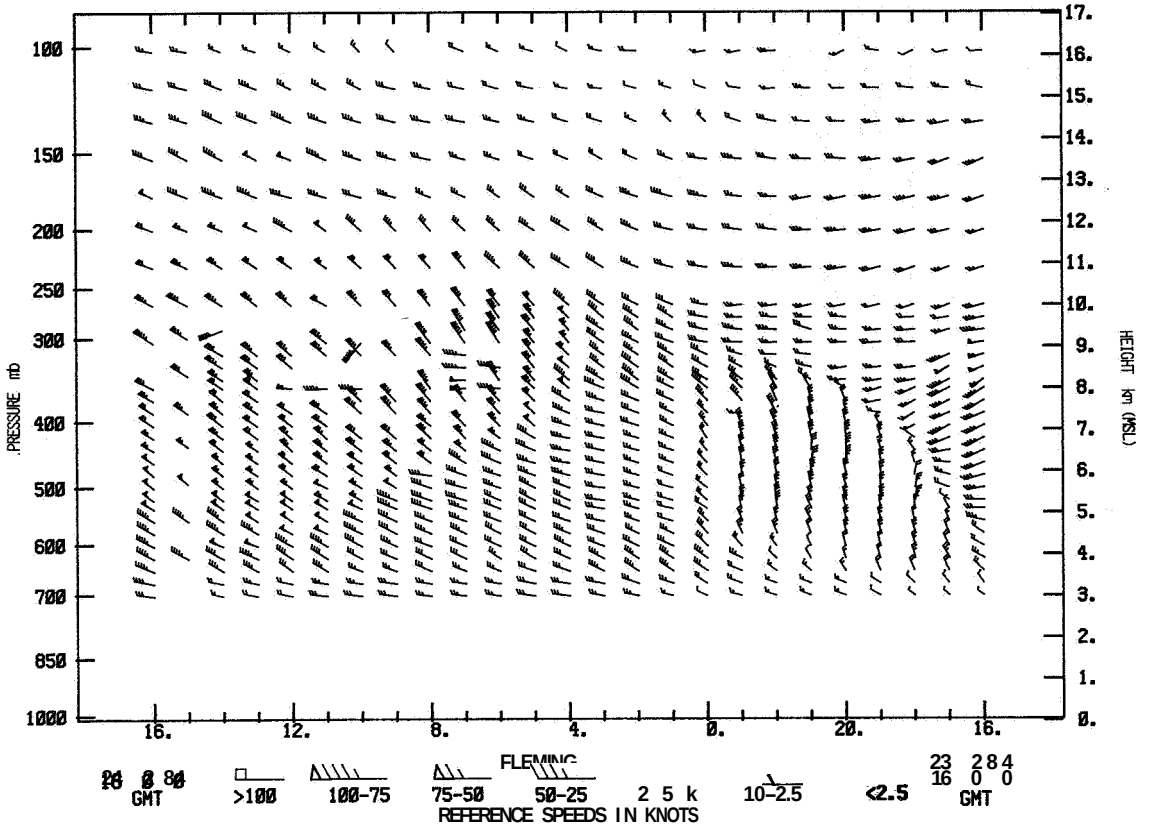

Figure 3–4. Sample of hourly–averaged winds measured by the 6-m wavelength radar at Fleming.

power and effective antenna area required. The VHF radars in the Colorado Network have a power–aperture product of 10^6 W-m^2: *400* W of average transmitted power and a 50 m x 50 m antenna. Figure 3–5 shows the percentage of time the Lay Creek radar (near Craig) was able to measure hourly winds as a function of height. The squares are the data points for the 3 μs pulse mode, and the circles are the data for the 9 μs mode. Both the u and v wind components passed the random sample consensus test, described in Chapter 2, Section E, for the percentage of time shown (as a function of height). The data are from 450 profiles (for each pulse mode) obtained from November 12 to December 12, 1983. The operating statistics from other systems are being developed and in general, we expect the same trend as shown in Fig. 3–5; however, the rapid decrease in height coverage that starts at about 16 km (9 μs mode) for the winter data will probahly start at about 13 km for summer data. The decrease in percentage coverage at about 12 km is due to signal dropout in the core of a jet stream.

Figure 3–6 shows what percentage of the data would have passed the random sample consensus if the algorithm had required that 8 or more of the 12 observations be in the largest subset. The decrease in percentage at about 5 km altitude (3 μs mode) is probably a result of moving clutter in the sidelobes, such as automobile traffic. Such clutter would tend to

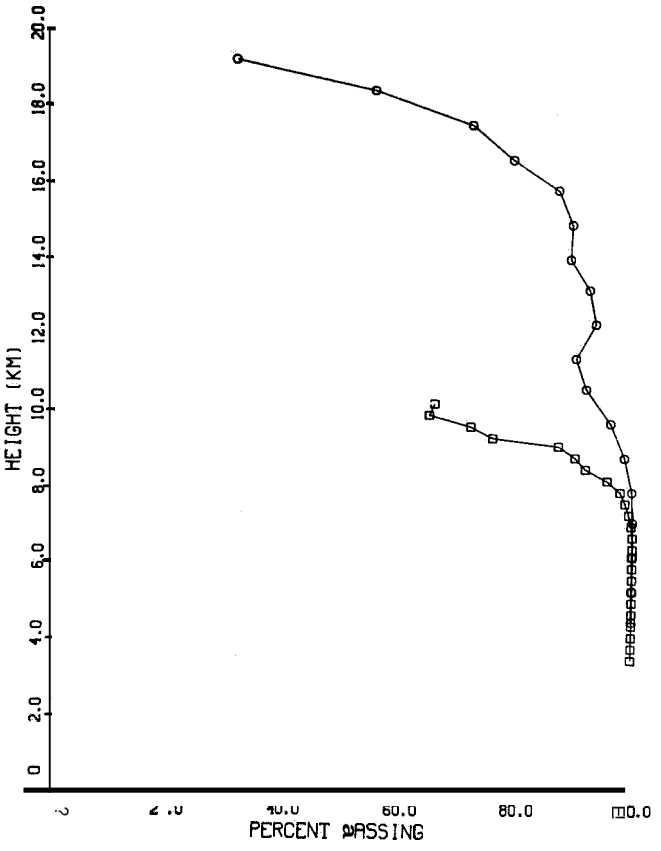

Figure 3-5. Percentage of time the 6-m radar at Lay Creek was able to measure wind profiles with a 3-μs pulse (squares) and a 9-μs pulse (circles). Power aperture product is the same for both modes. Data shown are from 450 profiles measured from Nov. 12 to Dec. 12, 1983. Twelve profiles are measured during each hour; 4 or more must pass the consensus test.

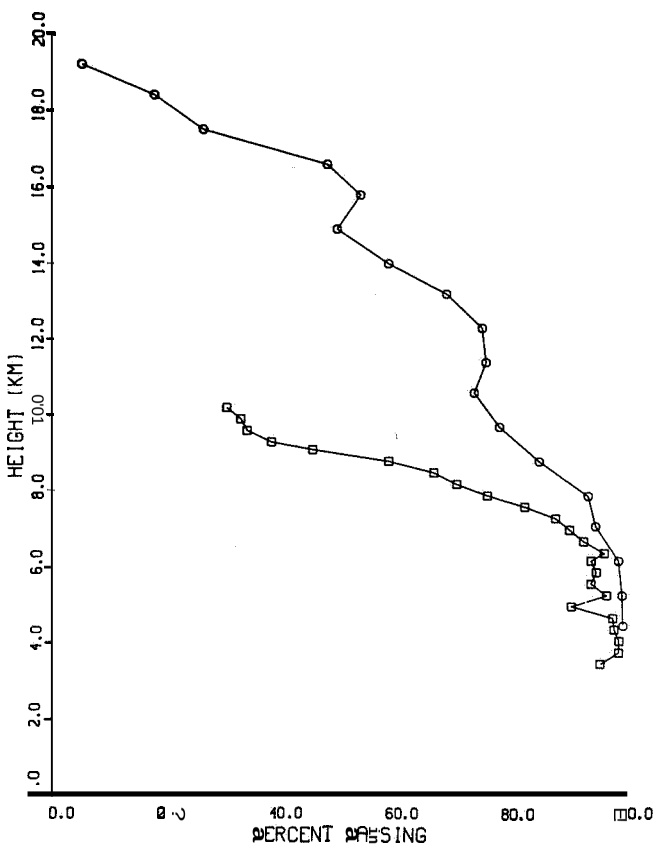

Figure 3-6. Same as Fig. 3-5 but 8 or more of the 12 profiles must pass the consensus test.

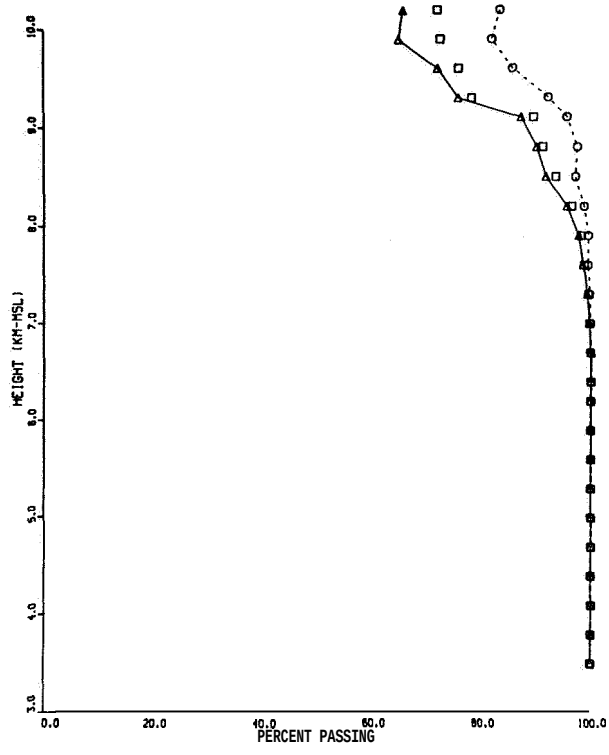

Figure 3–7. Percentage of time the 6-m radar was able to measure u (squares), v (circles) and both u and v (triangles) with the 3-μs mode. Same data as in Fig. 5. Four or more must pass the consensus test.

cause the data system to select a false velocity, whereas fixed clutter is rejected (to a large extent) by the data processing. Figure 3–7 shows the percentage of the u, v, and both u and v components that pass the consensus. We believe the difference in the u and v data reflects the difference in radar sensitivity (separate transmitters, receivers, and antennas) rather than a difference in radar reflectivity for the two pointing directions.

C. VHF Radar Problems

Some of the problems encountered with the VHF radars in the Colorado Network are associated with the particular hardware implementation we used and some are the result of VHF operation.

Problems associated with VHF operation:

1. Frequency allocations are difficult to obtain at VHF. The frequency allocation for the Colorado Network is on a non-interference basis with other users who occasionally produce interference.

2. Even when frequency allocations are obtained, the authorized bandwidth limits the height resolution of the radar. The bandwidth authorized for the Colorado Network is 400 kHz, so the minimum obtainable height resolution is about 400 m.

3. The weakest signal that can be detected by the VHF radars is about −145 dBm. It is difficult to avoid interference from the many communications systems that operate at nearby frequencies. We have had occasional interference problems with all our VHF systems.

4. A remote site with an acre or more of level ground is required. We selected our VHF radar sites in rural Colorado to be at least 10 mi from small towns or airports; sites were relatively easy to find, and all the sites are relatively free from moving clutter. However, the remote locations can lead to problems with primary power and telephone service. The radar site at Lay Creek has had very unreliable power; power outages occurred several times per week during the thunderstorm season. The computer at that site had to be modified *so* it could be reset by telephone. (All systems self-start after power failure unless the power remains off for more than 30 min; if this happens the computer must be reset.) The site near Craig has also had telephone problems; when telephone service is interrupted, rural locations are the last to be restored. Note in Fig. 3–4, for example, data for the 3 μs mode was lost during telephone transmission at 1200 GMT on February 24, 1984.

Problems related to WPL system hardware:

1. The minimum height that can be measured in the 3-μs pulse mode is about 1.7 m AGL. It should be possible to measure winds below 1 km AGL, but the combination of recovery time of the transmit/receive switch and switching transients limits the minimum height.

2. The power-aperture product of 10^6 W-m^2 does not always permit hourly wind measurements at all heights of interest. In particular, the core of the jet stream is a region of poor signal-to-noise ratio where signal dropout occurs. Note the data dropout at about 300 mb from 0600 to 1200 GMT on February 24, 1984, in Fig. 3–4. We believe this problem can be corrected by increased average transmitted power and/or increased antenna aperture.

3, Colinear-coaxial dipole arrays provide a low-cost, large-aperture antenna. Their radiation patterns are not of high quality, and antenna sidelobes have caused some problems. The enhanced echo observed with VHF zenith-pointing radars can sometimes be strong enough to be observed through an antenna sidelobe. This spurious signal from the zenith, if it is strong enough, can cause the velocity estimate for that height to be near zero. We believe this is the explanation for the group of wind vectors that show only west winds near 300 mb from 0600 to 1200 GMT on February 24, 1984 (Fig. 3–4). The north-pointing antenna measured almost zero radial velocity. The signal-to-noise ratio of the turbulence echo is low in this region (note the dropouts discussed above), *so* it could be smaller than the specular signal observed through an antenna sidelobe. The main lobe of the antenna points 15° off-zenith; a pointing angle

change to direct an antenna pattern null toward zenith could reduce the number of times this occurs. Other spurious echoes occur occasionally, but their origin cannot always be identified. A higher quality illumination pattern would no doubt eliminate some of them.

4. We have operated the radars at remote stations (one site is an 8 h drive from WPL) in an unmanned and automated mode. The remote locations cause maintenance problems, particularly with hardware that is not designed for long mean times between failures. Most of our problems are associated with high-voltage/vacuum-tube transmitters; the problems are easy to correct and the radar is usually returned to operation a short time after someone reaches the site. We have relatively unskilled local people available to correct problems that can be diagnosed by telephone, and they have been very valuable in saving time and travel. However, successful operation of unmanned Profilers requires that skilled personnel make routine visits for preventive maintenance.

All of the problems associated with our particular hardware implementation can be solved, so we conclude that routine operation of VHF wind Profilers is feasible provided that the fundamental constraints of frequency allocations, bandwidth, and interference, imposed by VHF operation, do not unduly compromise the measurement objectives.

D. UHF Radar Operations

The 915 MHz (33 cm wavelength) radar was installed near the Weather Service Forecast Office at Denver's Stapleton International Airport in January of 1983. Unlike the remote VHF radars, which have been operated in the same mode since they were built, the UHF radar has operated in many different modes for special experiments and comparisons with other instruments. Table 3.2 lists the operating parameters and radar characteristics. This radar uses three separate pulse widths and sequentially points in three directions. Each mode and each viewing direction are observed 12 times in an hour. Correction of the horizontal wind profiles for vertical velocity was implemented in May 1984. Data formats are the same as for the VHF radars.

E. UHF Radar Performance

Figures 3-8 to 3-10 illustrate the height coverage of the UHF radar. These figures show the results of 415 profiles (for each pulse width) acquired from November 5 to November 23, 1983. Circles show the north antenna data, squares show the east data, and triangles show the percent of the profiles where both the north and east data passed the consensus. Figure 3-8 shows data for the 1 μs pulse mode, with a largest subset required of 5 or more of the 12 observations. The radar is located at 1.6 km MSL; the first range gate is about 350 m AGL. Data are sampled every 2/3 μs or about every 100 m in height to about 4.3 km MSL. The consensus algorithm shows the problems caused by clutter in the lowest eight range locations (1.9-2.7 km MSL). The abrupt decrease in percentage passing at

Table 3.2--Stapleton radar characteristics and operating parameters

Radar			
Frequency	915 MHz		
Maximum bandwidth	2 MHz		
Peak power	5.6 kW		
Duty cycle	<25%		
Antenna aperture	≈10 m x 10 m		
Antenna pointing	zenith, 15' off-zenith to north and east		
Antenna type	offset paraboloidal reflector with offset horn feeds		
Two-way beamwidth	1.7'		
System noise temperature	240 K		
Operating parameters			
Mode	1	2	3
Data processing			
Pulse width	1 µs	3 µs	9 µs
Pulse repetition period	50 µs	64 µs	110 µs
Average power	110 W	260 W	450 W
Time domain averaging	136 pulses	80 pulses	46 pulses
Spectral averaging	8 spectra	32 spectra	32 spectra
Maximum radial velocity	±12.02 m/s	k15.97 m/s	±16.16 m/s
Spectral resolution (64 points)	0.376 m/s	0.499 m/s	.505 m/s
Heiqht sampling			
First height	0.35 km	1.64 km	2.7 km
Height spacing	100 m	290 m	870 m
Number of heights	24	24	18

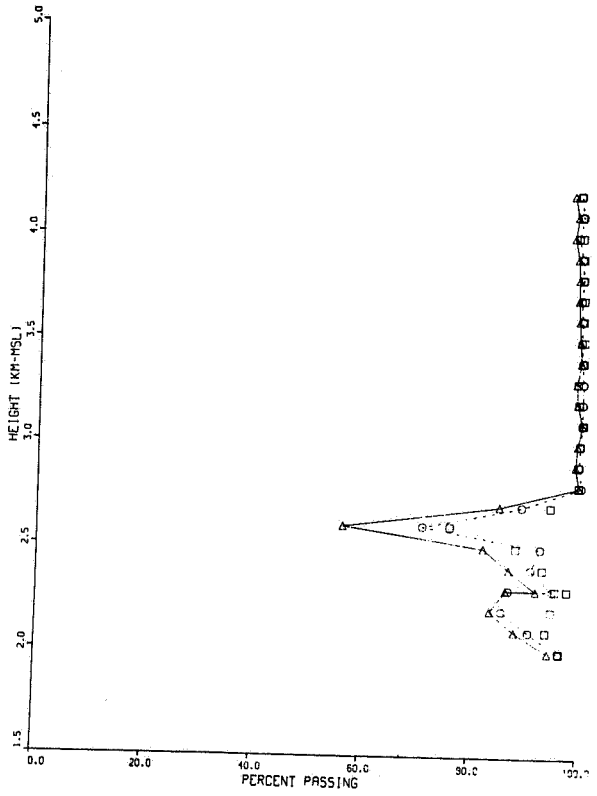

Figure 3-8. Percentage of time the UHF radar was able to measure hourly-averaged winds in the 1-μs pulse mode. East component (squares), north component (circles), and both components (triangle) passed the consensus test with 5 or more of 12 profiles to the largest subset. Data are from 415 profiles obtained Nov. 5 to Nov. 23, 1983.

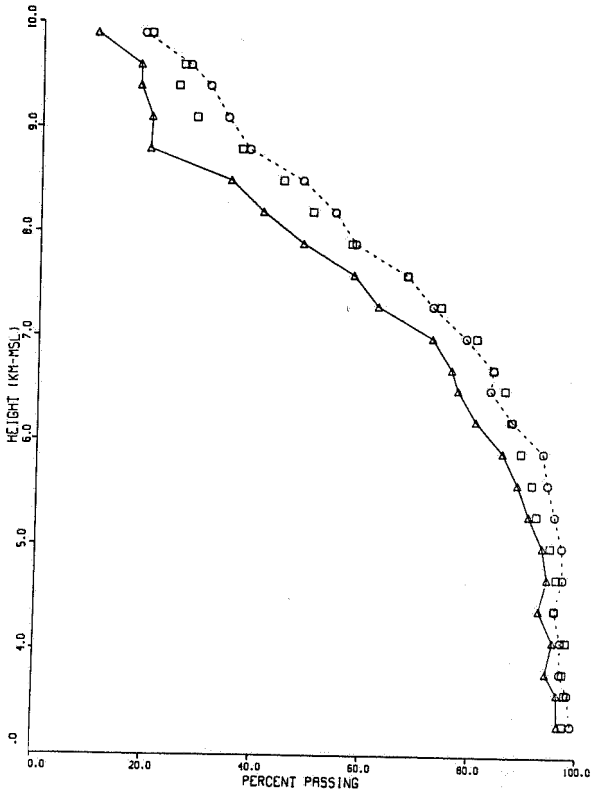

Figure 3-9. Same as Fig. 3-8 except the data are obtained with a 3-μs pulse and a largest consensus requirement of 8 of 12 profiles.

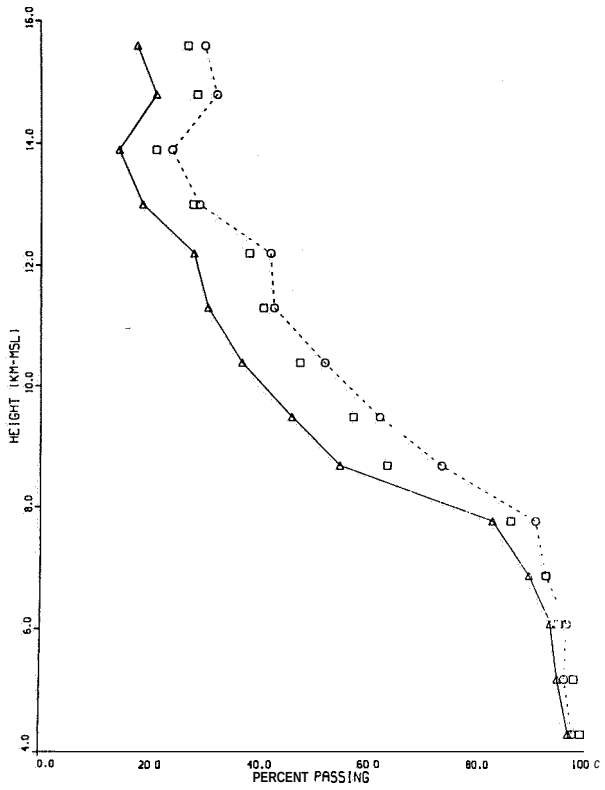

Figure 3–10. Same as Fig. 3–8 except the data are obtained with a 9-μs pulse and a largest consensus requirement of 8 of 12 profiles.

2.6 km is caused by traffic on a nearby interstate highway; moving clutter cannot be eliminated in the Doppler spectrum as readily as fixed clutter. The signal–to–noise ratio of the atmospheric scatter is higher at these lower altitudes than. it is at the upper heights where the winds are measured nearly all the time, but the clutter is strong enough to impair the ability of the radar to measure winds in the lowest 1.1 km AGL.

Figure 3–9 shows the 3 μs pulse data when the largest subset required is eight or more. Figure 3–10 shows the corresponding data for the 9 μs pulse mode. The increased height coverage with 9 μs pulses as compared with the height coverage with 3 μs pulses is much less pronounced for the UHF radar than for the VHF radar (Figs. 3–5 and 3–6). At the 60% passing level, the 9 μs pulse mode only increased the height coverage by about 1 km for the UHF radar. For the UHF radar the power–aperture product of the 9 μs mode is 6 dB greater than the 3 μs mode; however, for the VHF radars it is the same, so the height coverage difference for the two wavelengths is all the more dramatic. We believe the failure of the increased sensitivity of the 9 μs mode to increase the height coverage of the UHF radar is an indication that the inner scale of turbulence is less than half the radar wavelength (<16.5 cm) at 10 km MSL or below in at least some meteorological conditions. The 33 cm radar can measure winds to 14 km MSL in some cases, but its wavelength may be too short for routine tro-

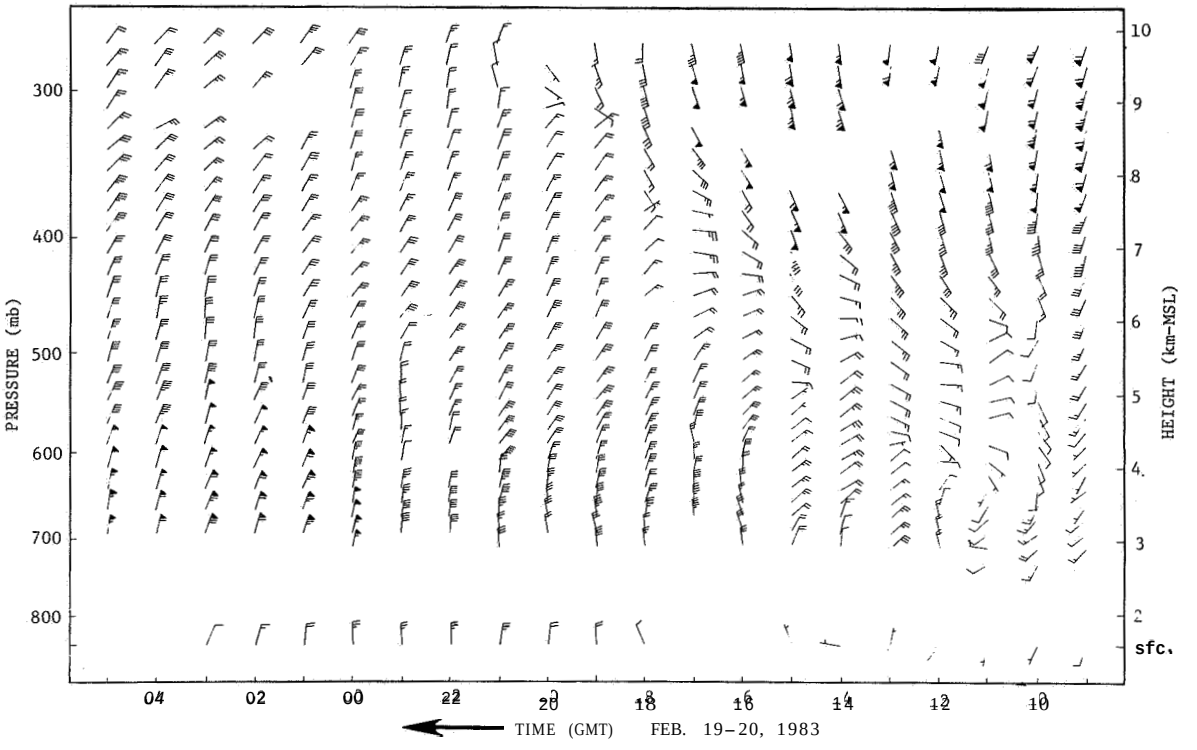

Figure 3–11. Data sample from the UHF radar at Denver–Stapleton. Measured data points were available every 30 min; hourly profiles are plotted. Likewise, the number of measured points in each profile is about twice the number plotted. At the time these data were acquired the minimum height of observation was about 1.1 km AGL; the radar is now able to measure winds starting at 350 m AGL.

pospheric coverage. Figure 3–11 illustrates the resolution of the UHF radar during a winter snowstorm.

F. UHF Radar Problems

Problems associated with using UHF radar for wind profiling:

1. The height coverage of the UHF radar may be limited more by the scattering mechanism than by sensitivity (power-aperture/noise temperature) considerations.

2. Clouds and precipitation detected from antenna sidelobes can he stronger than the refractive turbulence signal from the main lobe. Although this has no doubt occurred with our 33 cm radar, we do not have a procedure to identify when it happens.

Problems encountered that are related to our particular UHF hardware implementation:

1. A major airport is an extremely poor choice for a site for a sensitive clear-air radar. The ground clutter in the lowest 1.1 km height impairs our ability to measure winds close to the surface. The clutter power does not saturate the receiver or data system, so it would be much more tolerable if it were not caused partly by moving targets (automobiles, aircraft taxiing and flying).

2. The only component failures in a year of operation are the mechanical RF switches that select the antenna pointing direction. They have been replaced with another type of switch with a longer rated lifetime.

3. The maximum power-aperture product available is 8×10^4 W-m^2; the height coverage expected with this radar is less than expected with the VHF radars.

4. The UHF radar uses the same data processing as used with the VHF radars. However, the VHF radars require 5 or 6 s to acquire the time series of radar returns needed to calculate a 64 point Doppler velocity spectrum whereas the UHF radar acquires the same data in about 2/3 s. (The dwell time is proportional to the radar wavelength.) Therefore, software power spectral analysis does not represent a serious overhead time (about 1 s) for the W F radars, but it seriously reduces the incoherent integration time available for the UHF radar.

5. A zenith-pointing antenna position is included in the UHF radar because the scattering from hydrometeors can exceed that from refractive turbulence, and therefore a correction for particle fallspeeds must be made during precipitation. The correction has recently been implemented but has not been fully evaluated. The correction is made during clear air and precipitation. Hourly averaged vertical velocity measurements are combined with the hourly averaged horizontal wind measurements.

6. We have observed occasional interference from other transmitters. A request has been made to shift transmitted frequency to between 910 and 915 MHz to solve this problem.

G. Wind Measurements With Fixed-Beam Doppler Radar - Summary and Some Observations

The radar wind Profilers in the Colorado Network are fixed-pointing systems with two or three pointing directions. The two-beam systems have orthogonal viewing directions at 15° off-zenith; the three-beam systems also have a zenith-pointing position. The choice of elevation angle and the method of wind measurement is discussed by Strauch et al. (1984).

The meteorological assumptions needed to measure hourly averaged horizontal wind profiles with a two-beam system are that (1) the errors caused by vertical velocity will be negligible; and (2) the horizontal wind components, measured at separated volumes in space, are representative of the mean wind above the radar. Vertical velocity at the measurement volume causes an error in the measured horizontal wind component of w tan θ_e (m/s) where w is the vertical wind and θ_e is the elevation pointing

angle. For the Colorado radars we must assume $w < 0.25$ m/s for an hourly average if the error in the horizontal component is to be less than about 1 m/s. The representativeness assumption applies when the horizontal components are combined and presented as the vector wind above the radar location. The difference in the wind at the measurement volume and at the radar is (grad u_i)(h) cotan Θ_e where h is the measurement height and grad u_i is the mean gradient of the wind component in the direction that the component is translated. Gradients normal to the translation direction do not enter into the wind calculations; nevertheless, a tacit assumption of a locally uniform wind field underlies the two-beam measurement technique. It is important to note that vertical wind causes errors in the measured horizontal wind components. Horizontal gradients do not introduce an error in the horizontal wind component at the measurement location. In some applications the wind components would be assigned to their actual locations *so* there would be no error from horizontal gradients.

The meteorological assumptions needed to measure hourly averaged winds with a three-beam system are that horizontal gradients of w will cause negligible errors and that the wind components measured at separated volumes can be combined to form a vector wind. Horizontal wind accuracy of about 1 m/s requires that (grad w)(h) cotan Θ_e be less than 0.25 m/s. The assumption of a locally uniform wind field is unchanged with the addition of a third beam. Generally the third beam adds relatively little to the ability of the radar to measure hourly averaged horizontal winds. The zenith beam provides a direct measurement of w, and it measures the temporal scale of vertical fluctuations *so* it can indicate the temporal averaging period needed to reduce vertical motion contamination of horizontal measurements. The two-beam system will have significant errors in the measured horizontal components if the period of vertical velocity perturbations is long compared with the averaging time; the three-beam system allows a correction for this long-term vertical motion but only if the spatial wavelengths of w are large compared with the separation of the measurement volumes. Correction of the horizontal winds for vertical motion on a short-term basis (say every 2 min) without some knowledge of the spatial variations of w does not seem possible. The zenith beam is important at VHF for measuring the height of the tropopause (Gage and Green, 1982). At shorter wavelengths the vertical beam allows a correction for fallspeed of precipitation.

CHAPTER 4

ANALYSIS OF EXPECTED ACQUISITION COSTS (1984 DOLLARS) FOR WIND PROFILERS

A. Assumptions

This simple and relatively straightforward analysis of acquisition costs for a small number of wind Profilers is presented to help answer two questions: (1) What will be the approximate cost of a wind profiling radar to measure winds at a given height with a given resolution? (2) What are the frequency-cost tradeoffs?

The analysis shows that a VHF (50 MHz) type of wind Profiler designed to reach a given height will probably cost less than a 225 MHz or *400* MHz wind Profiler designed to reach the same height. A 50 MHz wind Profiler with a range of 20 km and coarse resolution will cost on the order of a quarter of a million dollars. A 50 MHz system with the same range capabilities but with high resolution (75 m) will probably cost nearly $1 million. This assumes that the necessary bandwidth is available and that there will be minimal interference. If, because of bandwidth and frequency allocation restrictions, the radar must operate at higher frequencies, the cost will more than double. The reader is cautioned that this analysis is only approximate and that numerous assumptions have been made. Results given in this chapter are best estimates and should be used only as preliminary guidance.

The assumptions that were used here are the following

1. The cost of a wind Profiler is determined by three items: antenna, power transmitter, and fixed costs such as computer, receiver, building, etc. The fixed costs are the same for all systems.

2. Only three possible frequency bands will be available, 50 MHz, 225 MHz, and *400* MHz.

3. A coaxial-colinear array antenna is used at 50 MHz and arrays of discrete Yagi-Uda antennas are used at 225 MHz and *400* MHz.

4. The transmitter uses high voltage vacuum tube amplification with forced-air cooling. The same type of transmitter is used in each frequency band.

5. The cost of land is zero, and no unique landscaping would be required.

6. Three beam systems are used. Significant averaging time (10 min) is used to derive a wind profile.

7. System integration costs are small compared with the cost of the major subsystems.

13. Cost Models

The cost of a wind Profiler is given by

$$C(pA) = C_T(p) + C_a(A) + C_f$$

where p is average power in watts, A is antenna aperture area in square meters, $C_T(p)$ is the cost of the power transmitter as a function of average power, $C_a(A)$ is the cost of the antenna as a function of the antenna area, and C_f are fixed costs independent of power or aperture area. The equation will he developed so that the power aperture product (pA) is the independent variable and average power (p) is a parameter.

Cost data for power transmitters in the *50–450* MHz band were obtained from a reputable and competitive manufacturer of electronic equipment. Table *4.1* gives the prices for various–sized pulsed *(10%* duty cycle) transmitters *(400* MHz) with high–power vacuum tubes and forced air cooling. Table *4.2* gives corrections to these prices for various frequency bands from *50* to *450* MHz. When the data in Table *4.1* are plotted on log–log paper, it becomes clear that a reasonable cost model for the power transmitter is

$$C_T(p) = C_o + K\, p^{C_1}$$

and straightforward algebra yields numerical values for the constants. A good approximation to the cost of a transmitter is given by

$$C_T(p) = (11 \times 10^3) + 56\ (p^{.9})$$

where p is average power in watts and the value of the equation is the cost in *1984* dollars. This cost is then scaled up or down as indicated by the frequency data in Table *4.2.*

Table *4.1.* Prices of *400* MHz power transmitters

Avg. power	.2KW	1KW	2.5KW	5KW	10KW
Cost	18K	37.5K	75K	128K	235K

Table *4.2.* Price corrections for different frequencies

Frequency	50 MHz	*200–425* MHz	450 MHz
Correction	*–10%*	0	+3%

The cost model for the antenna had to be developed separately at two different frequencies. At 200–400 MHz the antenna is assumed to be an N x N array of Yagi-Uda elements spaced d meters apart. The aperture area is given by $A = N^2 d^2$. If the cost of an element (with associated feed lines, switches, supports) is C_e then the cost model for the antenna is

$$C = N^2 C + K .$$

The Wave Propagation Laboratory has built such an antenna with two beams. The material and cost used in this 10 x 10 array are given in Table 4.3. So, the cost model (not including labor) for the WPL 400 MHz array is

$$C_a = 390 N^2 + 6000 .$$

Adding the capability for a vertical beam would add about $40 to the cost of an element.

The one company that has this type of antenna as a catalog item will deliver an 8 x 8 array of Yagi–Uda antennas with all of the associated cables, switches, etc., for $48.2K. The element cost less the site preparation then becomes $753. If we assume site preparation expenses of $8K, the cost of a 200–400 MHz array with N elements on a side spaced d meters apart is given by

$$C_a(A) = 753 N^2 + (8 \times 10^3) .$$

Noting that $A = N^2 d^2$, we obtain

$$C_a(A) = 753 A/d^2 + (8 \times 10^3) .$$

The antenna technology discussed above (Yagi–Uda antennas) is well-known and has been widely used at 400, 225, and 50 MHz. Another antenna technology, called coaxial–colinear (co–co) arrays, has found wide use at 50 MHz.

Table 4.3. Costs of materials used in WPL 400 MHz array

Quantity	Item	cost
100	Yagi–Uda antenna	$12K
100	feed cables	10K
50	transfer switches	9K
1	1:100 splitter	5K
	metal frame	3K
1	box	5K
1	switch driver	1K

Two things (other than the cost of land) determine the cost of co-co arrays. These are the length of the radiating elements and the length of the feed lines. So, the cost model depends on the area of the array and the linear dimension. If S is the length of one side of the array, a good cost model is

$$C_a = K_1 S + K_2 S^2 .$$

A 50 m × 50 m 50 MHz co-co antenna with beam switching costs $35K whereas a 100 m x 100 m version costs $87K. Both of these are three-beam systems that can measure vertical-and horizontal winds. Again it is easy to use this cost information to determine the coefficients in the cost model. The resulting equation is

$$C_a(A) = 3.4A + 530 \sqrt{A}$$

where A is the aperture area equal to S^2. There are significant questions as to whether coaxial-colinear arrays will work properly at higher frequencies so here we have used a proven technology at the higher frequencies.

The fixed costs (independent of power-aperture product) are listed in Table 4.4. These figures are the fixed costs for a WPL wind profiler similar to the five that have been built.

By combining the fixed cost with antenna cost and transmitter cost we can obtain expressions for the total cost of wind Profilers. At 50 MHz the cost is given by

$$C(pA) = \frac{3.4\ pA}{p} + \frac{530\ \sqrt{pA}}{\sqrt{p}} + 50.4\ p^{0.9} + 55000 .$$

For the frequency range of 200-400 MHz the cost is given by

$$C(pA) = \frac{753\ pA}{d^2 \lambda^2 p} + 56\ p^{0.9} + 64000 .$$

Table 4.4. Fixed costs of wind profiler

Item	cost
receiver	$ 8K
radar controller	12K
computer	17K
building	8K
Total	$45K

C. Cost Comparisons

The cost equations for three different frequencies are plotted against power-aperture product, with average power as a parameter, in Fig. 4–1. The power-aperture product of clear air radars generally varies over several orders of magnitude, and so the axes in Fig. 4–1 are scaled logarithmically. The parts of the lines that run horizontally are regions where the transmitter is too costly. The regions of diagonal lines are where the antenna is too costly. The curved lines are where approximately equal resources have been put into both the antenna and the transmitter, resulting in the best use of those resources. The line of economically optimum antenna and transmitter size for a given power-aperture product can be found by making plots similar to those in Fig. 4–1 except with smaller steps between parametric variables. Figure 4–2 is similar to Fig. 4–1 except the increment from one power curve to the next in Fig. 4–2 is a factor of 2. Clearly in Fig. 4–2 a minimum cost curve as a function of power-aperture product is defined.

If the sensitivity of the radar were proportional to only the power-aperture product it would be a simple matter to compare the minimum costs of the three frequencies in Fig. 4-2. However the relative sensitivity is also determined by the background noise, which in this case is galactic noise. Table 4.5 gives the relative noise temperatures of the galactic noise for the three frequencies. The noise temperature is a "fictitious" temperature directly proportional to the noise power. It is not difficult to make radar receivers at these frequencies with effective noise temperatures of 150 K, but a low noise receiver is of no value at 50 MHz because of the large galactic noise at that frequency. The galactic noise is also an important contribution at 200 MHz but is practically negligible at 400 MHz. The practical effect of this is that a 50 MHz wind Profiler has to be larger, i.e., have a larger power-aperture product, to achieve the same sensitivity as a 225 or 400 MHz wind Profiler. To quantify this, assume a receiver noise temperature of 150 K for each of the three frequencies and the average of the galactic noise temperatures in Table 4.5 as the external noise temperature. Then the 50 MHz radar will require 13 dB more power-aperture product than a 225 MHz radar to have the same sensitivity. Also a 50 MHz radar will need 17 dB more power-aperture product to have the same sensitivity as a 400 MHz radar.

The relative costs between different radars at different frequencies can be seen in Figs. 4–3 and 4–4. Some care is necessary in interpreting these figures. Figure 4–3 shows the cost as a function of power-aperture product for a 400 MHz wind Profiler. For comparison, 50 and 225 MHz radar cost curves that have been moved to the right, i.e., increased power-aperture product, by 17 dB and 4 dB respectively are shown. Note that the power-aperture product axis relates to the 400 MHz radar and not to the 50 or 225 MHz radar, even though the three radars will have approximately the same sensitivity to inertial subrange turbulence. It is clear that the 50 MHz radar has a cost advantage mainly because of the type of antenna used in it. Consequently, for large wind Profilers the 400 MHz radar will cost approximately twice as much as a 50 MHz radar.

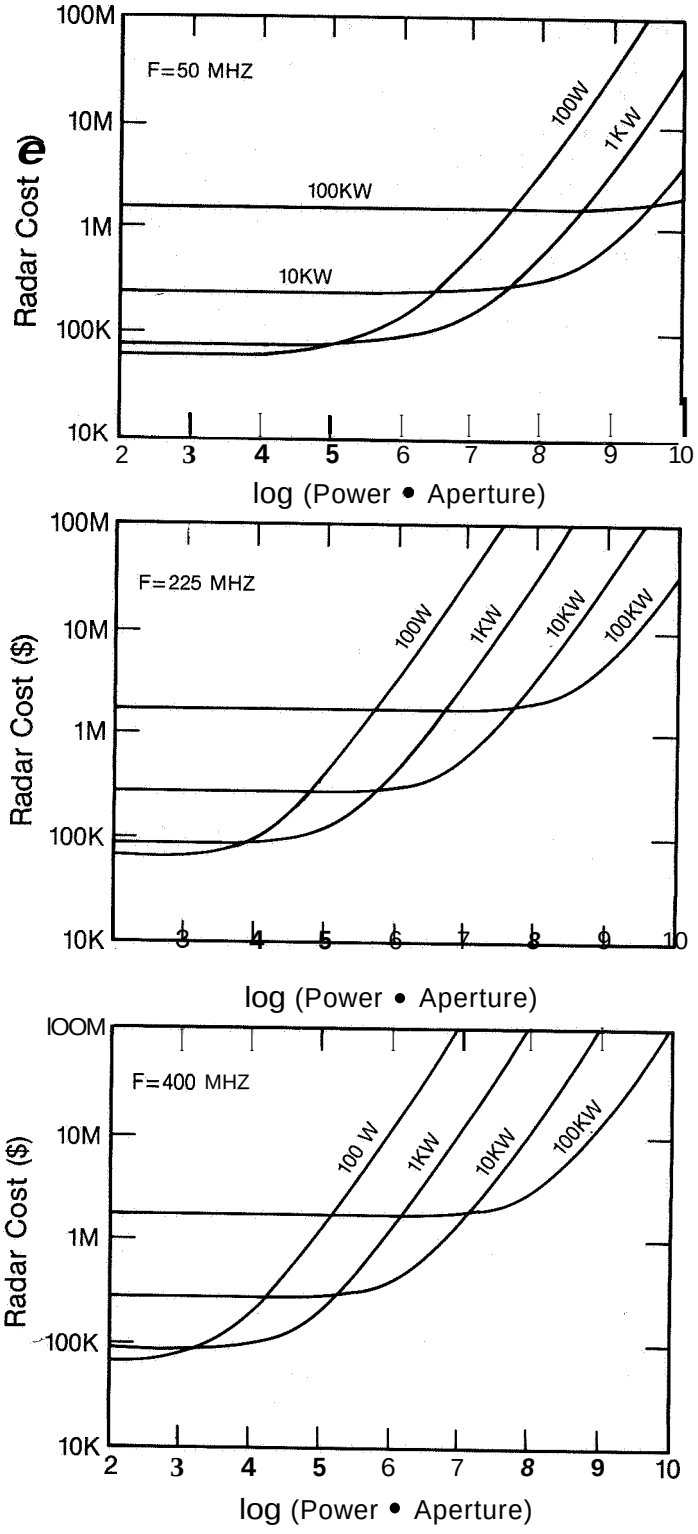

Figure 4-1a,b,c. Costs of radar wind profilers (a) 50 MHz; (b) 225 MHz; (c) 400 MHz.

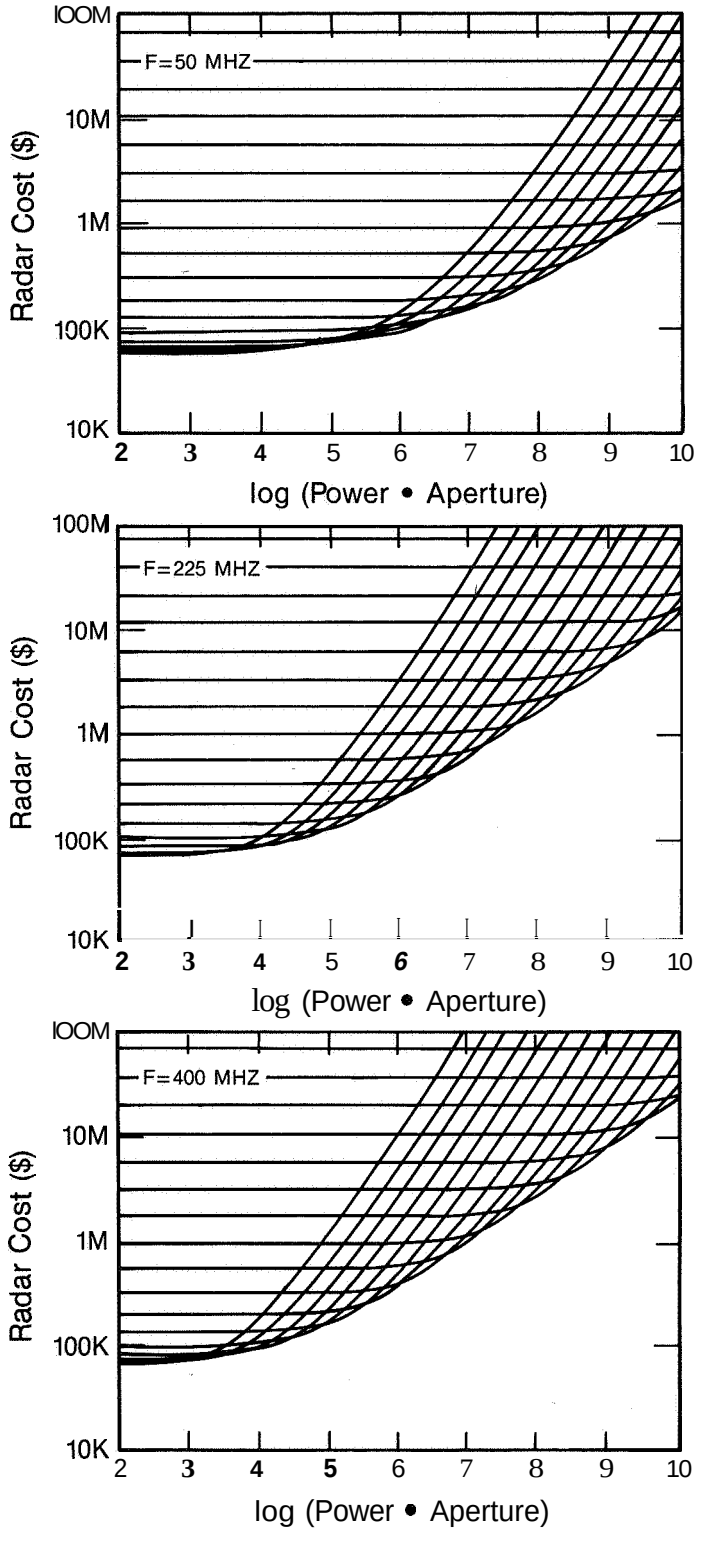

Figure *4-2.* Graphical determination of minimum radar ***cost*** for given power aperture product, (a) *50* MHz; (b) *225* MHz; *(c) 40Q* MHz.

Table 4.5. Galactic noise temperatures (K)

Freq.	Galactic center	Galactic pole	Avg.
50	20,000'	4,000'	12,000'
200	800°	100°	450°
400	120'	20"	70°

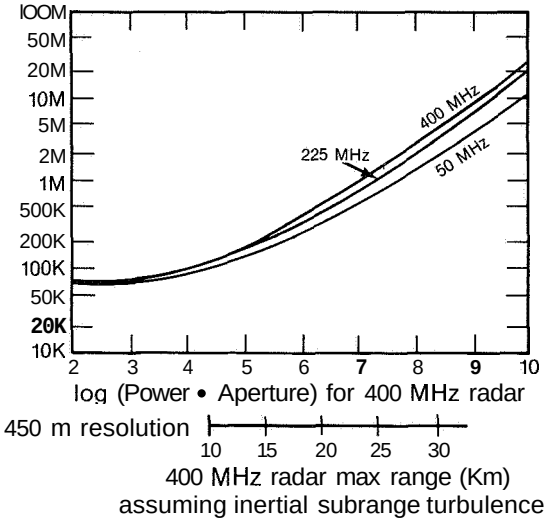

Figure 4-3. Cost of a 400 MHz wind profiler for a given power-aperture product. Also shown are costs for 225 and 50 MHz radars that will have similar height capability. The lower axis shows the maximum height for which wind measurements on 450 m resolution can be reliable made.

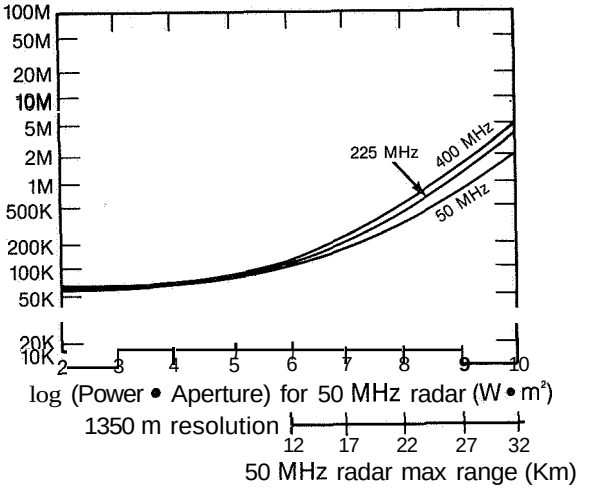

Figure 4-4. Cost of a 50 MHz wind profiler for a given power-aprture product. Also shown are costs for 225 and 400 MHz radars that will have similar height capability. The lower axis shows the maximum height for which wind measurements on 1350 m resolution can be reliably made.

Also shown on Fig. 4-3 is a maximum range scale for 400 MHz radar. This is based on limited experience in determining the maximum height to which winds can be measured with the WPL 400 MHz wind Profiler. During June and July of 1984 this system was able to reliably measure winds to 10 km with a reduced power-aperture product of 20×10^3 W-m^2. If we assume that the scattered power falls off at a rate of 2 dB/km as indicated by Nastrom, et al. (1981), then we can attach a maximum range scale as in Fig. 4-3. The assumption here is that the half-wavelength scale size turbulence is in the inertial subrange, but the altitude to which this assumption is valid is not known. Some experimental evidence suggests that at 25 km altitude the eddies reponsible for 400 MHz scattering are into the viscous cut-off region.

Figure 4-4 is a similar graph except the 50 MHz radar cost characteristic applies to the scale on the horizontal axis and the 225 and 400 MHz cost characteristics are moved to the right by 13 dB and 17 dB of power-aperture. Again we see that the 50 MHz wind Profiler has a cost advantage. The maximum range axis in this figure is derived from the WPL experience with 50 MHz wind Profilers. This experience shows that reliable wind measurements to 12 km are possible with a power-aperture product of 10^6 W-m^2. Applying the same assumption as before, i.e., the scattering falls off at 2 dB/km, we are able to show a maximum range scale in Fig. 4-4. In Fig. 4-4 there is no problem with viscous cut-off because of the long wavelengths used.

The maximum range scales in Figs. 4-3 and 4-4 assume a range resolution of 450 m and 1350 m respectively. To change to another range resolution simply requires that the power-aperture product be adjusted by the appropriate amount. For example, changing to a range resolution of 45 m requires that the power-aperture product be increased by a factor of 10 or one unit on the horizontal scale. On Fig. 4-3 we see that a 400 MHz radar to measure to 20 km with 450 m resolution would cost approximately $500K whereas if the resolution requirement were increased to 45 m, the cost would increase to approximately $1.5M.

Figure 4-3 and 4-4 do not agree on the maximum range even though both are assumed to he governed by inertial subrange turbulence and the scattering is assumed to fall off as 2 dB/km in both cases. The reason for this is that the assumptions of reliable range of wind measurement capability for 50 MHz and 400 MHz are necessarily based on limited operation time and subjective definitions of reliablity. For equal costs the maximum ranges from the two figures differ by about 2 km, so the error associated with the technique will not be less than this.

Reasonable "first guesses" for the cost of a particular radar to reach a certain height with a certain range resolution can be obtained from Figs. 4-3 and 4-4. A few general conclusions can be drawn after examining these figures:

1. It will be ~~very~~ expensive to measure to heights of 30 km with resolutions approaching that of a Jimsphere system. A system that reliably measures to 30 km with 25 m resolution would probably cost on the order of $15M. The system would probably need to be a 225 MHz radar because the 400 MHz radar would be limited by the viscous cutoff problem, and the required bandwidth for such high resolution would not be available at 50 MHz.

2. For the systems considered here, an increase in height coverage by 5 km, or an improvement in resolution of a factor of 10, would increase the cost of a large radar by a factor of about 4.

3. The 50 MHz system is cheaper because of the less expensive antennas. Because the co-co arrays are relatively inexpensive this technology should be considered for use at higher frequencies. It is unlikely that co-co technology is applicable at 400 MHz, but it may work at 225 MHz. If so the 225 MHz cost curves in Figs. 4-3 and 4-4 would move away from the

400 MHz curve and move closer to the 50 MHz curve. Rut, it seems unlikely they would ever go below the 50 MHz cost curve.

4. For altitudes below about 6 km the cost of one of these types of radars is relatively constant and is somewhere between $50K and $100K. This suggests that one should look very carefully at requirements. For example, if high resolution is required only at lower heights, the resolution requirement does not impose high costs; however, if high resolution is required at all altitudes of interest, it does impose high costs.

One final word of caution on using these results. The costs given here are €or acquisition costs of major subsystems (transmitter, antenna, computer, receiver) and the integration costs are assumed small with respect to these acquisition costs. However, this may not be a valid assumption for all contractors. It may be desirable to increase the costs given here by a applicable percentage to account for integration costs.

REFERENCES

Batten, L. J., 1973: Radar observations of the atmosphere. Univ. of Chicago Press, Chicago, Illinois.

Carter, D. A., 1982. Private communication. Aeronomy Laboratory, NOAA.

Doviak, R. J., and D. Zrnic, 1978. The weather radar equation--receiver bandwidth considerations. Preprints 18th Conf. on Radar Meteorol., Atlanta, Georgia, March 28–31, 484–489.

Fischler, M. A, and R. C. Bolles, 1981. Random sample consensus: a paradigm for model fitting with applications to image analysis and automated cartography. Commun. Assoc. Comput. Mach., 24:381–395.

Frisch, A. A., and S. F. Clifford, 1974. A study of convection capped by a stable layer using Doppler radar and acoustic echo sounders. J. Atmos. Sei., 31:1622–1628.

Gage, K. S., and J. L. Green, 1982. An objective method for determination of tropopause height from VHF radar observations. J. Appl. Meteorol., 21:1159–1163.

Gossard, E. E., W. D. Neff, R. J. Zamora, and J. E. Gaynor, 1984. Fine-structure of atmospheric refractive layers and implications for over-the-horizon propagation and radar sounding systems. Preprints, 22nd Conf. on Radar Meteorol., Zurich, Switzerland, September 10–13, 461–469.

Johnson, D. L., and W. W. Vaughan, 1978. Sequential high-resolution wind profile measurements. NASA Technical Paper 1354, December 1978.

Hildebrand, P. H., and R. S. Sekhon, 1974. Objective determination of the noise level in Doppler spectra. J. Appl. Meteorol., 13:808–811.

Hill, R. J., 1978. Spectra of fluctuations in refractivity, temperature, humidity, and the temperature-humidity cospectrum in the inertial and dissipation ranges. Radio Sci. 6:953–961.

Hogg, D. C., and W. W. Mumford, 1960. The effective noise temperature of the sky. Microwave Journal 3:80–84.

Labitt, M., 1981. Coordinated radar and aircraft observations of turbulence. Project Report ATC 108, MIT Lincoln Laboratory, 39 pp.

Nastrom, G. D., B. B. Balsley, and K. S. Gage, 1981. Changes with season of C_n^2 at Poker Flat, Alaska, from MST Doppler radar observations. Proc. 28th Conf. on Radar Meteorology, American Meteorological Society, Boston, Mass.

Nathanson, F. E., 1969. Radar Design Principles. McGraw Hill, New York, 626 pp.

Schmidt, G., R. Rüster and P. Dzechowsky, 1979. Complementary code and digital filtering for detection of weak VHF radar signals from the mesosphere. IEEE Trans. Geosci. Elec., GE-17, 154-161.

Strauch, R. G., 1976. Theory and application of the FM-CW Doppler radar. Ph.D. Thesis, University of Colorado.

Strauch, R. G., D. A. Merritt, K. P. Moran, K. B. Earnshaw, and D. van de Kamp, 1984. The Colorado Wind - Profiling Network. J. Oceanic Atmos. Technol., in press.

Whalen, A. D., 1971. Detection of Signals in Noise. Academic Press, New York, 411 pp.

APPENDIX A.

A TRANSCEIVER MODULE OF THE MU RADAR

S. Kato, T. Ogawa, T. Tsuda, and T. Sato

Radio Atmospheric Science Center, Kyoto University,
Gokanosho, Uji 611, Japan

and

I. Kimura, and S. Fukao
Department of Electrical Engineering, Kyoto University, Sakyo-ku,
Kyoto 606, Japan

A Japanese group working on radar remote sensing has been constructing the MU (Middle and Upper Atmosphere) radar since 1981, which is a pulse-modulated monostatic Doppler radar operating at 46.5 MHz with a bandwidth of 1.65 MHz. It is situated at 34.85°N and 136.13°E, where the L value is 1.208 and the dip angle of the local magnetic field is 42.38°. The general design concept of the MU radar was studied by Fukao et al. (1980), although several modifications were carried out in accordance with recent investigations. An updated block diagram is shown in Fig. A-1. One of the main characteristics is that the MU radar adopts an active array system in which each antenna is connected to a solid-state transceiver module (TR module).

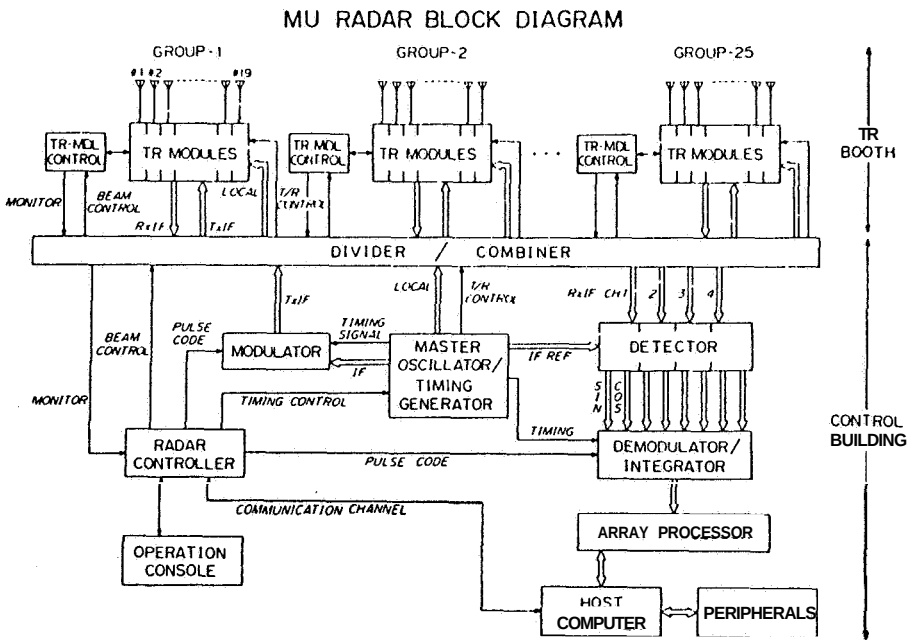

Figure A-1. A block diagram of the MU radar.

The MU radar will attain a peak power of 1 MW with a duty factor of 0.05 by using 475 TR modules so as to observe three components of wind velocity in the altitude range 2–300 km with good height resolution. However, only 57 TR modules (3/25 of the whole system) have been installed up to now, so that the present peak transmitting power is 120 kW. In this report, we describe a block diagram of the TR module and a preliminary result of the power amplifier which is the main part of the TR module.

The TR module used in the MU radar is mainly composed of two units: a mixer (MIX unit) and a power amplifier (PA unit) whose block diagrams are shown in Fig. A–2a and b, respectively. The former generates the RF wave for transmission and converts the received echo to the IF signal. An arrow in the figure indicates a control signal from the radar controller. A 41.5-MHz local signal fed to mixers passes through a digitally controlled 8–bit phase shifter which can change its value up to 1,000 times in a second, so that the MU radar has the ability to steer its antenna direction quickly and flexihly. The MIX unit also contains a buffer amplifier and a gate for the transmitting signal and preamplifier for the received one whose noise figure is less than 5 dB.

The PA unit amplifies the RF signal supplied from the MIX unit up to 63.7 dBm (2350 W), and feeds it to the crossed Yagi antenna. The younger stage amplifier operates in A–class and gains 39.5 dB, while the final stage one is composed of four push–pull amplifiers whose gain is 12 dB. A TR switch attains an isolation of 100 dB between TX and RX signals by using high power PIN diodes. A band–pass–filter is inserted after the TR–switch and prevents unnecessary harmonics from transmitting. Phase and intensity of the transmitting signal and the value of VSWR are monitored by using a directional coupler. The output circuit can give linear, right and left circular polarizations. Signal level at three points and gain of both driver and final amplifers are shown in Fig. A–2b. An over–all gain of the PA unit is about 50 dB.

Figure A–3 shows input output characteristics of the PA unit. The output increases linearly up to 2350 W for the input signal in the range from 5 to 13 dBm, and saturates because of an action of the APC (automatic power control). Considering loss in connecting cables to the antenna, the final radiation power will become 2050 W.

The TR module of the MU radar is manufactured by the Communication Equipment Works of Mitsubishi Electric Co.

REFERENCE

Fukao, S., S. Kato, T. Aso, M. Sasada, and T. Mikihira 1980. Radio Sci., 15: 225–231.

a)

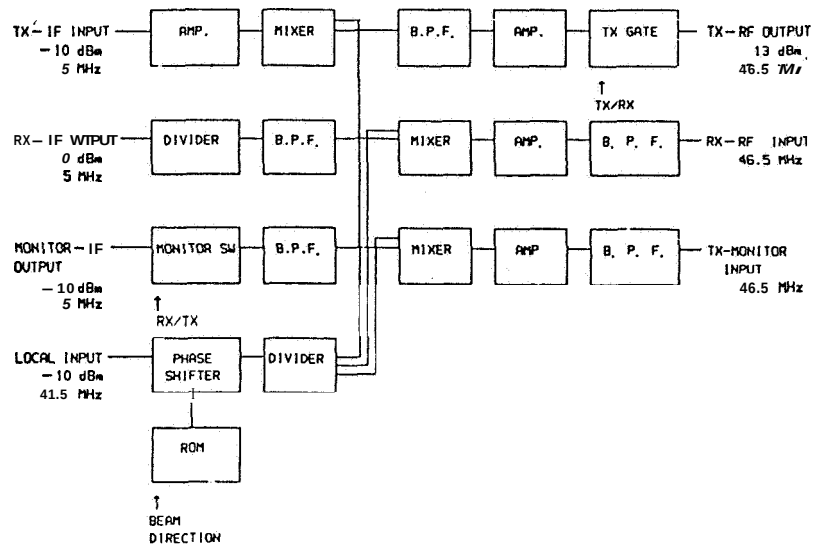

Figure A-2(a). Block diagram of the MIX unit of the transceiver module used in the MU radar.

b)

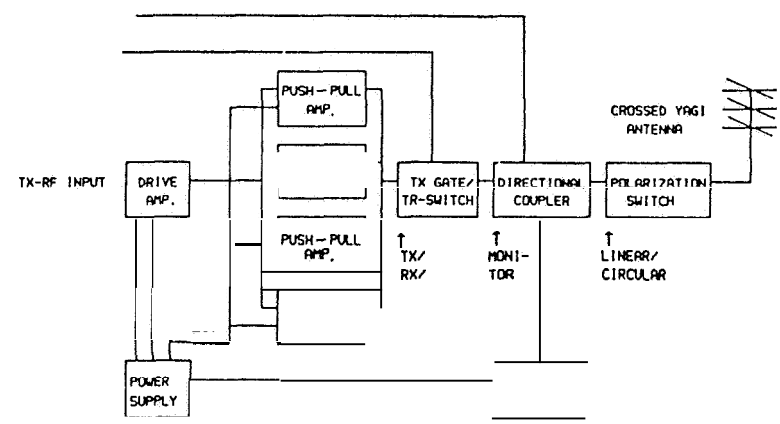

SIGNAL LEVEL	13 dBm		52.5 dBm			63.7 dBm (2350 W)
GAIN	-	39.5 dB	-	12 dB	- 0.6 dB	

Figure A-2(b). Block diagram of the PA unit of the transceiver module used in the MU radar.

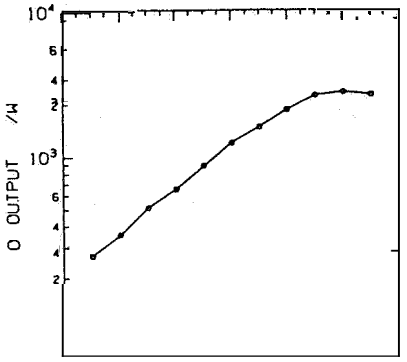

Figure A-3. Input/output characteristics of the PA unit.

APPENDIX B.

PULSE COMPRESSION USING BINARY PHASE CODES

D. T. Farley
School of Electrical Engineering
Cornell University
Ithaca, NY 14853

INTRODUCTION

In most MST applications pulsed radars are peak power limited and have excess average power capacity. Short pulses are required for good range resolution, but the problem of range ambiguity (signals received simultaneously from more than one altitude) sets a minimum limit on the interpulse period (IPP). Pulse compression is a technique which allows more of the transmitter average power capacity to be used without sacrificing range resolution. As the name implies, a pulse of power P and duration T is in a certain sense converted into one of power nP and duration T/n. In the frequency domain, compression involves manipulating the phases of the different frequency components of the pulse. A short pulse consists of contributions from a wide band of frequencies, all of which are in phase at one point in space-time. Changing the phase relations on transmission lengthens the pulse, but it can be reassembled into a short pulse upon reception by proper processing if the phases have not been perturbed in some unknown way in the meantime (i.e., by the scattering process). This is essentially the idea behind frequency 'chirping'.

Another way to compress a pulse is via phase coding, especially binary phase coding, a technique which is particularly amenable to digital processing techniques. This method has been used extensively in recent years in radar probing of the atmosphere and ionosphere, and it is the method we will discuss here. The general topic of pulse compression is dealt with in Cook and Bernfeld (1967), Barton (1975), Brookner (1977), and other texts.

BARKER CODES

A class of codes known as Barker codes (Barker, 1953) has been used extensively in ionospheric incoherent-scatter measurements. The Barker coded pulse is considered to be made up of n 'bauds', each of duration T, so the total duration is nT, with the maximum value of n being 13. The phase of each baud is 0 or 180 degrees (±1), in a sequence that depends on n. The pulse is decoded upon reception by passing it through a 'filter' whose impulse response is the reverse in time of the transmitted pulse (the pulse 'played backwards', so to speak). Such a filter is said to be 'matched' to the pulse. In practice these matched filters are usually specially designed acoustic surface wave devices or conventional filters plus digitizers, digital delay lines, and some add/subtract circuitry or equivalent software.

From another point of view, the decoding process consists of cross-correlating the received signal with a replica of the transmitted pulse; hence, when an undistorted coded pulse is passed through such a decoder, the output is the autocorrelation function (ACF) of the pulse. As an example, the phase coding sequence and the ACF of a 5-baud Barker coded pulse are listed below.

```
+ + + - +
. . . 0 0 0 1 0 1 0 5 0 1 0 1 0 0 0 . . .
```

If the compression process were perfect, only the 5 would be present in the above ACF; the 1s represent undersired range 'sidelobes'. In Barker codes (n up to 13) the sidelobes are always unity and in the pattern above, and the central peak is n. For ionospheric applications the sidelobes are generally not a problem since, for n equal 13, say, the power corresponding to the central peak is 169 times greater than that in each of the 12 sidelobes. (Note that the signal-to-noise ratio in the central peak is increased by the compression by a factor of 13, not 169, since the noise is the sum of 13 independent samples.)

The above discussion is valid for scatter probing of the atmosphere as long as the correlation time of the scattering medium is long compared to the total (uncompressed) duration of the coded pulse. In practice this is always the case for MST applications but may not be true for incoherent scatter from the ionosphere, for example. Detailed calculations of what happens in the latter case are given by Gray 'and Farley (1973), and a general discussion of the 'ambiguity function' of a Barker coded pulse as a function of target-induced Doppler shift is given in Cook and Bernfeld (1967). Gray and Farley also discuss the use of multiple coded pulse sequences in the measurement of the ACF of the scattering medium. The effect of the coding is usually minimal; in typical situations the 'true' ACF is convolved with a function whose width is about one baud. Finally, although 13 bauds is the longest possible Barker sequence (unity sidelobes), there are many longer sequences with sidelobes that are only slightly larger. As an example, a 28-baud sequence with a maximum sidelobe level in the ACF of 2 is listed by Gray and Farley and has been used by Woodman et al. (1980) for observations with the **SOUSY** radar.

COMPLEMENTARY CODE PAIRS

The codes discussed above have range sidelobes which are small, but which may still cause problems in MST applications. Ideally we wish to use high compression ratios (long codes) to get the best possible altitude resolution, but if we do so the 'wanted' signal from an altitude in the upper stratosphere, say, may be contaminated by range sidelobe returns from lower altitudes, since the scattered signal strength is a strong function of altitude, typically decreasing by 2-3 dB per kilometer. This problem can be completely eliminated, at least in principle, by the use of a special class of binary phase codes known as complementary codes.

The existence of complementary codes was first pointed out by Golay (1961) and has been mentioned in the radar literature (e.g., Rabiner and

Gold, 1975), but the severe restriction on their use--phase changes introduced by the target must vary only on a time scale much longer than the interpulse period (IPP)--have prevented them from being utilized much in practice. The Doppler shifts encountered in military applications and in incoherent scatter from the ionosphere are much too large, for example, but the very small Doppler shifts associated with MST radar observations are entirely compatible with the use of such codes. The medium correlation time is typically tens or hundreds of times longer than the IPP.

Complementary codes are again binary phase codes and they come in pairs. They are decoded exactly as are Barker codes, by a 'matched' filter/delay line combination whose impulse response is the time reverse of the pulse. The range sidelobes of the resulting ACF output will generally be larger than for a Barker code of comparable length, but the two pulses in the complementary pair have the property that their sidelobes are equal in magnitude but opposite in sign, so that when the outputs are added the sidelobes exactly cancel, leaving only the central peak; i.e., the compression is perfect. As the simplest possible example, consider the 2-baud complementary pair below

Code:	+ +	(first pulse)
	+ −	(second pulse)
ACP:	0 +1 +2 +1 0	(first pulse)
	0 −1 +2 −1 0	(second pulse)
	0 0 +4 0 0	(sum)

Representing the above pair as (A, B) it is easy to show that the sequence (AB, $A\bar{B}$), where $\bar{B}$ is the complement of B, is also a complementary pair that is twice as long. Proceeding in this way one can obviously generate long n-baud code pairs, where n is any power of two. It turns out that n can also be ten, or ten times any power of two. Further properties of these sequencies are given by Golay (1961). In the first reported MST studies using these codes at SOUSY (Schmidt et al., 1979) and Arecibo (Woodman, 1980) n was 32 and the baud lengths were 2 μs and 1 μs, respectively (300 m and 150 m resolution).

There are two practical limitations on the maximum value of the compression rate n: (1) as n increases the effect of ground clutter extends to higher and higher altitudes; (2) the computing requirements for decoding increase with n. The first is the most serious limitation; the computing requirements can usually be handled one way or another. One process that often simplifies the computing is coherent integration (summing N successive voltage samples from a given altitude before doing any other processing). Since coherent integration and decoding linear operations they can be interchanged; e.g., samples from 100 pulses, say, can be coherently integrated and then decoded all at once. In dealing with the first limitation one must achieve some compromise between three competing goals: (1) the desire to confine strong ground clutter effects to the lowest possible range of altitudes (i.e., use short pulses); (2) the desire to avoid range ambiguity (use a long IPP); and (3) the desire to use the full average power capabilities of the transmitter to achieve maximum sensitivity.

MORE COMPLEX COMPLEMENTARY CODING SCHEMES

More complicated schemes can partly alleviate the ground clutter/range ambiguity problem. The cross correlation function (XCF) of the basic complementary transmitted sequency A, B, A, B, ... with the decoding function A, B is periodic with a period 2T, where T is the interpulse period (between A and B), but there are also substantial non-zero values of the XCF in the vicinity of T. For example, for the 4-baud pair (+++-, ++-+) the XCF is

... 0008000 ... 0040400 ... 0008000 ...

At delays near T from the 'wanted' return, in other words, the range sidelobes of the individual pulses add rather than cancel, whereas the main peak does cancel. The 4 s in the above represent the most important source of range ambiguity. These can be eliminated by transmitting the more complex sequence A, B, A, B, A, B, A, $\bar{B}$, ... and decoding by cross correlating with A, $\bar{B}$, A, $\bar{B}$. XCF for this scheme consists of single identical spikes at intervals of 2T; i.e., the first range sidelobes is pushed out to twice the interpulse spacing. By extending this idea the first sidelobe can be pushed out to even higher multiples of T. In this way a substantial range of altitudes could be probed at a very high pulse repetition frequency (PRF). In actual practice, though, some altitudes would be lost because of the necessity of blanking the receiver during actual pulse transmission and because of receiver saturation by ground clutter. Gonzales and Woodman (1981) used such a scheme for HF partial-reflection studies of the mesosphere at Arecibo.

QUASI-COMPLEMENTARY CODE SETS

The results presented so far have all been based on the assumption that the transmitted pulses were perfectly coded. In practice of course this won't be true; the phase shifts will require a finite amount of time and will not be exactly 180 degrees, etc. As a result, the range sidelobes for the complementary code pairs will not cancel exactly; the location of the sidelobes will depend on what sort of error is made by the transmitter. Sulzer and Woodman (unpublished manuscript, 1982) have developed a technique to minimize this problem. Rather than transmit just a pair of complementary 32-baud codes, they transmit a sequence of 48 different 32-baud pulses. Each is decoded individually and the results are combined coherently, so in a sense the whole sequence can be considered to be a single code. But from another point of view we can think of the sequence as 24 quasi-complementary pairs, each with a different set of small range sidelobes, due partly to errors in transmission and partly to the fact that the pairs are not perfectly complementary. Because the sidelobes produced by the individual pairs have a more or less random distribution, the resultant sidelobes of the entire sequence are lower and more uniform than those of a single (imperfect) complementary pair. This is no accident of course; the codes were chosen by an extensive computer search requiring about 350 hours (!) using a Harris computer and an FPS

AP120B array processor. The major disadvantage of this technique is that no coherent integration before decoding is possible; at present only the Arecibo Observatory has the digital preprocessing equipment required for the extensive high-speed decoding.

A similar idea has been developed by the same authors for mesospheric observations at Arecibo. To achieve the desired resolution of 600 m (4 μs) and fully utilize the transmitter, one would ideally use a 52-baud Barker code, which unfortunately does not exist. A good approximation to this can be achieved by a pseudo-random sequence of pseudo-random 52-baud codes found by a 10 hour computer/array processor search.

CYCLIC CODES

These codes (also called maximal length sequences) are a well-known class of periodic code which repeats at intervals of $N=2^n-1$ bauds and can be generated by an n-bit shift register. The ACFs of such sequences have periodic peaks of amplitude N at intervals of N times the baud length but are unity everywhere else. Hence if the periodic major range sidelobes cause no range ambiguity problems, very high compression ratios can be achieved. These codes are used widely in radar astronomy, since the interval between sidelobes can be made larger than the target size and ground clutter is unimportant. In MST work, however, such codes are useful only for bistatic radar systems.

REFERENCES

Barker, R. H., 1953. Group synchronizing of binary digital systems, in Communications Theory, W. Jackson (ed.), 273-287, Academic Press, New York.

Barton, D. K. (ed.), 1975. Radars, Vol. 3, Pulse Compression, Artech House.

Brookner, E. (ed.), 1977. Radar Technology, Artech House. (See especially chapter 8 by C. E. Cook.)

Cook, C. E., and M. Bernfeld, 1967. Radar Signals: An Introduction to Theory and Applications, Academic Press, New York.

Golay, M. J. E., 1961. Complementary series, IRE Trans. Info. Theory, IT-7, 82-87.

Gonzales, C. A., and R. F. Woodman, 1981. A high power HF radar for probing the mesosphere (abstract), URSI General Assembly, Washington, D.C.

Gray, R. W., and D. T. Farley, 1973. Theory of incoherent-scatter measurements using compressed pulses. RadioSci., 8:123-131.

Rabiner, L. R., and B. Gold, 1975. Theory and Application of Digital Signal Processing. Prentice-Hall.

Schmidt, G., R. Ruster, and P. Czechowsky, 1979. Complementary code and digital filtering for detection of weak VHF radar signals from the mesosphere. IEEE Trans. Geosci. Electron., GE-17:154-161.

Woodman, R. F., 1980. High-altitude resolution stratospheric measurements with the Arecibo 430-MHz radar. Radio Sci., 15:417-422.

Woodman, R. F., R. P. Kugel, and J. Rottger, 1980. A coherent integrator-decoder preprocessor for the SOUSY-VHF radar. Radio Sci., 15:233-242.

APPENDIX C.

ELIMINATION OF RANGE-ALIASED ECHOES IN VHF RADARS

R. G. Strauch
NOAA/ERL/Wave Propagation Laboratory
Boulder, Colorado 80303

Very High Frequency (VHF) radars designed to measure tropospheric wind profiles usually detect scattering to a maximum height of about 20 km. If the antenna elevation angle is 45 degrees or more above the horizon, the maximum range of interest is less than 30 km. A VHF pulsed Doppler radar wind Profiler can, therefore, be operated at high pulse repetition rates (~5 kHz). The maximum bandwidth allowed (by frequency allocation or by the antenna) is about 0.5 MHz (at most) so a radar with uncoded pulses can operate with a duty cycle of 1 to 10%, depending on the desired height resolution. This is approximately the duty cycle allowed in many transmitters. Therefore it is often possible to operate a tropospheric wind Profiler that utilizes all the average power available from the transmitter without the complexity of coded pulses. However, the VHF radar can detect echoes from the mesosphere on occasion and, with high pulse repetition rates, these echoes will occur at the same apparent range as the tropospheric echoes of interest. These mesospheric echoes may, at times, be stronger than the tropospheric signals. The range-aliased mesospheric echoes can be greatly attenuated or effectively eliminated as described below.

First, suppose that the phase of the transmitted pulse varies randomly from pulse to pulse. This random phase occurs if the transmitter uses a pulsed oscillator instead of a pulsed amplifier, as in a microwave radar with a magnetron (oscillator) transmitter. If the transmitter uses an amplifier the phase can be varied from pulse-to-pulse by introducing a phase shift on a low-level reference oscillator just prior to each transmitted pulse. The phase of the reference oscillator is kept constant while all echoes from the unambiguous range interval are received. (The unambiguous range interval is 0 to cT/2 where c is velocity of propagation and T is the pulse repetition period.) Then, as in a magnetron microwvae Doppler radar, the signals from range-aliased targets will be incoherent and cause an increase in noise, but they will not produce a Doppler spectrum that can compete with (or be mistaken for) the tropospheric Doppler spectrum. It is possible to choose any ambiguous range interval $[n\ cT/2 < R < (n + 1)cT/2]$ for coherent reception while targets at all other ranges are incoherent by selecting the phase of the reference oscillator used during reception to be equal to that used in previous transmitted pulses. Range-aliased signals that appear as white noise in the Doppler spectrum are much less troublesome than if they were coherent. However, because VHF radars with high pulse repetition rates can use time domain integration of the video samples from consecutive pulses, the range-aliased echoes can be greatly attenuated or effectively eliminated rather than made incoherent (causing increased noise).

Next, let the phase of the transmitted pulse change from pulse to pulse with a psuedo-random binary code. Then signals in the range 0 to $cT/2$ will add in the time domain integrator just as though the transmitter had constant phase, but range-aliased signals will add or subtract depending on the phase of the code during reception relative to the phase during transmission of a prior pulse. If the signal phase of the range-aliased targets remains constant during the time domain integration period, the range-aliased signals will cancel if there are as many positive as there are negative elements in the code. A psuedo-random code can cancel the signals (except for at most 1 pulse) for all range-aliased intervals. If the range-aliased signals are in motion but have small velocity compared with $\pm \lambda/4MT$, where M is the number of samples averaged in the time domain, then the cancellation of range-aliased echoes is still effective. If this were not so, one could not perform time domain integration on the signals from the range of interest. In fact, when targets are in motion, the cancellation of the range-aliased signals is more efficient than the coherent addition of the desired signals, because in the latter case signals must remain nearly in phase throughout time MT, while in the former case cancellation occurs during subintervals of MT.

The VHF radars in the Colorado Wind Profiler Network have been designed to operate at high pulse repetition rates with uncoded pulses and to be able to reject mesospheric echoes on the basis of the above considerations. We have not as yet implemented the mesospheric echo cancelling feature.

APPENDIX D.

TOPIC 3. TECHNIQUES FOR MEASUREMENT OF HORIZONTAL AND VERTICAL VELOCITIES: OPTIMUM POINTING ANGLE

R. G. Strauch
NOAA/ERL/Wave Propagation Laboratory
Boulder, Colorado 80303

The factors that influence the choice of pointing angle for measurement of vertical profiles of the horizontal wind with monostatic Doppler radar are summarized in this paper.

We assume that fixed pointing directions are used; this avoids the costs and complexities of large mechanically or electronically steered antennas. Three antenna beam-pointing directions are needed to measure the vector wind; for simplicity the pointing directions are chosen to observe orthogonal horizontal wind components u and v, and the vertical component w. Horizontal winds are measured with an antenna elevation pointing angle θ_e that allows observation at all altitudes of interest.

The radial Doppler velocities V_i measured by the radar are related to the wind as follows:

$$V_1 = u \cos\theta_e + w \sin\theta_e$$

$$V_2 = v \cos\theta_e + w \sin\theta_e$$

$$V_3 = w$$

where the antenna azimuth angles for V_1 and V_2 are assumed to be 0" and 90° respectively. At each altitude h the three measurements are made at volumes separated in space, so an assumption of horizontal uniformity is needed to combine the measurements to form a wind profile assumed to apply in the vertical direction above the radar location. Two types of errors can result from this assumption: first, u and v measured at the observation volume will be in error by $h(\Delta w/\Delta x)$ and $h(\Delta w/\Delta y)$ respectively; and second, the measured u and v will differ from the u and v directly above the radar by $(\Delta u/\Delta x)\, h \cot\theta_e$ and $(\Delta v/\Delta y)\, h \cot\theta_e$ respectively.

It is commonly assumed that w can be ignored for sufficiently long averaging times so that horizontal winds can be measured with just two pointing directions. In some clear-air cases the averaging time needed may be hours (much longer than is commonly used), and during precipitation the measured Doppler velocity spectra may be from a combination of scattering from refractive turbulence and hydrometeors. Hydrometeors generally trace the mean wind but also have fall speeds that may be as large as 9 m/s (even larger for hail, Atlas et al., 1973). The hydrometeor scattering signal can be stronger than the signal from refractive turbulence, even for VHF radars. If the horizontal winds are measured without correction for vertical motion, then the (two) pointing angles used are generally the same as for radars that use three pointing directions.

Factors that dictate high elevation angles are the following:

1. If the physical axis of the antenna is directed toward the zenith (the usual case for large phased arrays or large fixed reflectors) the elevation pointing angle should be as high as possible to keep the effective aperture nearly the same as for zenith pointing. The loss in sensitivity varies as csc θ_e and is given in Table D-1.

2. The elevation pointing angle should be as high as possible to minimize the range to a given height. The range is $h/\sin \theta_e$ and the loss in sensitivity varies as $(\text{range})^2$. This loss is double that of the effective aperture loss as shown in Table D-1.

3. The height resolution of the radar depends on the range resolution and the cross-beam dimensions of the antenna illumination. The antenna elevation angle should be high enough so that the height resolution is not degraded by cross-beam resolution at the highest altitude of interest. We want radar range resolution ΔR to determine height resolution because range resolution is controllable by system bandwidth whereas cross-beam resolution is fixed by antenna dimensions. Thus, the cross-beam dimension, $h_m \beta_2 \cot\theta_e$, should be less than $\Delta R \sin \theta_e$ where h_m is the maximum height of interest and β_2 is the two-way antenna beamwidth. Cross-beam height resolution at a height of 20 km is given in Table D-1 for two-way beamwidths of 2°, 3°, 4°, and 5".

4. The elevation angle should be as high as possible to minimize the effects of horizontal gradients of the wind as discussed earlier.

Opposing these factors that mandate elevation angles near zenith are those that dictate lower elevation angles:

Table D-1.--Loss Factor and Resolution for Various Elevation Angles

θ_e (deg)	Aperture loss (dB)	$(\text{Range})^2$ loss (dB)	Cross-beam height (m)			
			2°	3"	4"	5"
90	0	0	0	0	0	0
85	0.016	0.032	60	90	129	150
75	0.15	0.30	187	280	375	467
60	0.62	1.24	400	600	800	1000
45	1.5	3.0	700	1050	1400	1750

1. The elevation angle should be as low as possible to produce accurate wind measurements because uncertainty in the measurement of radial velocity causes an uncertainty in horizontal wind that increases with elevation angle. If vertical velocities are neglected,

$$\text{STD DEV } (\hat{v}_h) = [\text{STD DEV } (\hat{v}_i)] \sec \theta_e$$

where the superflex denotes an estimated quantity. Our ability to obtain unbiased estimates of v_i with low standard deviation depends on radar wavelength, signal-to-noise ratio, observation time, and the width of the Doppler spectrum (Zrnic, 1979). We want to obtain estimates at low signal-to-noise ratios where STD DEV ($\hat{v}_i$) may be 1 m/s or more for individual observations. If we derive average horizontal winds from N independent observations with an uncertainty of 1 m/s, then sec θ_e must be at most $\sqrt{N}$ if the individual radial measurements have an uncertainty of 1 m/s. Table D-2 gives the uncertainty in horizontal wind for an uncertainty in measured radial velocity of 1 m/s. For a VHF radar that obtains hourly wind averages from 15 observations, the elevation angle should not be greater than 75'.

2. Bias errors in the wind measurements caused by errors in antenna pointing direction increase with increasing elevation angle. Table D-2 gives the bias error for antenna beamwidths of 2°, 3°, 4°, and 5° when the antenna pointing is in error by 1/4 of the beamwidth, a value that should be achieved in practice with a non-steerable antenna.

3. At long wavelengths (6-10 m) enhanced radar reflections are observed on a zenith-pointing beam. These reflections are caused by horizontally stratified atmospheric layers; their intensity decreases as the antenna elevation angle decreases from zenith. However, if the antenna is pointed too close to zenith, the effective pointing angle will be biased toward zenith, and this pointing error will bias wind measurements toward low values. At 15' off-zenith this effect should be negligible (Röttger, 1980).

Table D-2.--Uncertainty and Bias of Wind Measurements for Various Elevation Angles

θ_e (deg)	STD DEV $(\hat{v}_h)$ (m/s)	Bias errors (%)			
		2°	3°	4"	5°
90	∞	---	---	---	---
85	11.5	11	17.6	24.9	33
75	3.9	3	5	7	9
60	2	1.5	2	3	4
4	1.4	0.9	1.3	1.8	2.6

Conclusion: The selection of the elevation angle for measurement of vertical profiles of horizontal winds and Doppler radar must satisfy conflicting demands. Elevation angles near zenith result in intolerable uncertainties in wind measurement; elevation angles too far off-zenith result in a loss of sensitivity that must be compensated by increased transmitted power or antenna size. An elevation angle of 75" yields an acceptable compromise for typical clear-air radars.

REFERENCES

Atlas, D. A., R. C. Srivastava, and R. S. Sekhon, 1973. Doppler radar characteristics of precipitation at vertical incidence. Rev. Geophys. Space Phys., 11:1-35.

Röttger, J., 1980. Reflection and scattering of VHF radar signals for atmospheric refractivity structures. Radio Sci., 15:259-276.

Zrnic, D. S., 1979. Estimation of spectral moments for weather echoes. IEEE Trans. Geosci. Elec., GE-17:113-128.

APPENDIX E.

PROPOSED WHITE SANDS MISSILE RANGE WIND PROFILING RADAR

R. G. Strauch
NOAA/ERL/Wave Propagation Laboratory
Boulder, Colorado 80303

WPL proposes to construct a wind profiling radar for White Sands Missile Range that will be an instrument for meteorological support for weapons testing and an instrument for atmospheric research. The proposed radar combines instrumentation techniques developed by WPL in radars that operate continuously and unattended and automatically provide vertical profiles of the horizontal wind. The WPL radars (a total of six units) operate at 6 m, 74 cm, and 33 cm wavelength; the WSMR radar would operate at 1.33 cm wavelength to take advantage of military frequency allocations.

The attached tables describe the radar. All of the hardware except the transmitter and antenna would be identical to that used in WPL radars. The radar/computer interface computer, communications, and software are generic to all WPL radars. The only changes would be in providing improved primary power to the digital hardware and improved lightning protection on power and telephone lines. All of the other radar system components have also been used in one or more WPL radars. The transmitter would have the same output capability that is used in the WPL 74 cm radar. The antenna would consist of two phased arrays of colinear-coaxial dipole elements constructed from low-loss/phase-stabilized cable. This type of antenna is used on the 6 m radars. The major difference is that in the WSMR radar, a single transmitter will feed one of three antenna pointing directions sequentially, whereas the WPL 6 m radars have a separate antenna and transmitter for simultaneous pointing. The power division and antenna switching are similar to that used with the 74 cm radar. Note that the switching is all at moderate power levels following an 8:1 power division. The antenna illumination shown has a simple 2:1 taper. The present 6 m radars do not have tapered illumination. There may be preferable switching arrangements to the one shown; this would be studied and a single array of dipoles would be tested before committing to this design.

Table E-1.--Proposed White Sands Radar

Frequency = 225 MHz
Wavelength = 1.33 m
Peak power = 32 kW
Average power = 160 W maximum
Duty cycle = 5% maximum
Pulse width = 1, 3, 9 microseconds
Pulse repetition period = 180 microseconds
Antenna aperture = 21.3 × 21.3 m (16λ x 16λ)
Power/aperture = 8×10^4, 24×10^5, 7.2×10^5 w-m^2
Antenna scanning - 3 position-sequential scanning
Antenna positions - zenith, 14.48 deg. off-zenith toward north and east
Antenna type - two arrays of coliner-coaxial dipole elements
One-way bandwidth - 3.75 degrees

Table E-2.--Proposed White Sands Radar Operating Parameters

Mode	1 psec	3 psec	9 psec
Time domain averaging	120	110	100
Spectral averages	8	16	32
Dwell time (64-point spectra)	11.1	20.3	36.9 sec.
Maximum radial velocity	215.4	±16.8	±18.5 m/s
Maximum horizontal velocity	±61.6	±67.2	±73.9 m/s
First height AGL	0.3	1.8	3.6 km
Number of heights	24	24	18
Height spacing	0.1	0.29	0.87 km

APPENDIX F

UNITED STATES DEPARTMENT OF COMMERCE
National Oceanic and Atmospheric Administration
Environmental Research Laboratories
325 Broadway
Boulder, Colorado 80303

January 16, 1984 R/E/WP6:RBC

TO: Distribution

FROM: R/E/WP6 - R. B. Chadwick R. B. Chadwick

SUBJECT: How many beams must a wind Profiler have if a wind Profiler is to profile winds.

The answer to the old question "how much wood would a woodchuck chuck..." depends on two things, the woodchuck and the wood. Similarly, questions about profiling wind depend on the Profiler and on the wind. The purpose of this memo is to present a simple wind model suitable for Profiler analysis and comparison. The model is used to compare the assumptions inherent in wind profiling with different numbers of beams (two through eight).

The problem with wind profiling is that even though the winds are desired at locations directly above the radar, most of the measurements must be made at points slightly removed from the desired location. Fortunately, there is a well-known, widely-used technique (Taylor's series expansion) which is applicable in this instance. A Taylor series is used to approximate a function at a point closely spaced to a "known" point by using successively higher derivatives. As higher order derivatives are used, the approximation becomes better, but any memo that starts out by referring to woodchucks should not attempt to include higher order derivatives, so here we will be concerned only with first-order derivatives. The more exact, higher-order analysis will be left to others. Also, we will assume a steady-state model with no changes in time. So, this model is very simple, being only one step above a model with no changes.

If u, v, and w are scalar wind components in a coordinate space with unit vectors $\vec{i}$, $\vec{j}$, $\vec{k}$, the Taylor approximation to the vector wind about the desired point above the radar is:

$$\vec{V} = \left(u + x\frac{\partial u}{\partial x} + y\frac{\partial u}{\partial y} + z\frac{\partial u}{\partial z}\right)\vec{i} + \left(v + x\frac{\partial v}{\partial x} + y\frac{\partial v}{\partial y} + z\frac{\partial w}{\partial z}\right)\vec{j} + \left(w + x\frac{\partial w}{\partial x} + y\frac{\partial w}{\partial y} + z\frac{\partial w}{\partial z}\right)\vec{k}$$

Here x, y, and z are displacements in the $\vec{i}$, $\vec{j}$, and $\vec{k}$ directions from the desired point above the radar. Even this simplest of models has 12 unknown parameters and would require a combination of 12 measurements and equations to solve in general. Fortunately the set of 12 unknowns can be reduced by

reducing the region of definition to just the x and y axis. The justification for this is that all of the measurement points for one height are on either the x-axis or the y-axis. It is convenient to define the vector wind as two functions, one valid over the x-axis and the other valid over the y-axis. The two functions are:

$$\vec{f}_x(x) = \left(u + x\frac{\partial u}{\partial x}\right)\vec{i} + \left(v + x\frac{\partial v}{\partial x}\right)\vec{j} + \left(w + x\frac{\partial w}{\partial x}\right)\vec{k}$$

$$\vec{f}_y(y) = \left(u + y\frac{\partial u}{\partial y}\right)\vec{i} + \left(v + y\frac{\partial v}{\partial y}\right)\vec{j} + \left(w + y\frac{\partial w}{\partial y}\right)\vec{k}$$

As in a previous memo, define unit vectors in each beam direction, north, east, south, west, and vertical as:

$$\vec{n} = \sin\phi\,\vec{j} + \cos\phi\,\vec{k}$$

$$e' = \sin\phi\,\vec{i} + \cos\phi\,\vec{k}$$

$$\vec{s} = -\sin\phi\,\vec{j} + \cos\phi\,\vec{k}$$

$$\vec{w} = -\sin\phi\,\vec{i} + \cos\phi\,\vec{k}$$

$$\vec{v} = \vec{k}$$

The measurements made by each beam are then inner products of these unit vectors and the vector wind at the measurement point. So those measurements are:

$$Vn = \vec{n} \cdot \vec{f}_y\,(d)$$

$$Ve = \vec{e} \cdot \vec{f}_x\,(d)$$

$$Vs = \vec{s} \cdot \vec{f}_y\,(-d)$$

$$Vw = \vec{w} \cdot \vec{f}_x\,(-d)$$

$$vv = 3 \cdot \vec{f}_x\,(o) = \vec{f}_y\,(o) \cdot \vec{v}$$

where d is the displacement from the vertical beam measurement point to the other measurement points.

The above set of equations can be evaluated to give:

$$Vn = \left(v + d\frac{\partial v}{\partial y}\right)\sin\Phi + \left(w + d\frac{\partial w}{\partial y}\right)\cos\Phi$$

$$Ve = \left(u + d\frac{\partial u}{\partial x}\right)\sin\Phi + \left(w + d\frac{\partial w}{\partial x}\right)\cos\Phi$$

$$Vs = -\left(v + d\frac{\partial v}{\partial y}\right)\sin\Phi + \left(w + d\frac{\partial w}{\partial y}\right)\cos\Phi$$

$$Vw = -\left(u + d\frac{\partial u}{\partial x}\right)\sin\Phi + \left(w + d\frac{\partial w}{\partial x}\right)\cos\Phi$$

$$Vv = w$$

This is five equations in seven unknowns and cannot be solved without additional information. It is possible to add one more unknown and two equations. As discussed in a previous memo, these two equations are valid for this problem.

$$\frac{\partial u}{\partial x} + \frac{\partial v}{\partial y} + \frac{\partial w}{\partial z} = 0$$

$$w = \Delta\frac{\partial w}{\partial z} + w_o$$

where A is the range cell and w_o is the vertical velocity from the adjacent range cell. At this point we have eight unknowns

$$u,\ v,\ w,\ \frac{\partial u}{\partial x},\ \frac{\partial v}{\partial y},\ \frac{\partial w}{\partial z},\ \frac{\partial w}{\partial y},\ \frac{\partial w}{\partial x}$$

and seven equations.

The two basic assumptions in the model to this point are: 1) higher order terms than first spatial derivatives are zero; 2) all time derivatives are zero. This model is simple, having no time variations and only linear spatial variations, but it is such that any proposed Profiler configuration must be able to work with this set of equations and, given certain assumptions, solve them to obtain values of wind parameters.

This simple model can be used to compare the assumption necessary to measure wind profiles with different numbers of beams. The results of this type of comparison are shown in Table 1. Across the top are the eight parameters of the model. If an I appears under a parameter, it implies that the parameter is measured indirectly, a D implies direct measurement and 0 implies that the parameter must be assumed zero to solve the equations. For a four-beam and a five-beam system, there are at least two different ways of assuming which parameters are zero and these are labeled case 1 and 2. Case 1 €or the four-beam problem was described in detail in a previous memo.

The last column is the cost of the antennas for that particular arrangement. For a three- and a five-beam system there are two ways to get a vertical beam and this results in two different costs for the antenna system. The second figure is the cost of an antenna system with a separate antenna for the vertical beam. The first figure is for a single antenna with the switching necessary to generate a vertical beam. An eight-beam system is one with four azimuth angles and two elevation angles.

Table 1. Assumptions and costs of using different numbers of beams to measure the parameters of the wind model. I implies measured indirectly, D implies measured directly, and 0 implies must be assumed. zero.

	U	V	W	$\frac{\partial u}{\partial x}$	$\frac{\partial v}{\partial y}$	$\frac{\partial w}{\partial z}$	$\frac{\partial w}{\partial y}$	$\frac{\partial w}{\partial x}$	Antenna cost
two-beam	I	I	0	0	0	0	0	0	40K
three-beam	I	I	D	0	0	0	0	0	60K, 75K*
four-beam (case 1)	I	I	I	I	I	I	0	0	50K
four-beam (case 2)	I	I	0	0	0	0	I	I	50K
five-beam (case 1)	I	I	D	I	I	I	I	0	70K, 85K*
five-beam (case 2)	I	I	D	I	I	I	0	I	70K, 85K*
eight-beam	I	I	I	I	I	I	I	I	70K

Note that a four- and eight-beam system would not measure w directly, rather w is determined by non-vertical measurements. During the early days of the dual-Doppler radar program, the vertical winds were estimated from the horizontal winds and initial estimates. The technique did not work well because the elevation angles were always very small so that vertical winds hardly contributed to any of the measurements. The situation with the Profiler is completely different because the vertical winds contribute heavily to all measurements and hence, it will be easy to accurately determine w even though it is not measured directly.

An eight-beam Profiler (two beams at different elevation angles) will provide eight measurements and produce ten equations for the eight unknowns. This is more than enough to solve the system, and the extra equations could be used to make consistency checks or reduce effects of noise.

* two separate arrays

APPENDIX G.

PROFILER MEASUREMENTS

The statistical nature of atmospheric motions from scales of a few kilometers to approximately 1000 km has been neglected because measurement techniques have not been available (Lilly and Petersen, 1982). One attempt to fill in this gap has been to use navigational winds measured from Boeing 747 passenger jet aircraft operated by Continental Airlines between Chicago, Los Angeles and Honolulu (Lilly and Petersen, 1982). This data set does not totally fill the gap, but along with measurements by Vinnichenko (1970), Nastrom and Gage (1983), Balsley and Carter (1982), and Chen and Wiin-Neilssen (1978), the existing data (when converted to common spatial spectra) show an approximate $k^{-5/3}$ to k^{-2} behavior over several decades of wavenumber for the one-dimensional spectra.

These spectra could be converted to frequency spectra using Taylor's hypothesis, which may be valid over a certain part of the wavenumber spectra. It would be useful to see what the average frequency dependence of the kinetic energy is at the airline altitudes over these routes. However, the Profiler can provide more site-specific data that can be used to compute the time-lagged velocity correlation vs. height as well as other parameters needed for shuttle operations.

We have taken a data sample from the Profiler system in Platteville, Colorado, as an example of some of the Profiler measurement correlations. Here, the off-zenith beams are range gated every 1.44 km vertically starting at 2.8 km (above ground level) and going to 20.1 km.

The data were sampled approximately every 90 sec, passed through a running consensus window (Fischler and Bolles, 1981), and interpolated to values every 2 min. Figure G-la shows the east component of wind at 10 km starting at 21:38:53 on October 21, 1983, and continuing for 86 hrs. The spike-like structures on the trace are caused by electromagnetic interference. Figure G-lb shows the same data set when the sliding consensus window has been used with 12 data points. Figure G-lc shows the correlation function for this height and velocity component. Here the correlation function falls to about 0.75 at 3 hrs.

We can also look at a lower range gate and compute the velocity correlation. Some examples are shown in Fig. G-2a and G-2b for October 21, 1983, starting at 21:38:53. Figure G-2a shows the edited (consensused) time series for the east velocity component at 3 km. Figure G-2b shows the autocorrelation function for the E-W velocity component. Notice that at 3 h time lag this velocity component still has a correlation of 0.6.

Figure G-3a shows the edited east component at 6 km, and Fig. G-3b the autocorrelation function. At a lag of 3 hrs, there is a correlation of about 0.7 .

At higher elevations, the backscattered signal is much lower, and the measured velocities are much noisier. Figure G-4a shows the raw data at 12 km without the consensus algorithm being applied. Figure G-4b shows the consensused data, applied over 1 h. Although the plot is cleaned up considerably, there are still some fairly large noise spikes near the beginning and at several other places. These cause a rapid dropoff in the autocorrelation function (Fig. 5-5) vs. time in the first hour. By applying the consensus algorithm over 2 h, we can edit out more of the obviously "bad" data points. This is reflected in the subsequent autocorrelation function (Fig. 5-6), although not all of the obviously bad points were removed.

As a further example of the utility of the profiler wind measurements vs. height, are shown in figures G-7 through G-30. Figure G-6 is a template showing the wind information. One can see from these examples the obvious utility of the remote wind profiles for both real-time operation and atmospheric research. The real time wind profiles may be extremely useful during a launch and then could be processed to obtain correlation information for wind climatology.

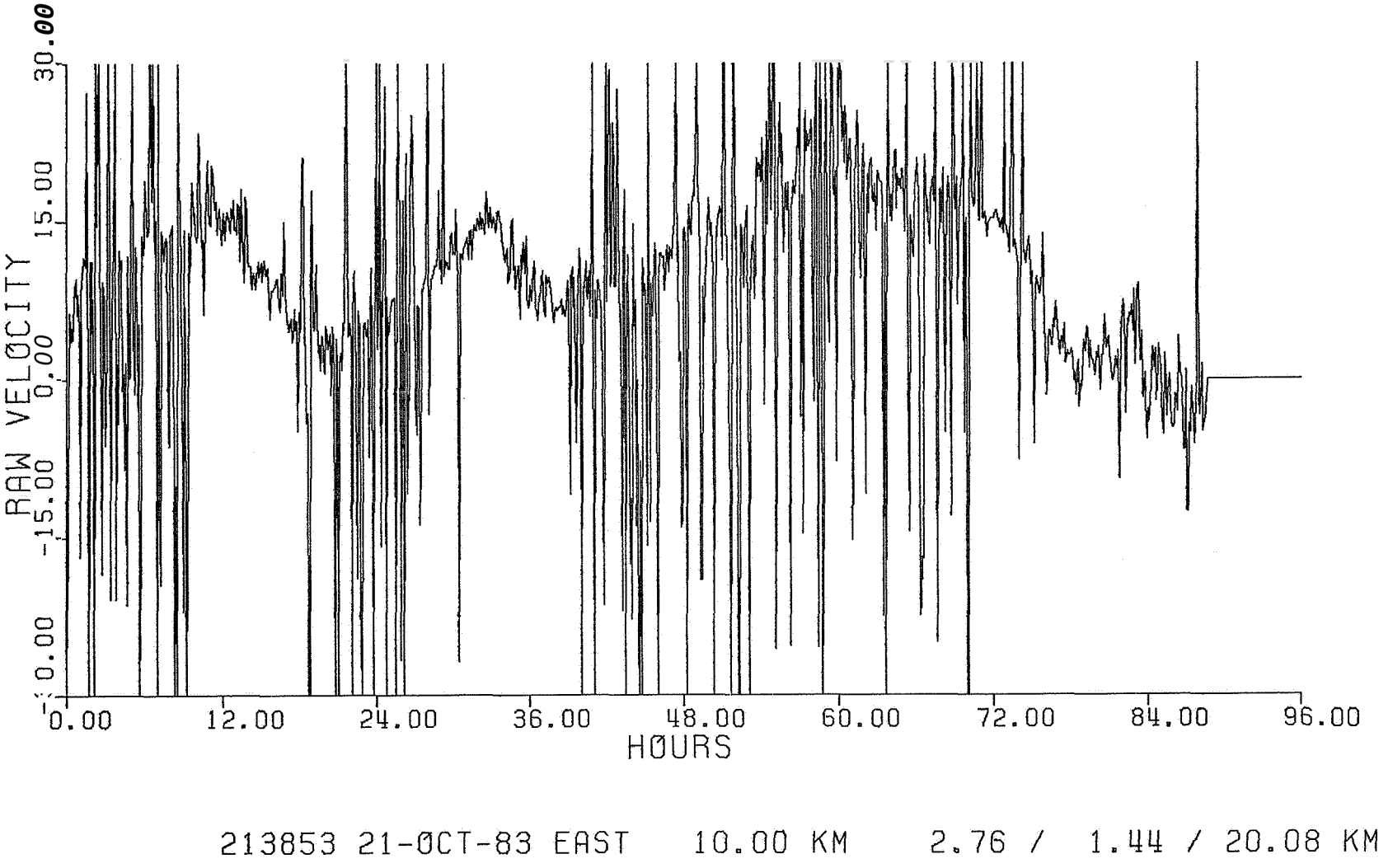

Figure G-1a. Profiler east component of velocity at 10 km. Starting time 21:38:53 on 21 October 1983.

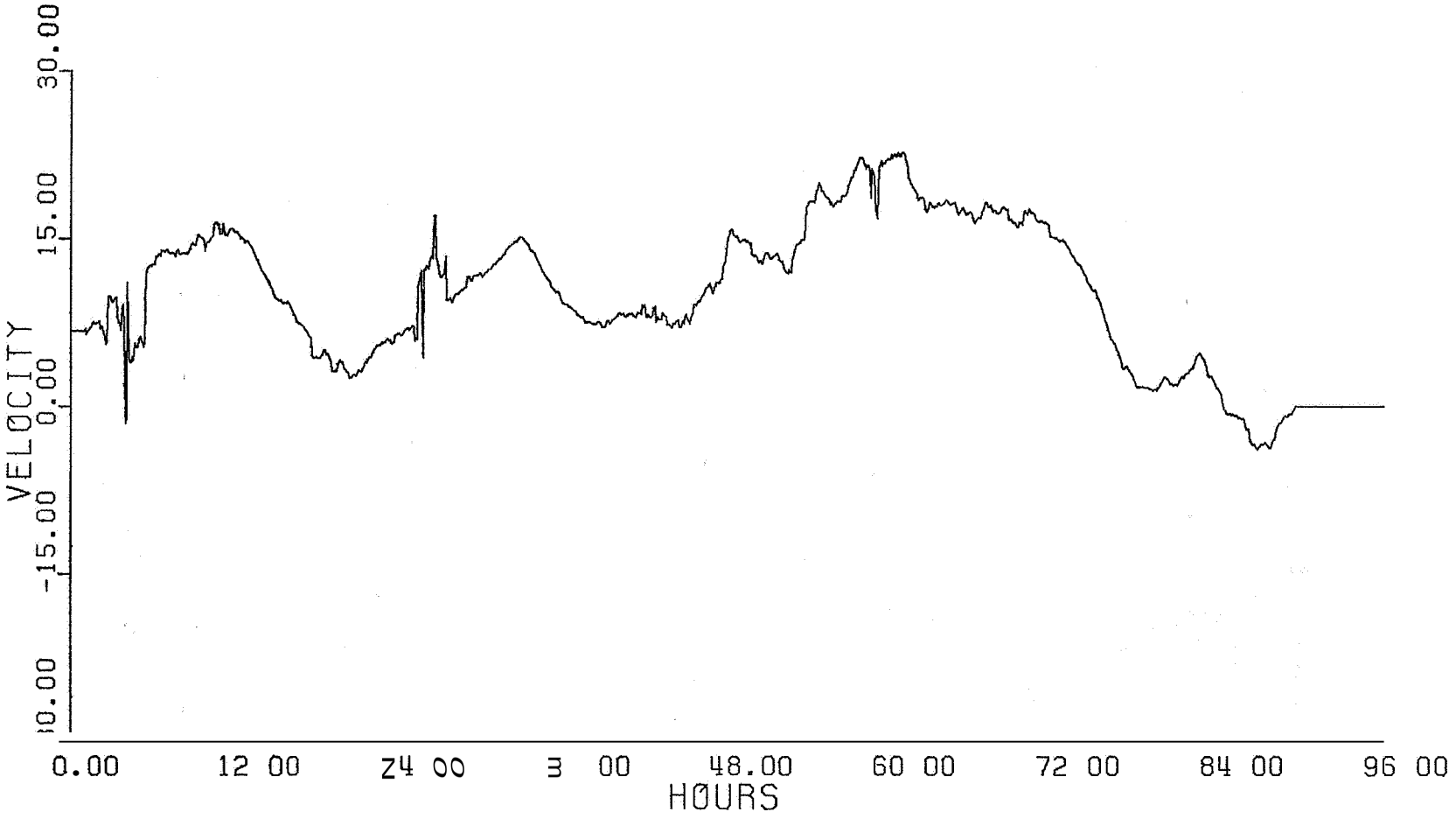

Figure G-1b. Profiler east component at 10 km using consensus algorithm where 4 out of 10 points must pass. Window width is 9 m/s. Starting time 21:38:53 on 21 October 1983.

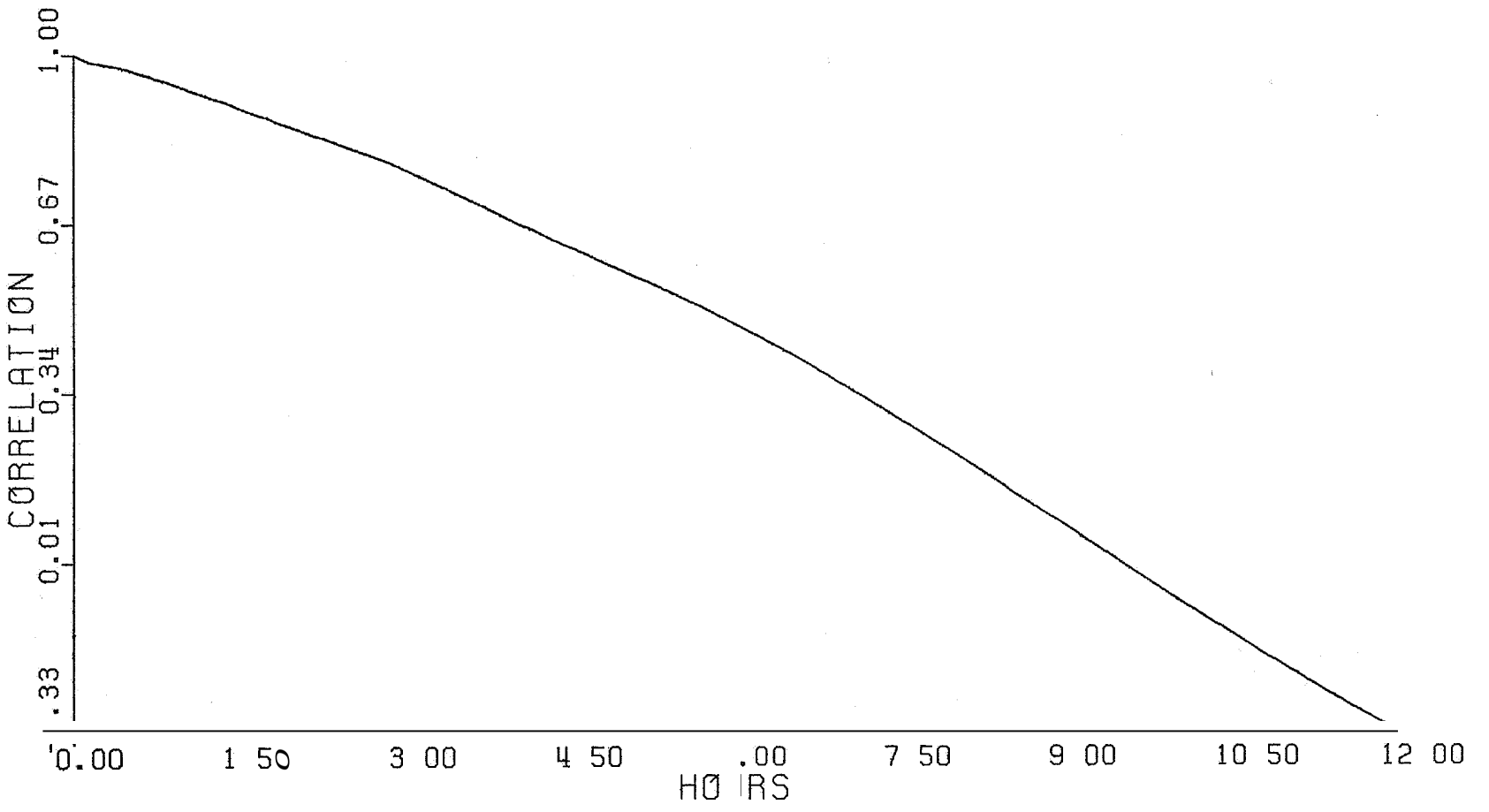

Figure G-1c. Autocorrelation function for east component of velocity at 10 km. Starting time 21:38:53 on 21 October 1983.

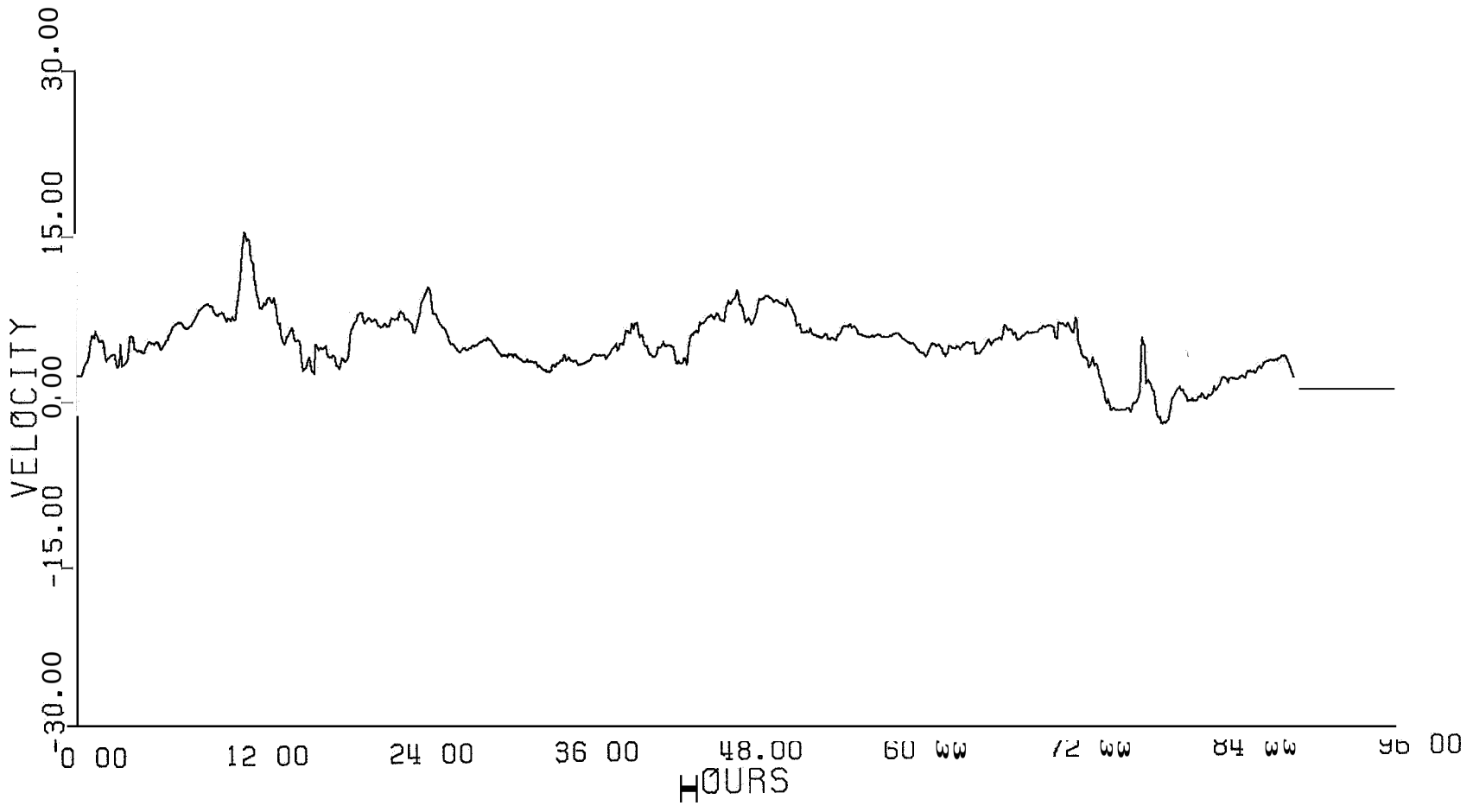

Figure G-2a. Profiler east component of velocity at 3 km using consensus algorithm with the same window as (G-1b). Starting time 21:38:53 on 21 October 1983.

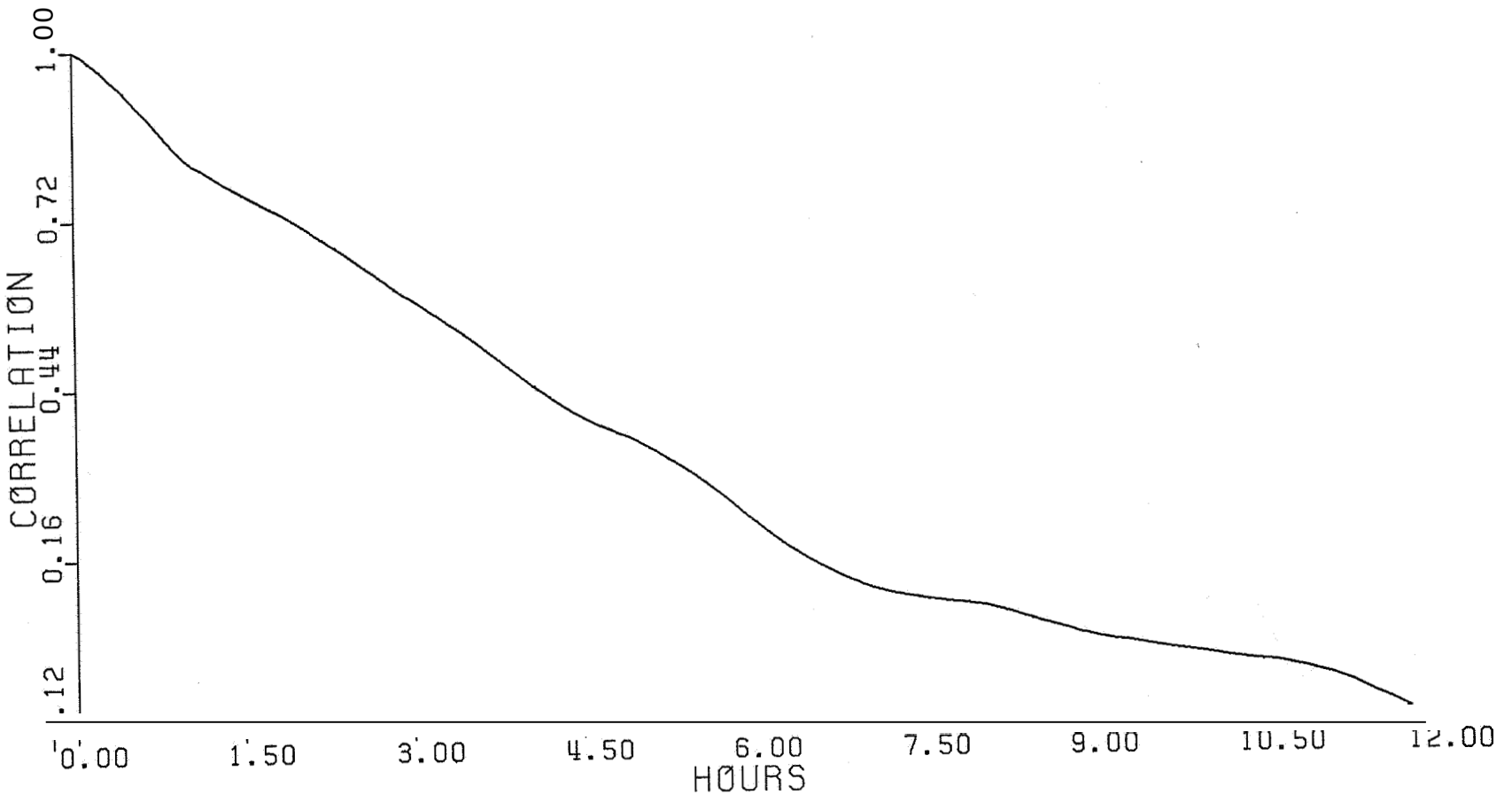

Figure G-2b. Autocorrelation function for east component of velocity at 3 km. Starting time 21:38:53 on 21 October 1983.

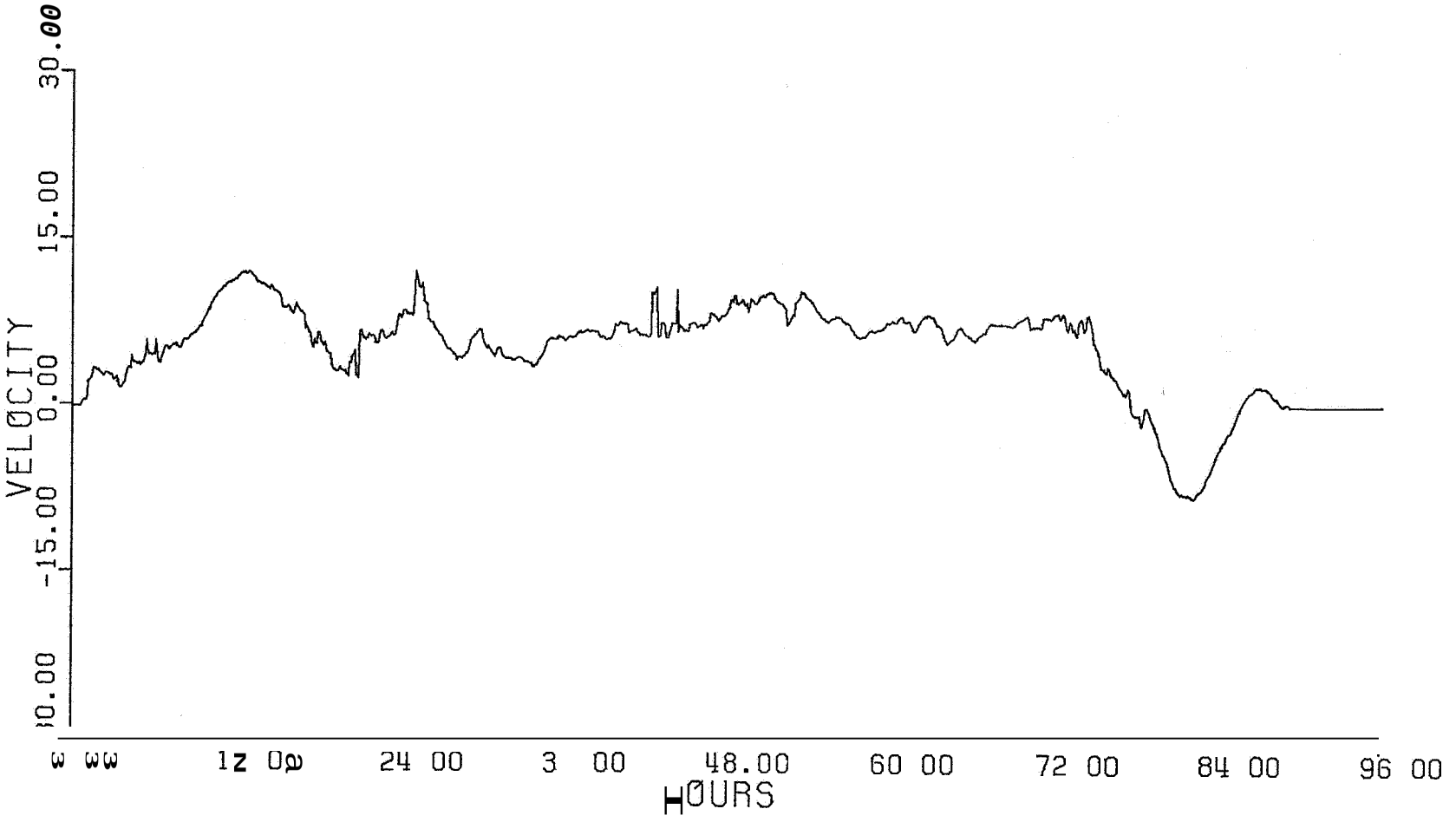

Figure G-3a. Profiler east component of velocity at 6 km using consensus algorithm with the same window at (G-1b). Starting time 21:38:53 on 21 October 1983.

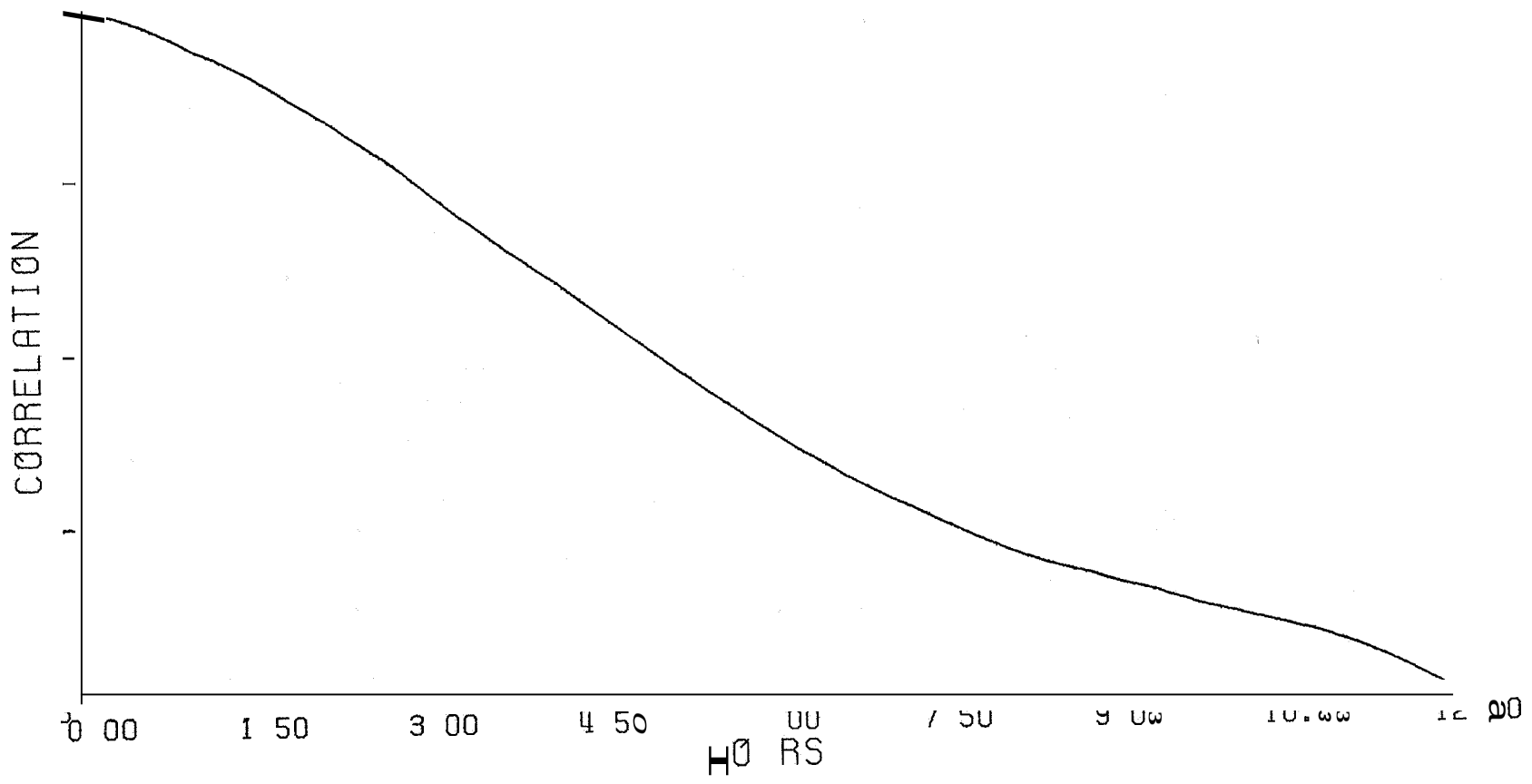

Figure G-3b. Autocorrelation function for east component of velocity at 6 km. Starting time 21:38:53 on 21 October 1983.

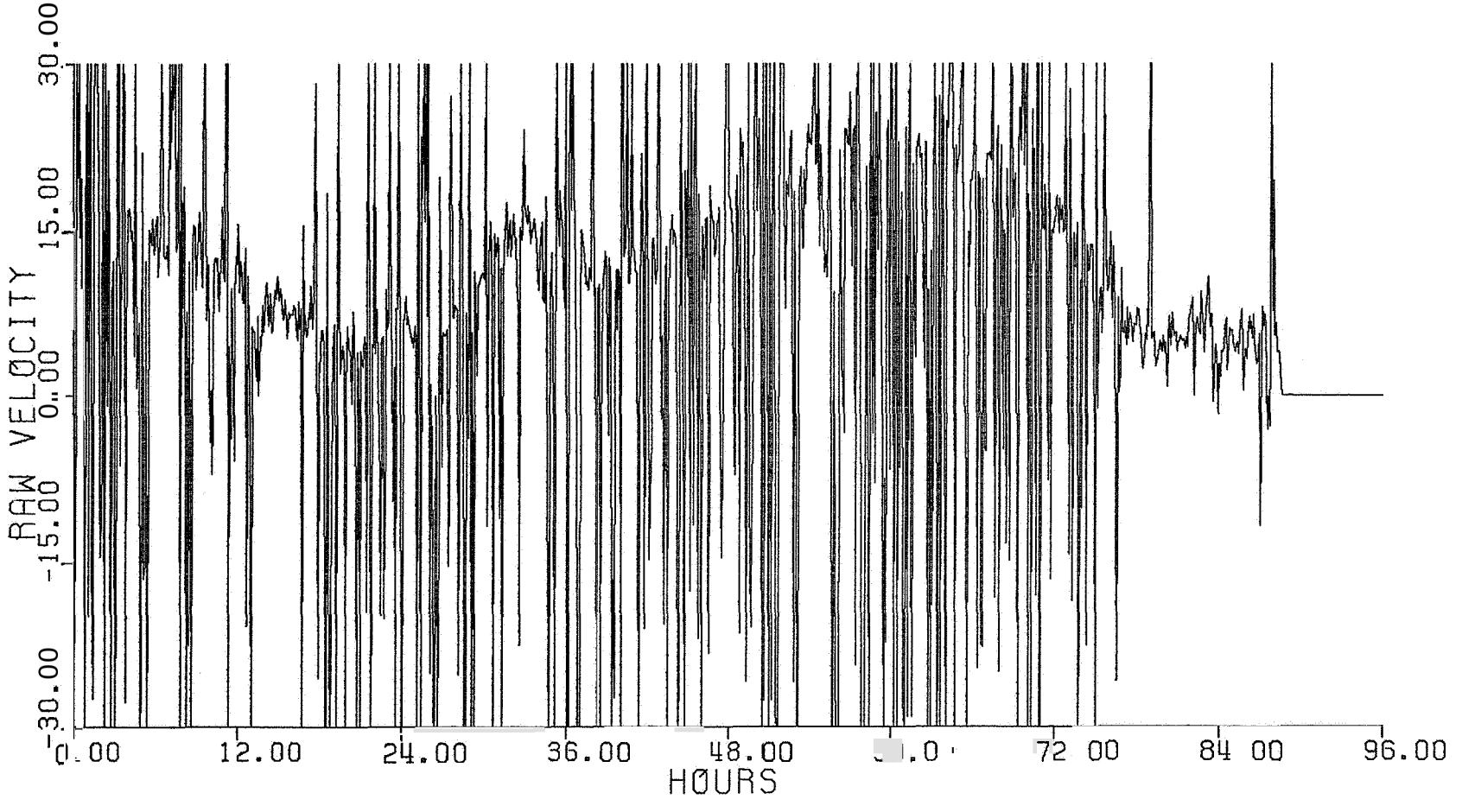

Figure G-5a. Profiler east component of velocity at 12 km. Starting time 21:38:53 on 21 October 1983

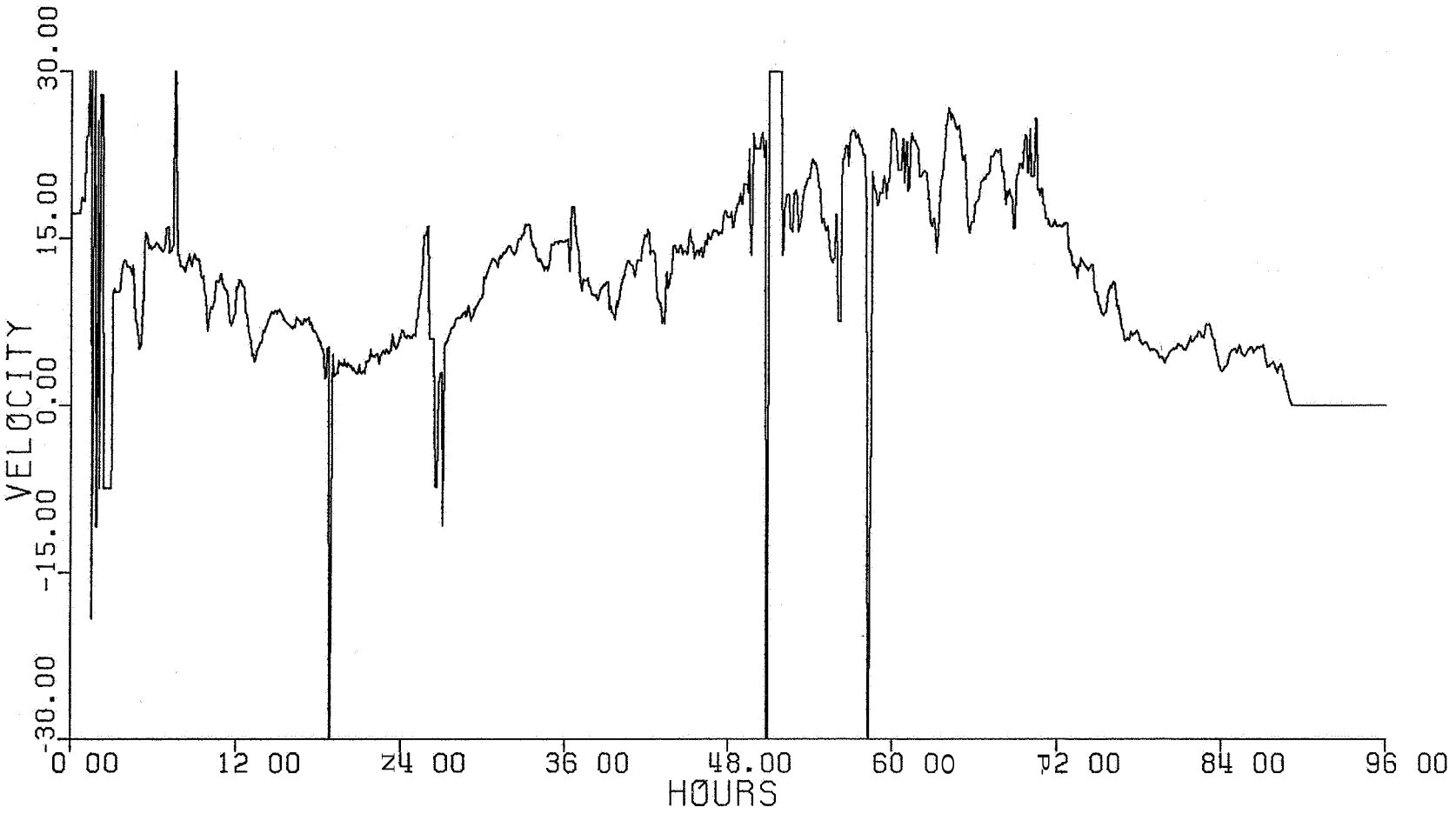

Figure G-4b. Profiler east component of velocity at 12 km using consensus algorithm with the same window as (G-1b).

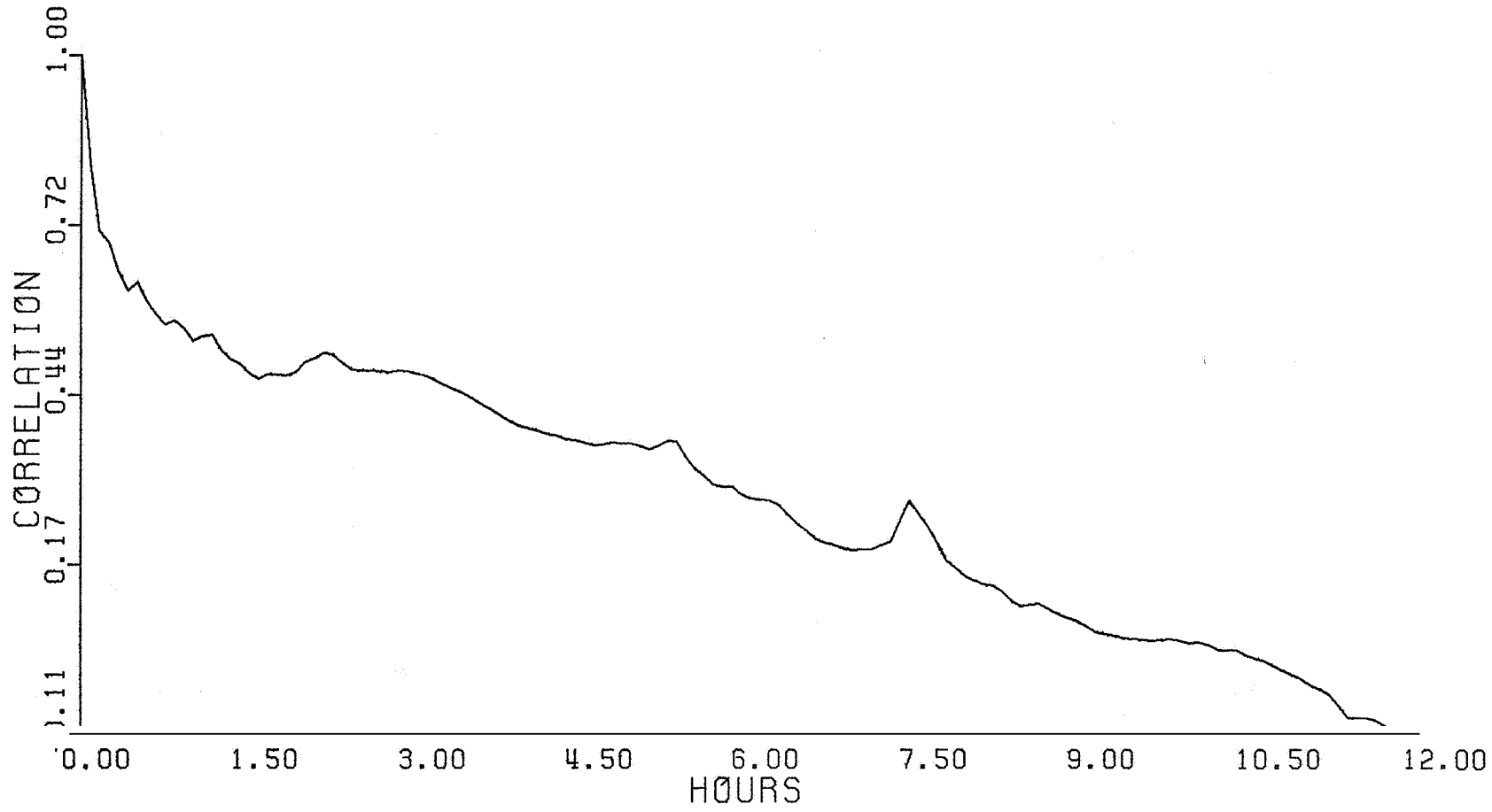

Figure G-4c. Autocorrelation function for the east component of velocity using consensus algorithm and with the same window as (G-1b).

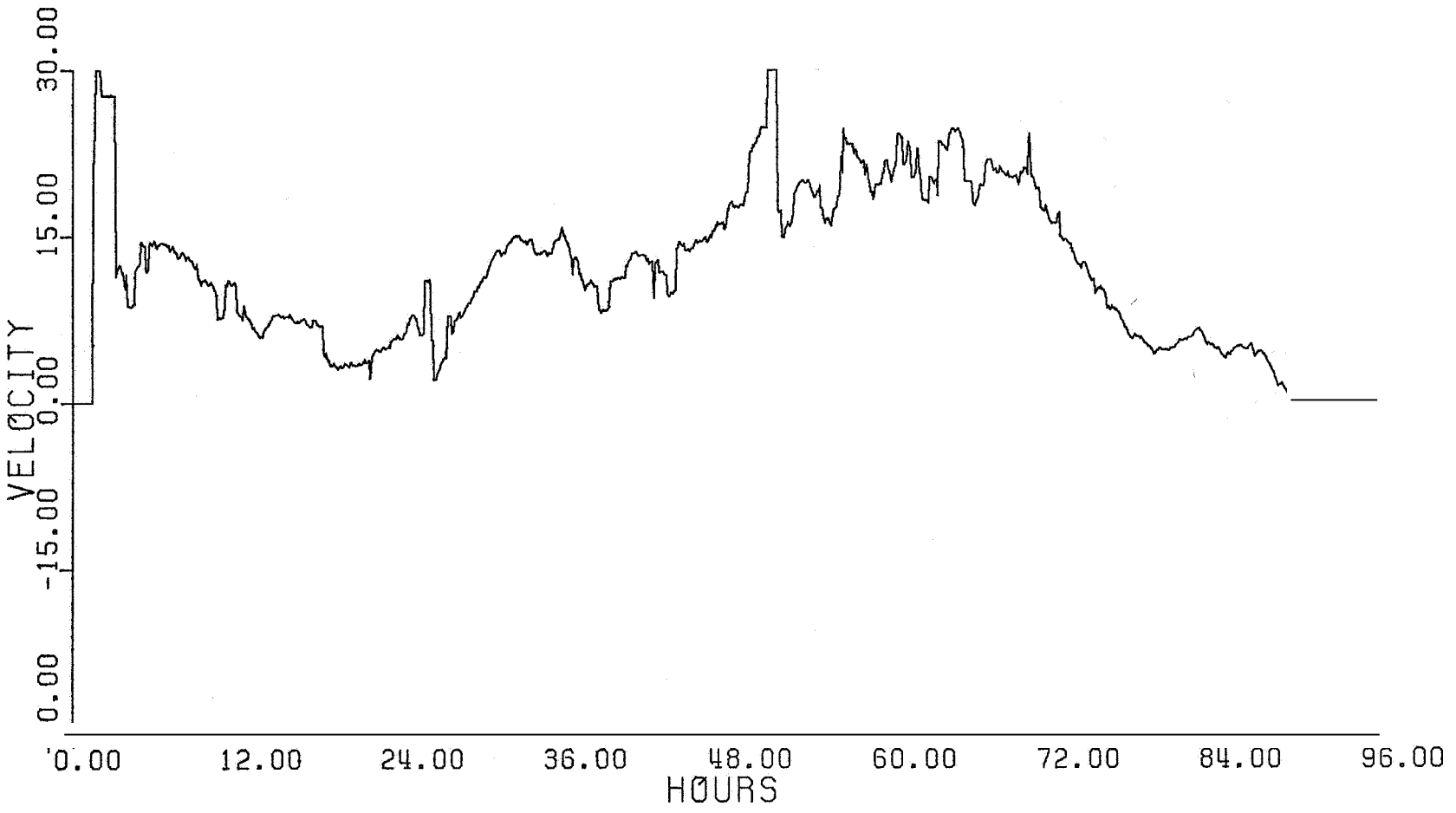

213853 21-0CT-83 EAST 12.00 KM

2.76 / 1.44 / 20.08 KM 8 0F 24 C0NSENSUS 9.00 M/S

Figure G-5a. Profiler east component of velocity at 12 km using consensus window where 8 of 24 points must pass and a 9.0 m/s window.

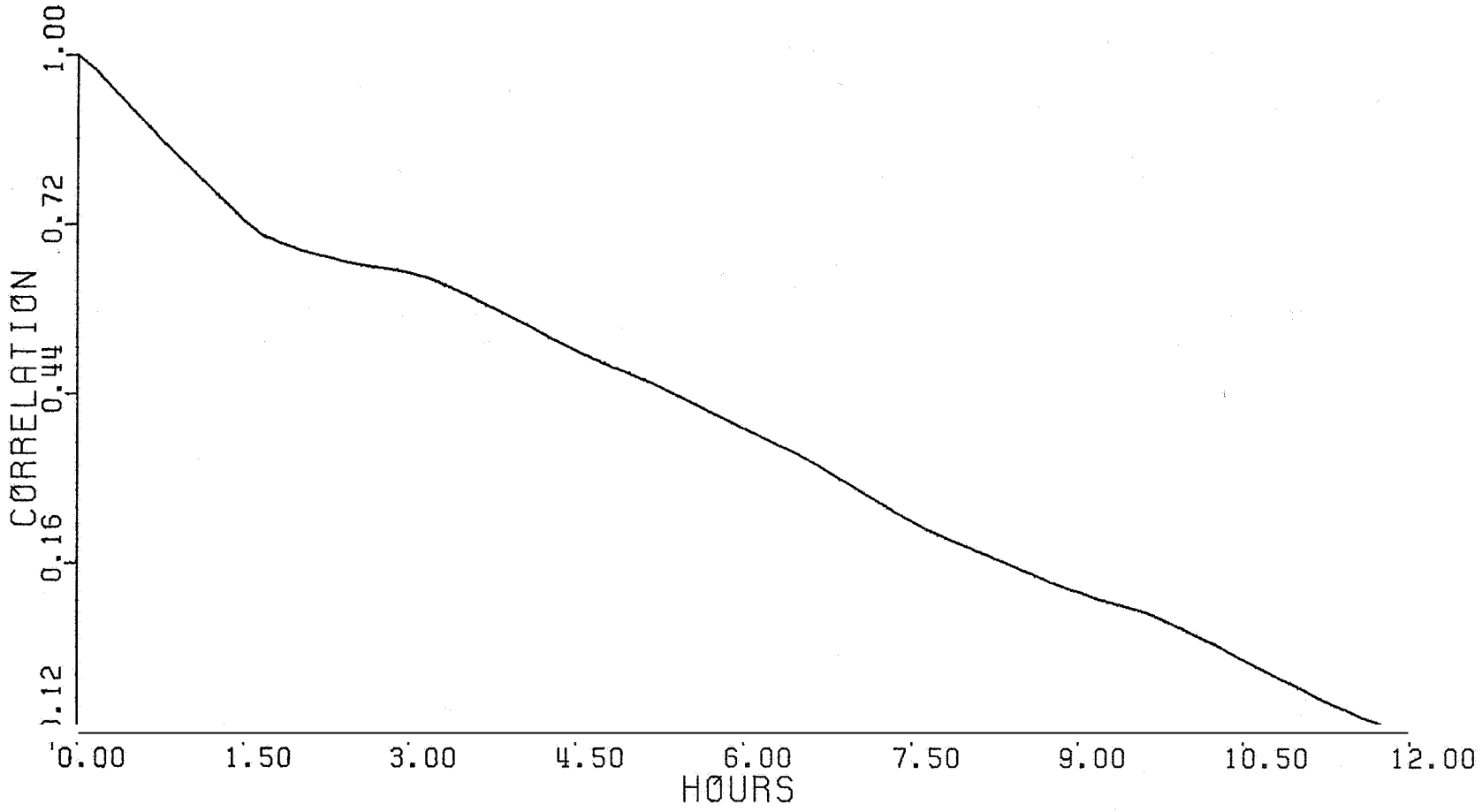

Figure G-5b. Autocorrelation function for east component of velocity at 12 km using the G-5a window in the consensus algorithm.

Figure Explanation

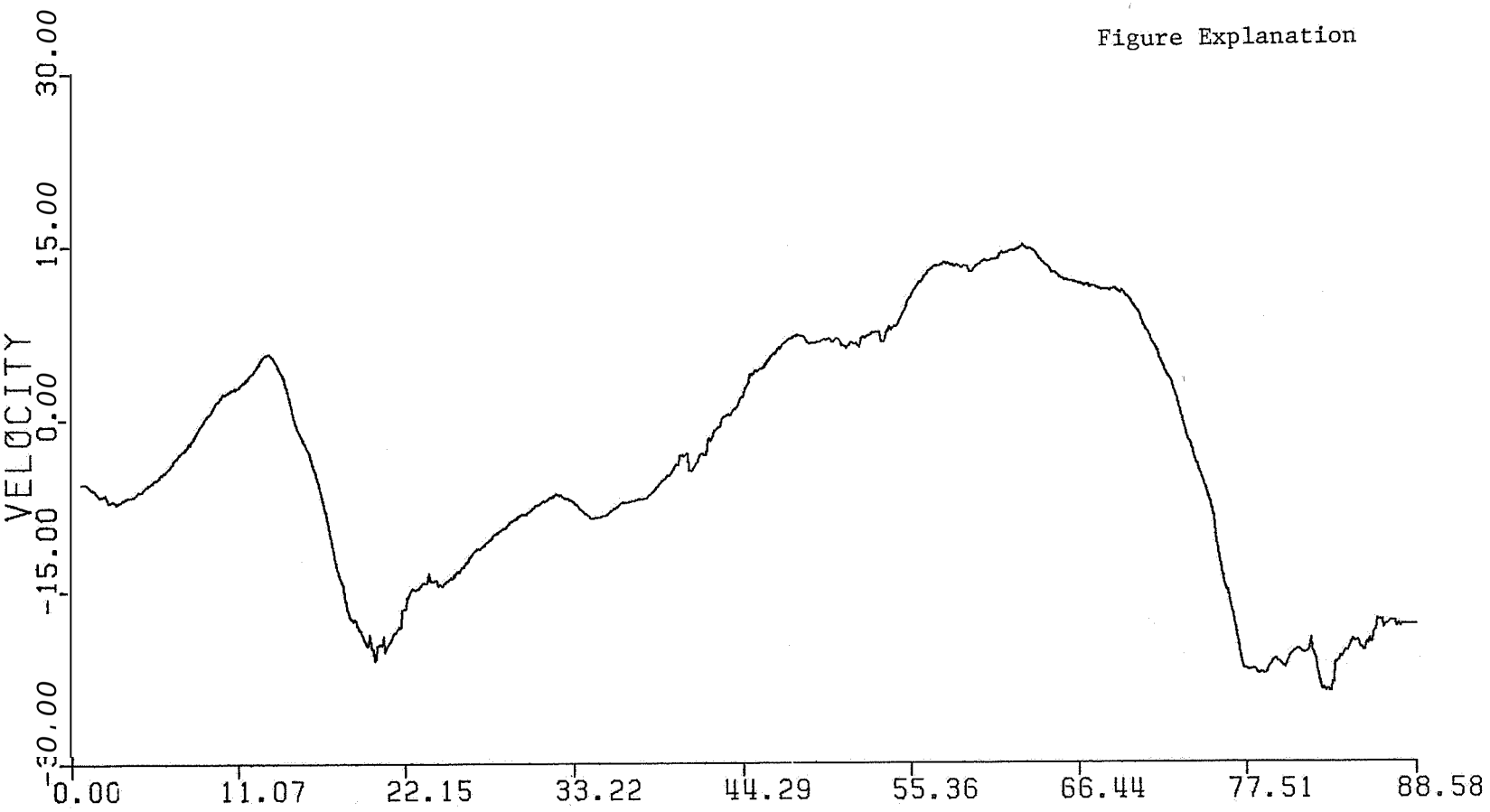

(Hours after start time)

Start time Date Wind speed component Index/Height above ground

First range gate elevation / Range gate length / Maximum range gate height No. of points to pass Wind width

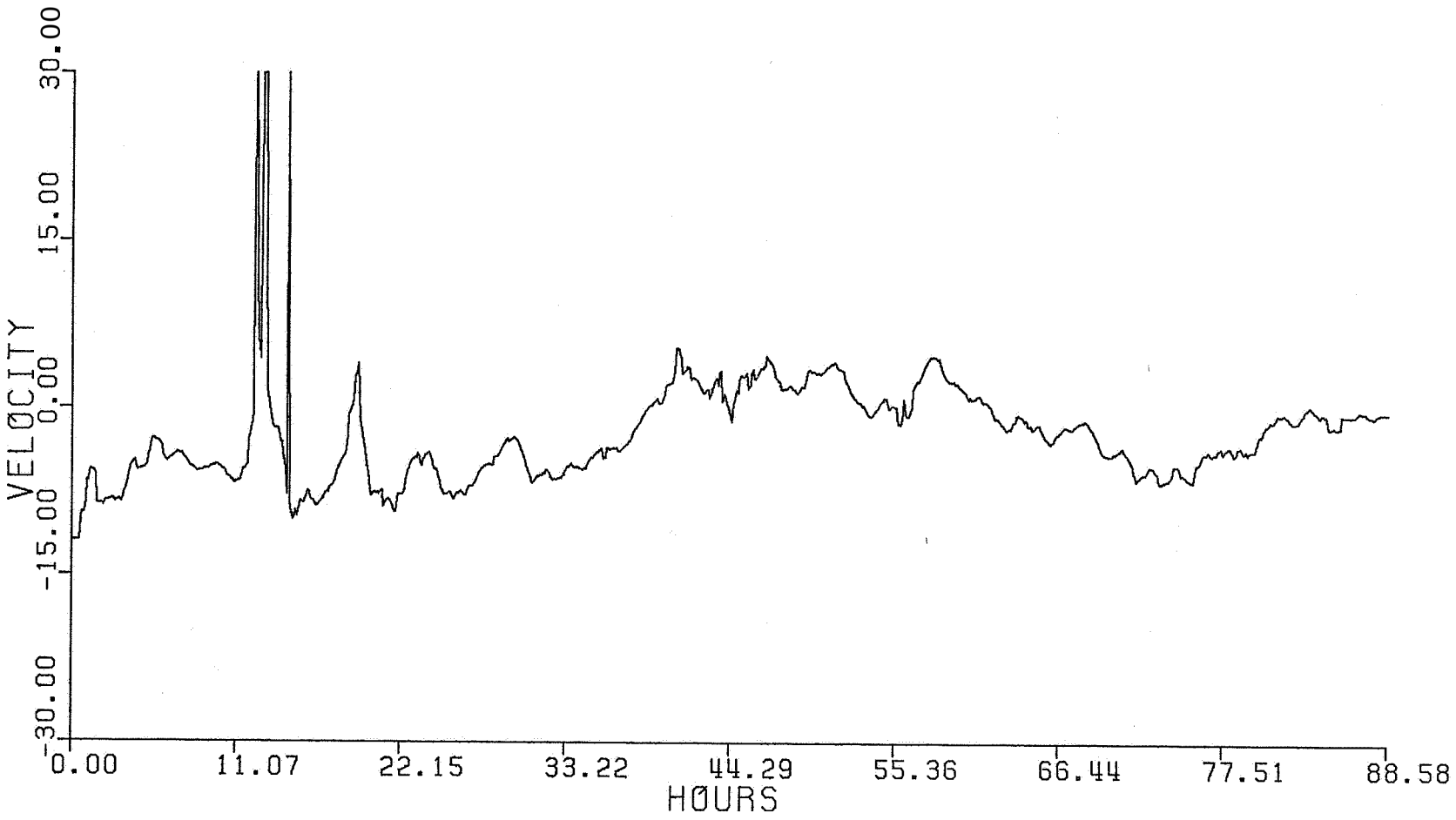

213853 21-ØCT-83 NØRTH 3.00 / 2.34 KM

2.34 / 1.45 / 19.76 KM 4 ØF 12 CØNSENSUS 9.00 M/S

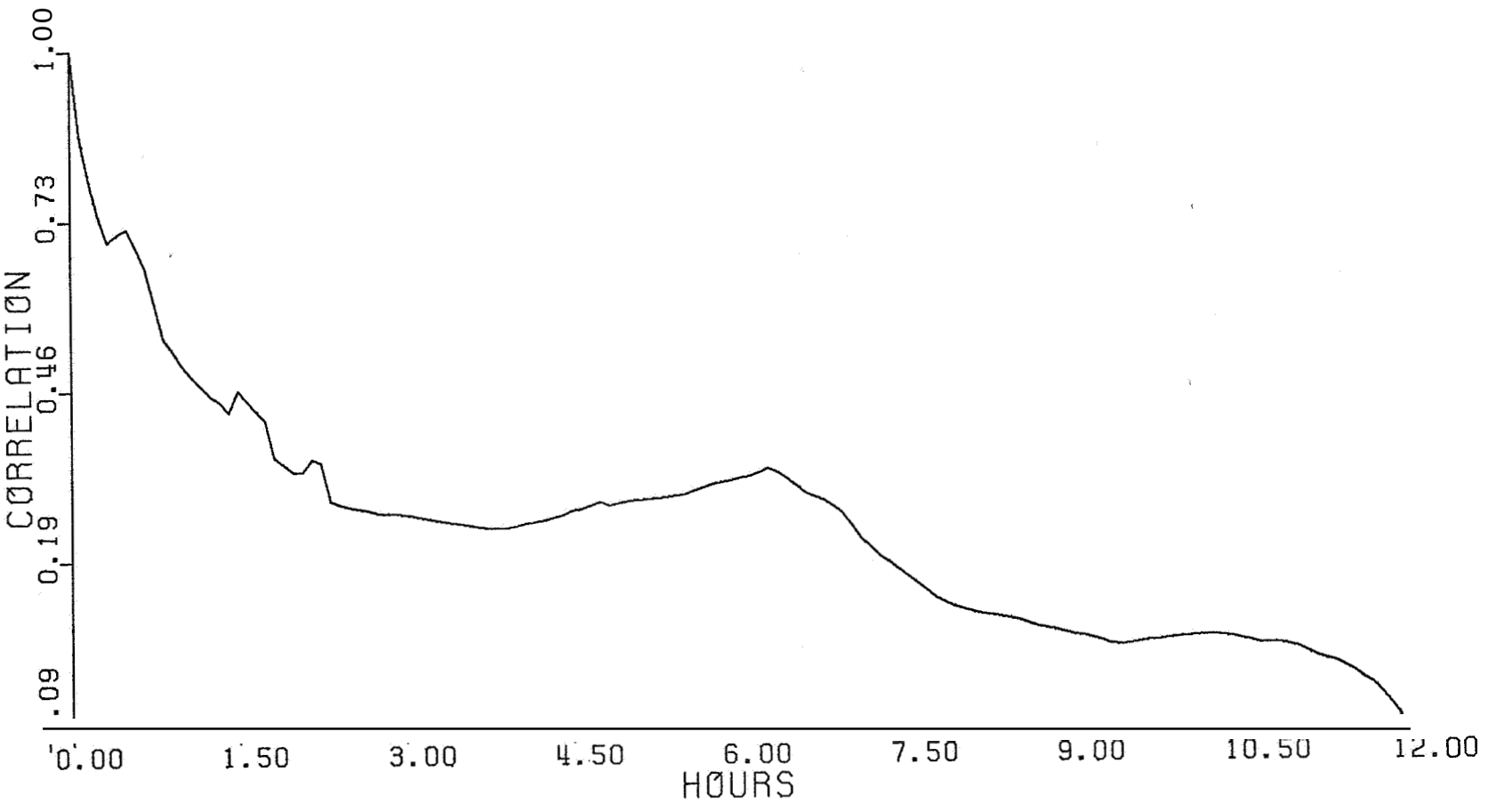

213853 21-OCT-83 NORTH 3.00 / 2.34 KM

2.34 / 1.45 / 19.76 KM 4 OF 12 CONSENSUS 9.00 M/S

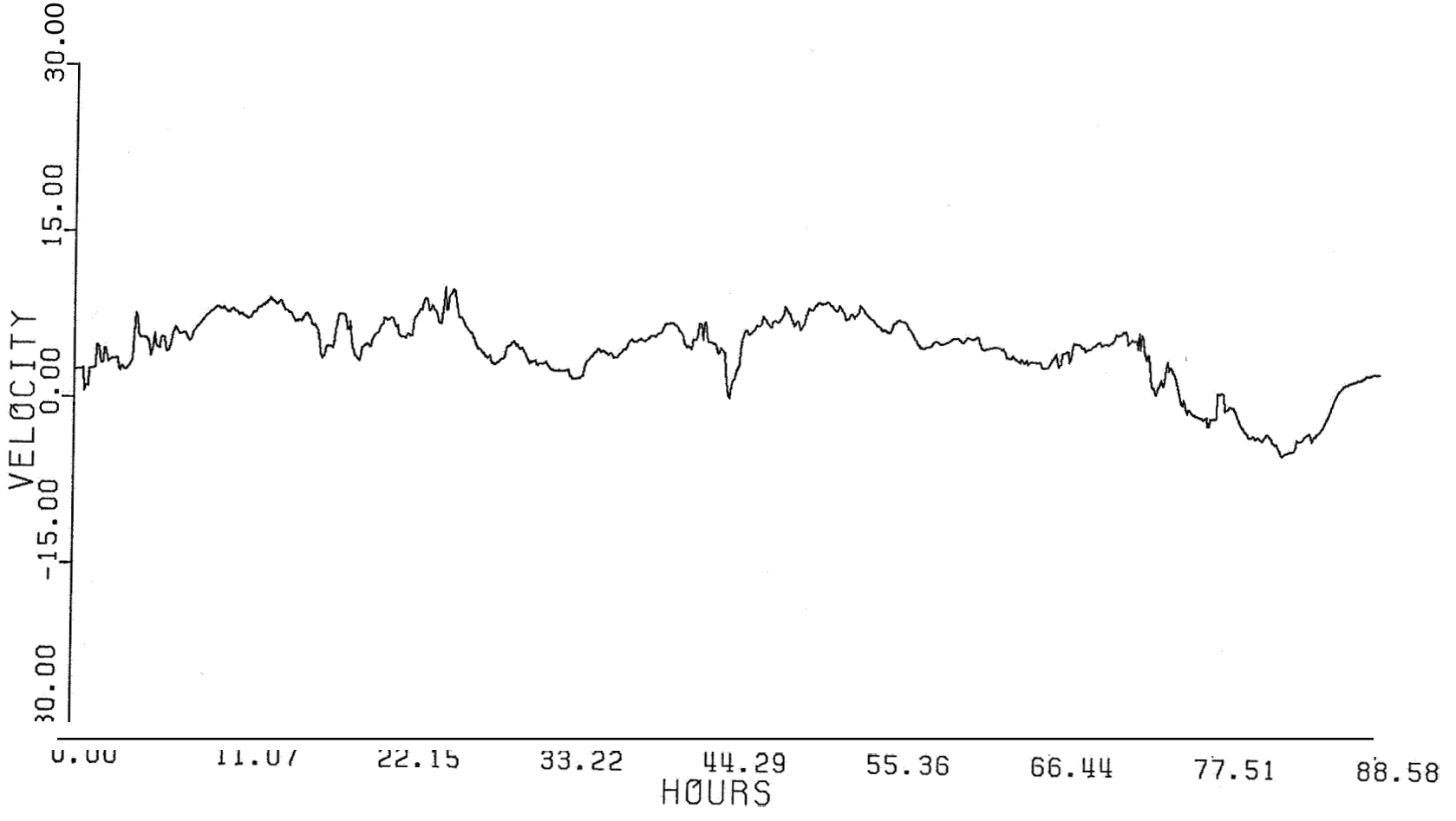

213853 21-OCT-83 EAST 4.50 / 4.20 KM

2.76 / 1.44 / 20.08 KM 4 OF 12 CONSENSUS 9.00 M/S

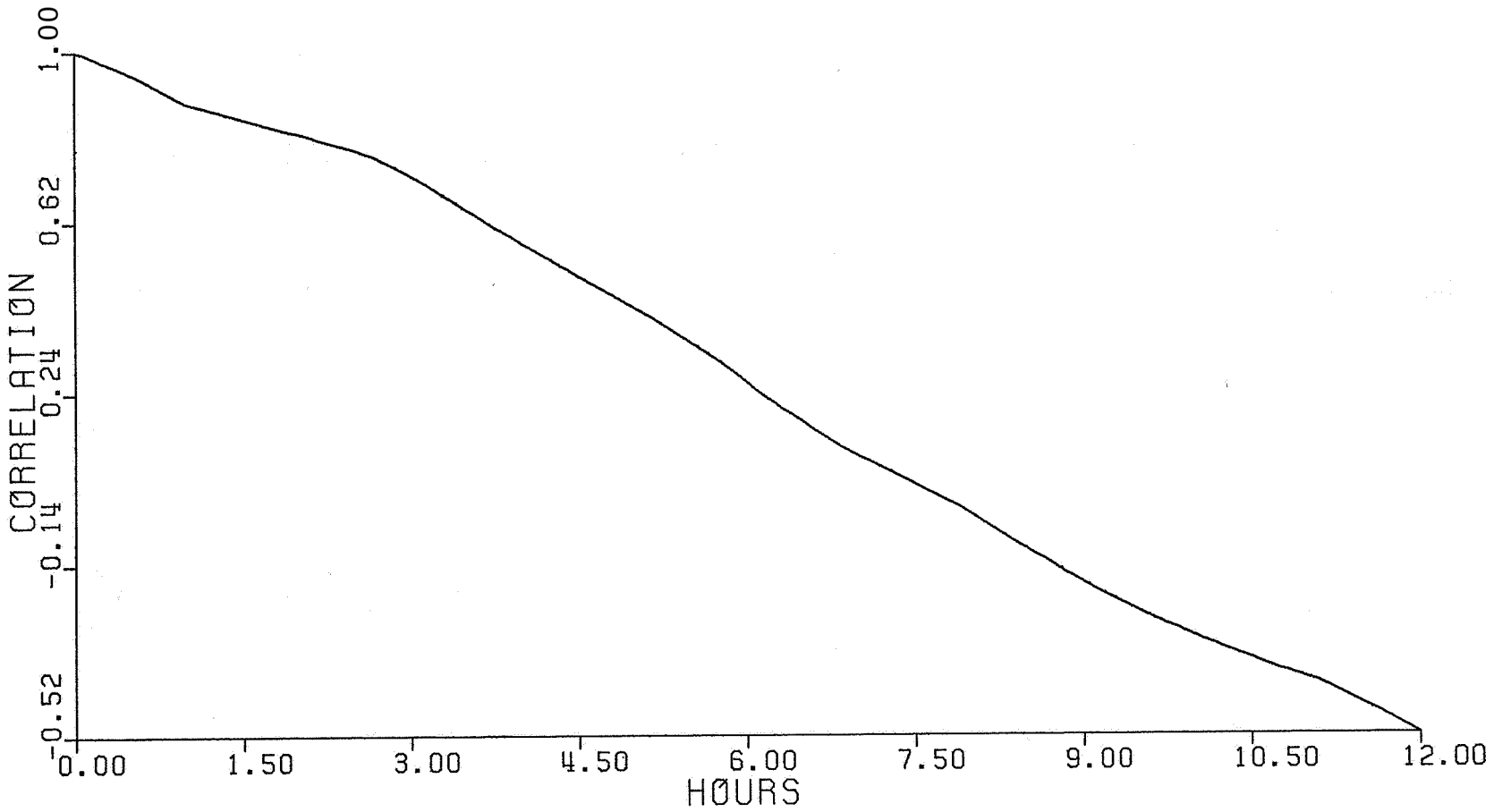

213853 21-OCT-83 EAST 4.50 / 4.20 KM

2.76 / 1.44 / 20.08 KM 4 OF 12 CONSENSUS 9.00 M/S

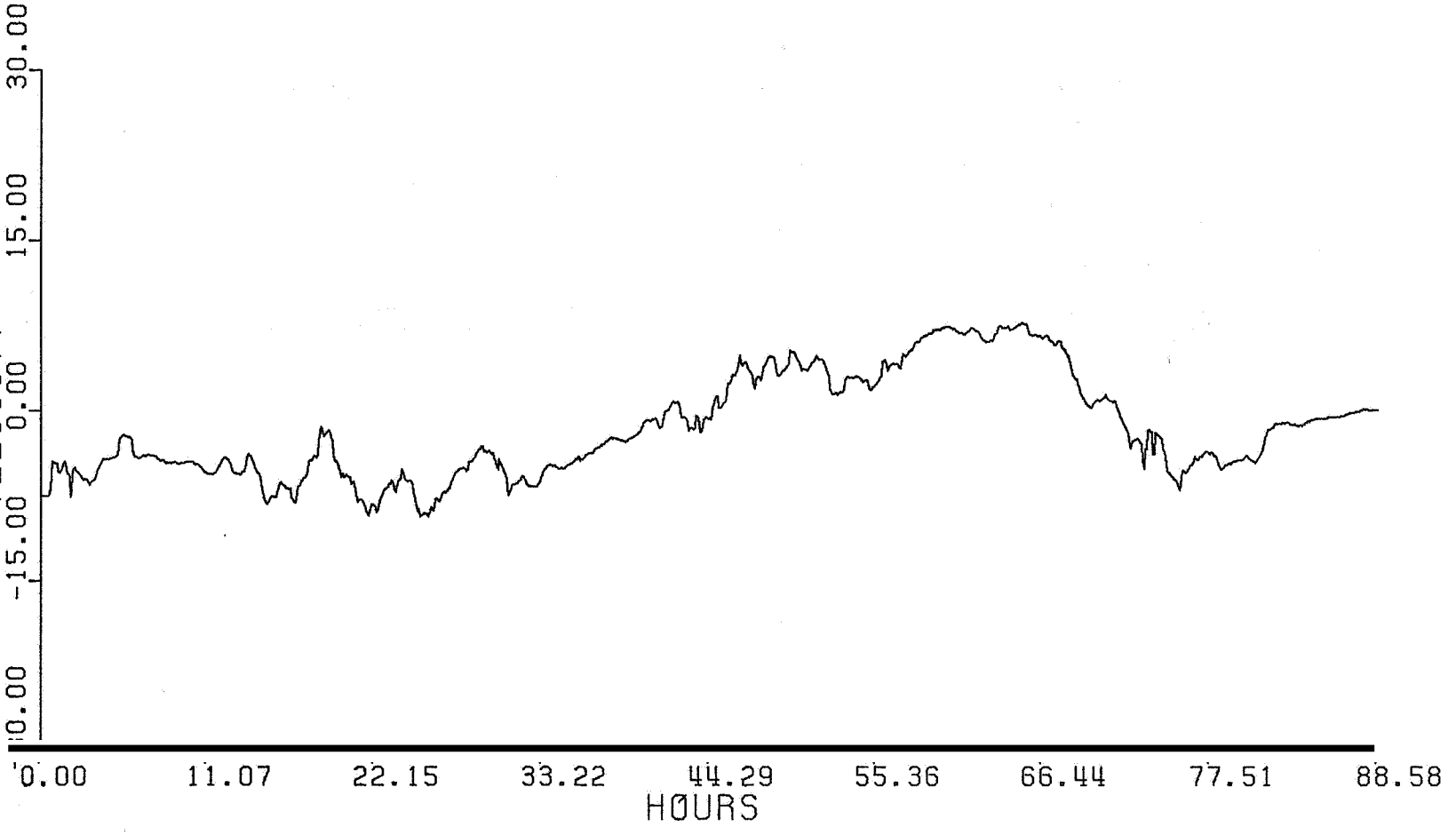

213853 21-OCT-83 NORTH 4.5 / 3.79 KM

2 34 / 1.45 / 19.76 KM 4 OF 12 CONSENSUS 9.00 M/S

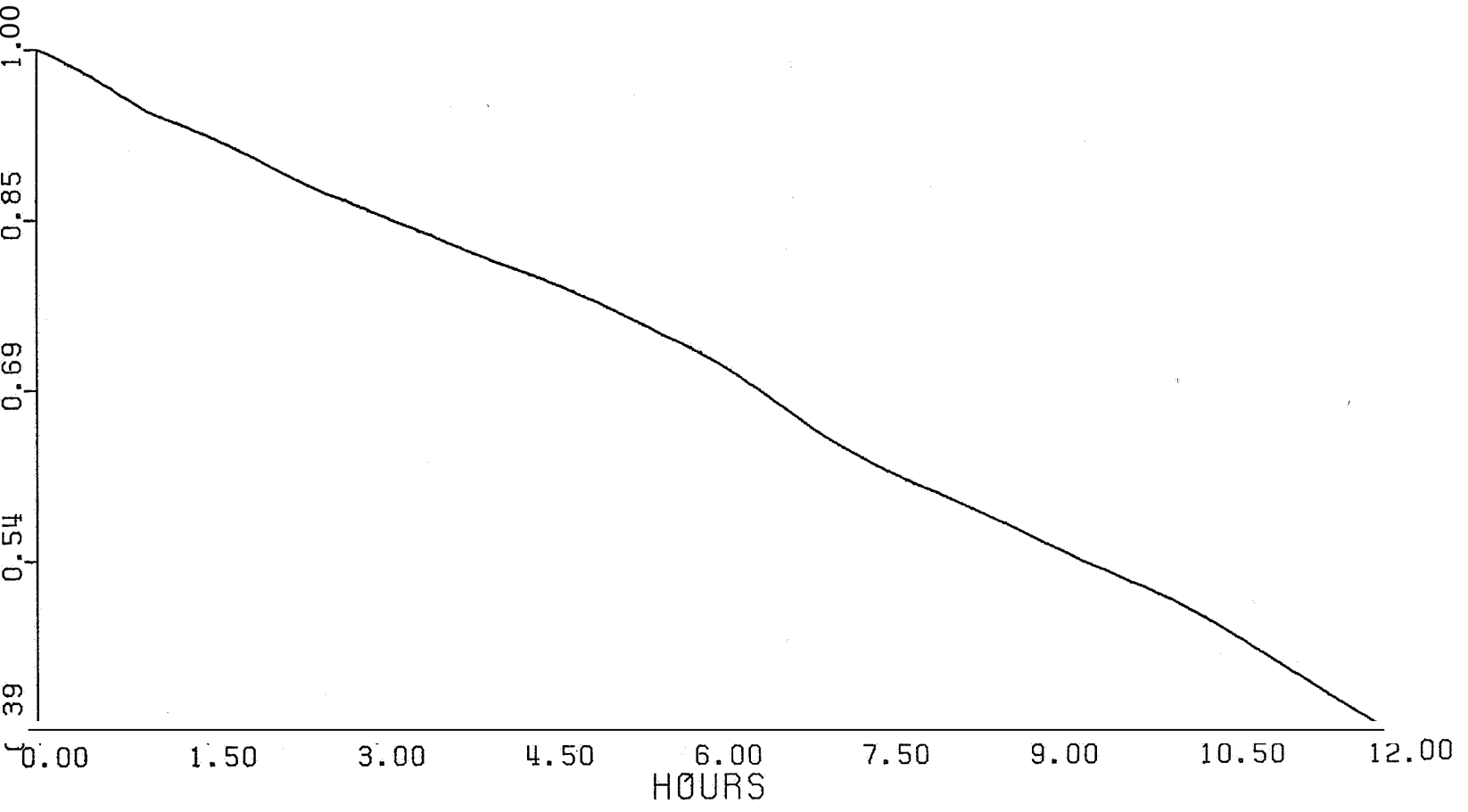

213853 21-OCT-83 NORTH 4.50 / 3.79 KM

2.34 / 1.45 / 19.76 KM 4 OF 12 CONSENSUS 9.00 M/S

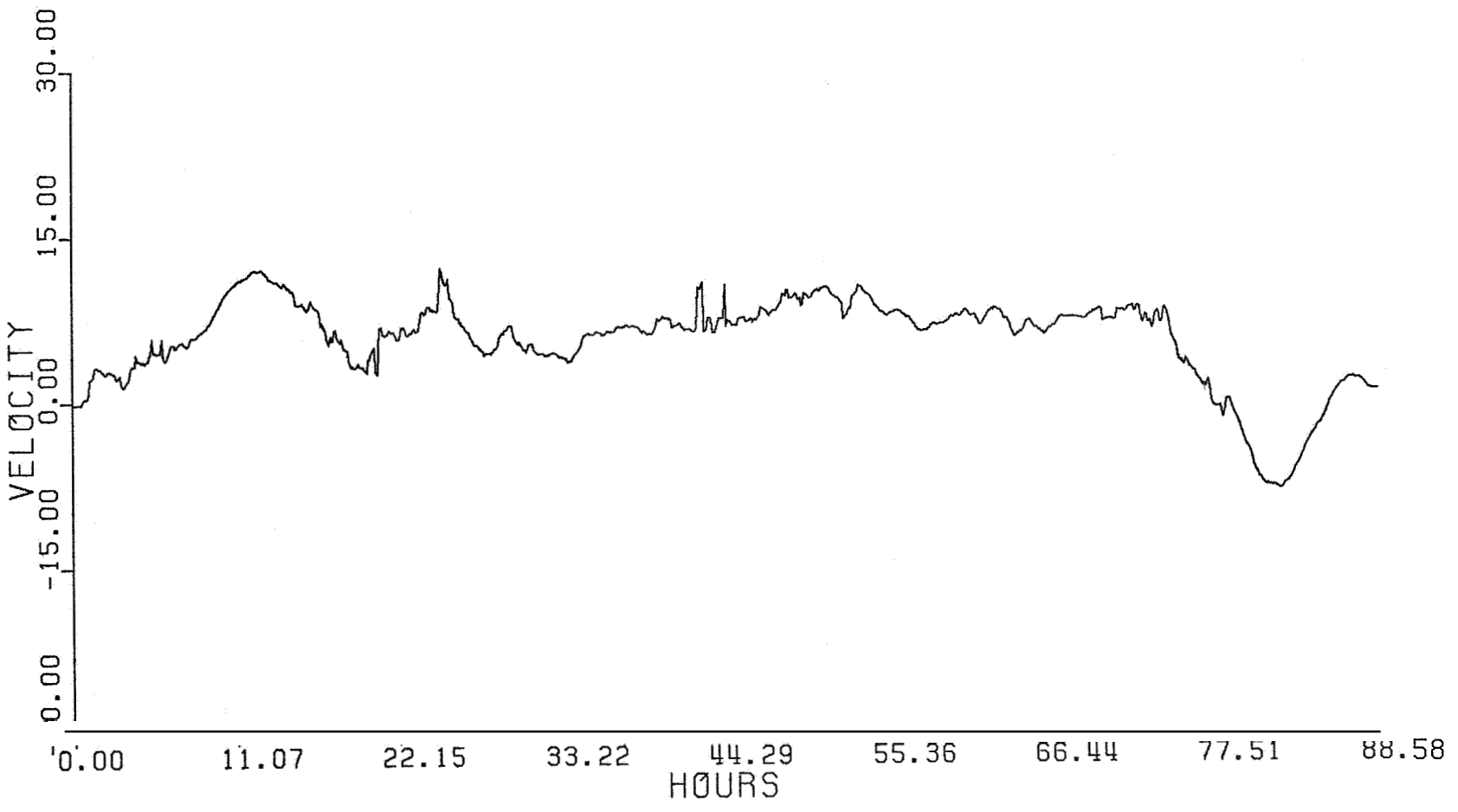

213853 21-OCT-83 EAST 6.00 / 5.65 KM

2.76 / 1.44 / 20.08 KM 4 OF 12 CONSENSUS 9.00 M/S

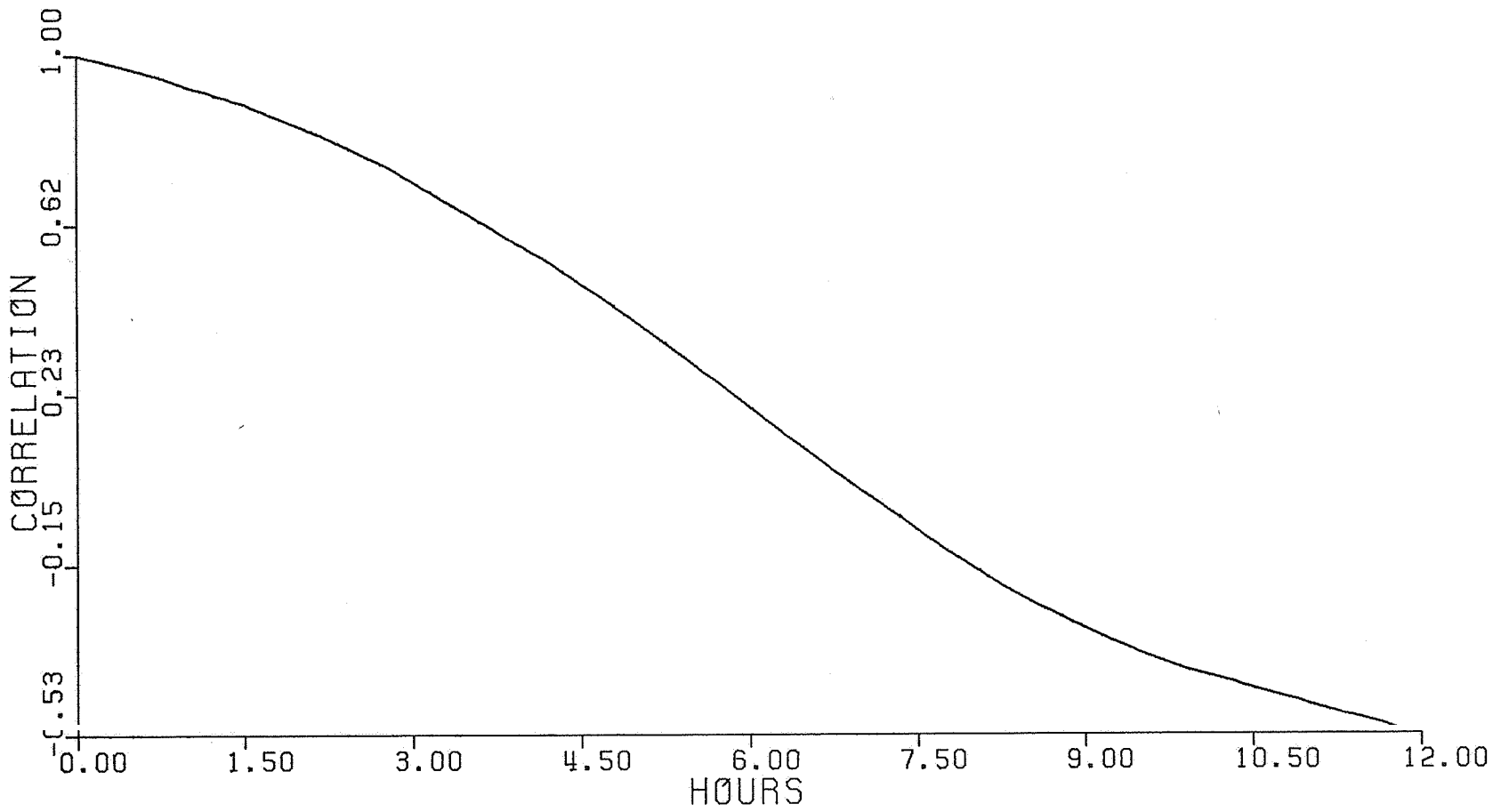

213853 21-ØCT-83 EAST 6.00 / 5.65 KM

2.76 / 1.44 / 20.08 KM 4 ØF 12 CØNSENSUS 9.00 M/S

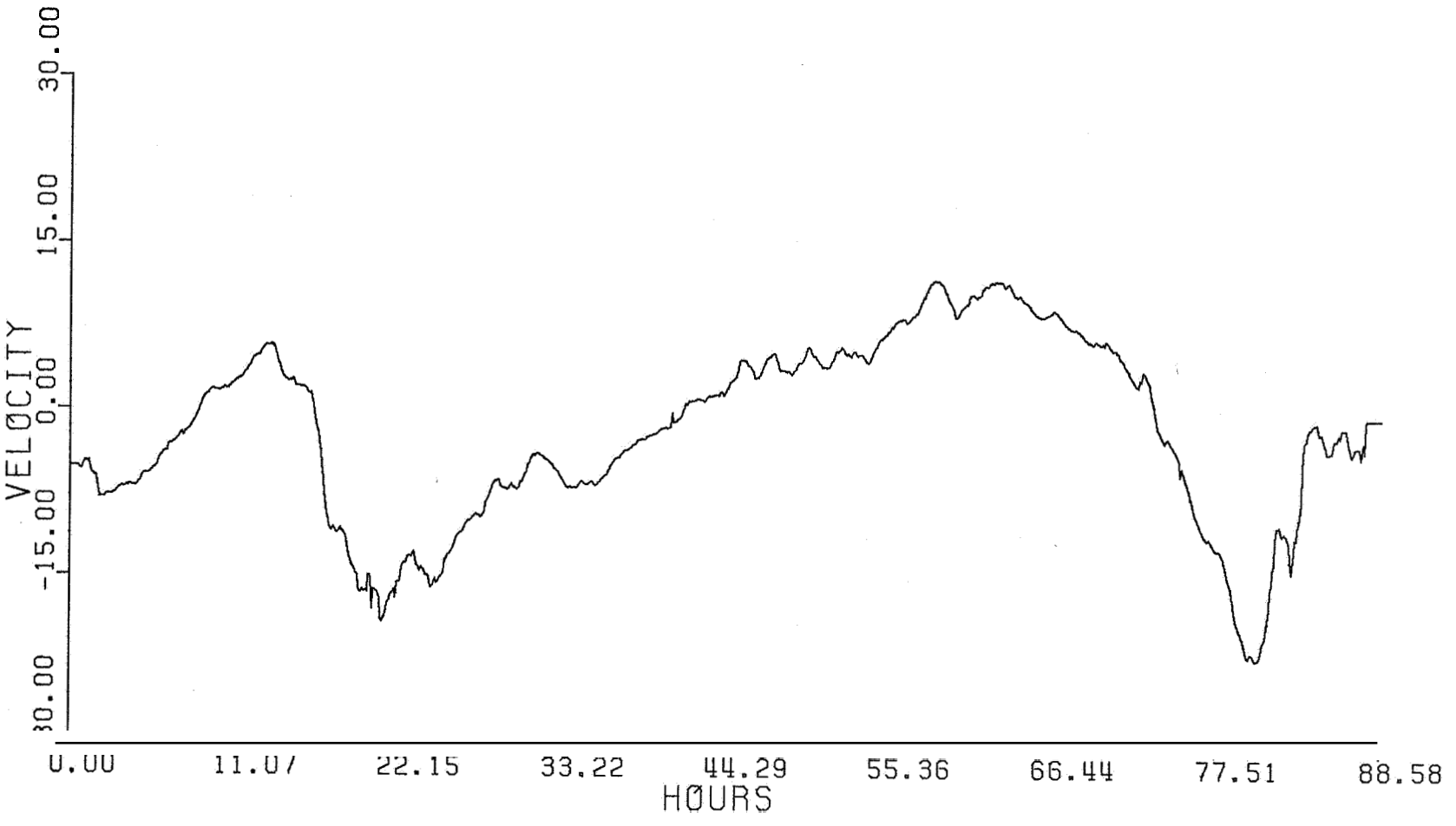

213853 21-ØCT-83 NØRTH 6.00 / 6.69 KM

2.34 / 1.45 / 19.76 KM 4 ØF 12 CØNSENSUS 9.00 M/S

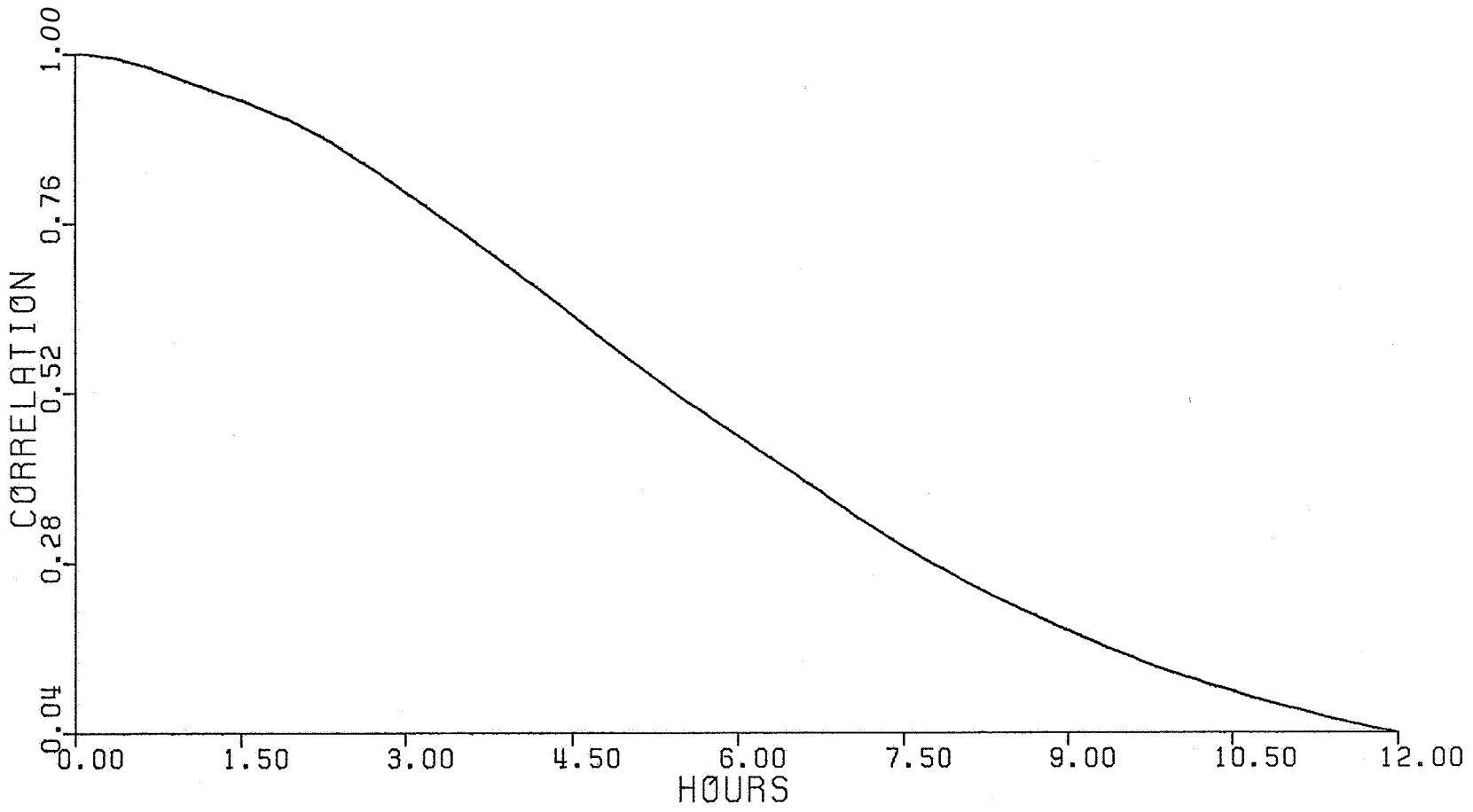

213853 21-OCT-83 NORTH 6.00 / 6.69 KM

2.34 / 1.45 / 19.76 KM 4 OF 12 CONSENSUS 9.00 M/S

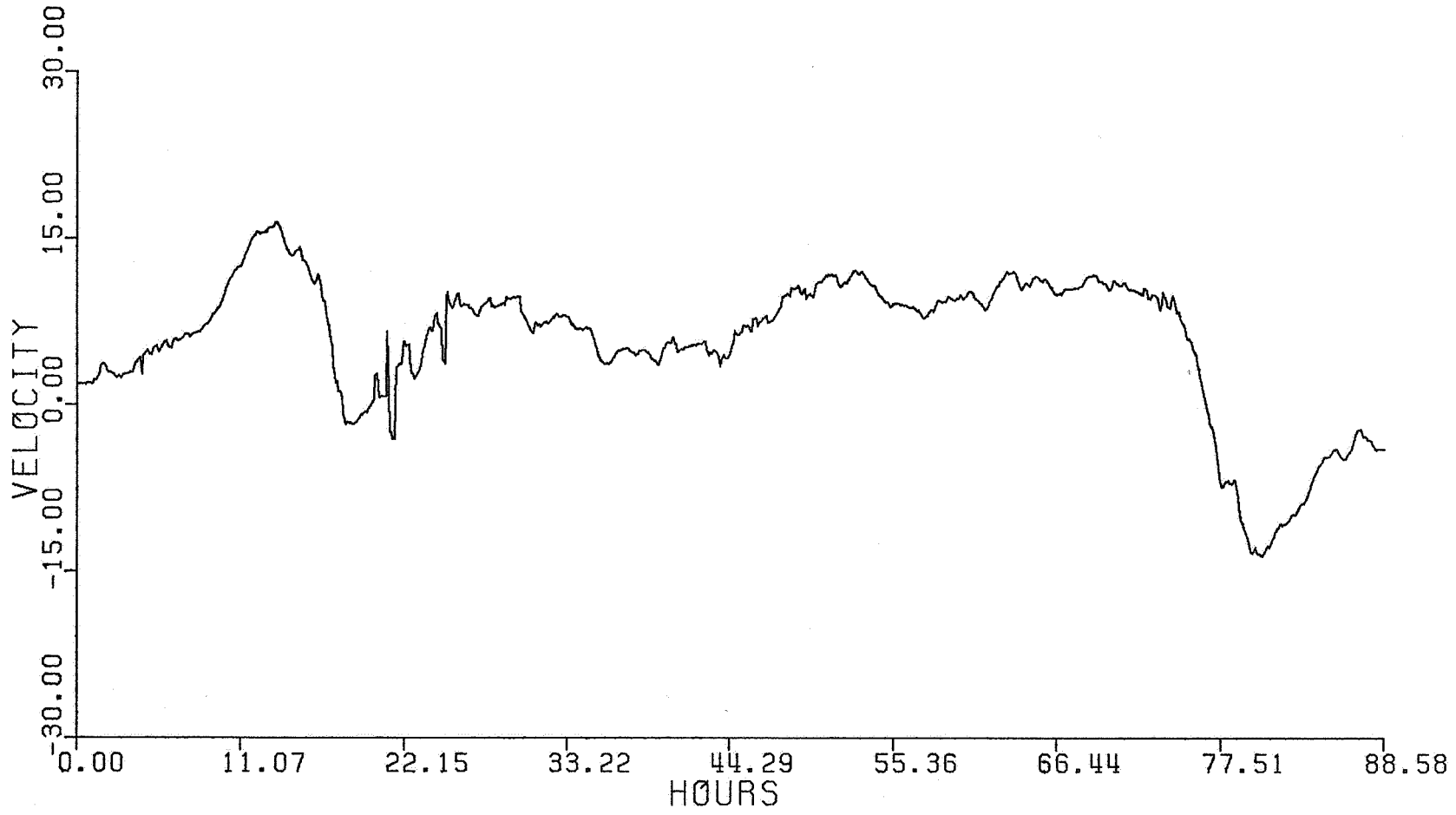

213853 21-0OT-83 EaST 7.50 / T.09 KM

G-17

2.76 / 1.44 / 20.08 KM 4 0F 12 CONSENSUS 9.00 M/S

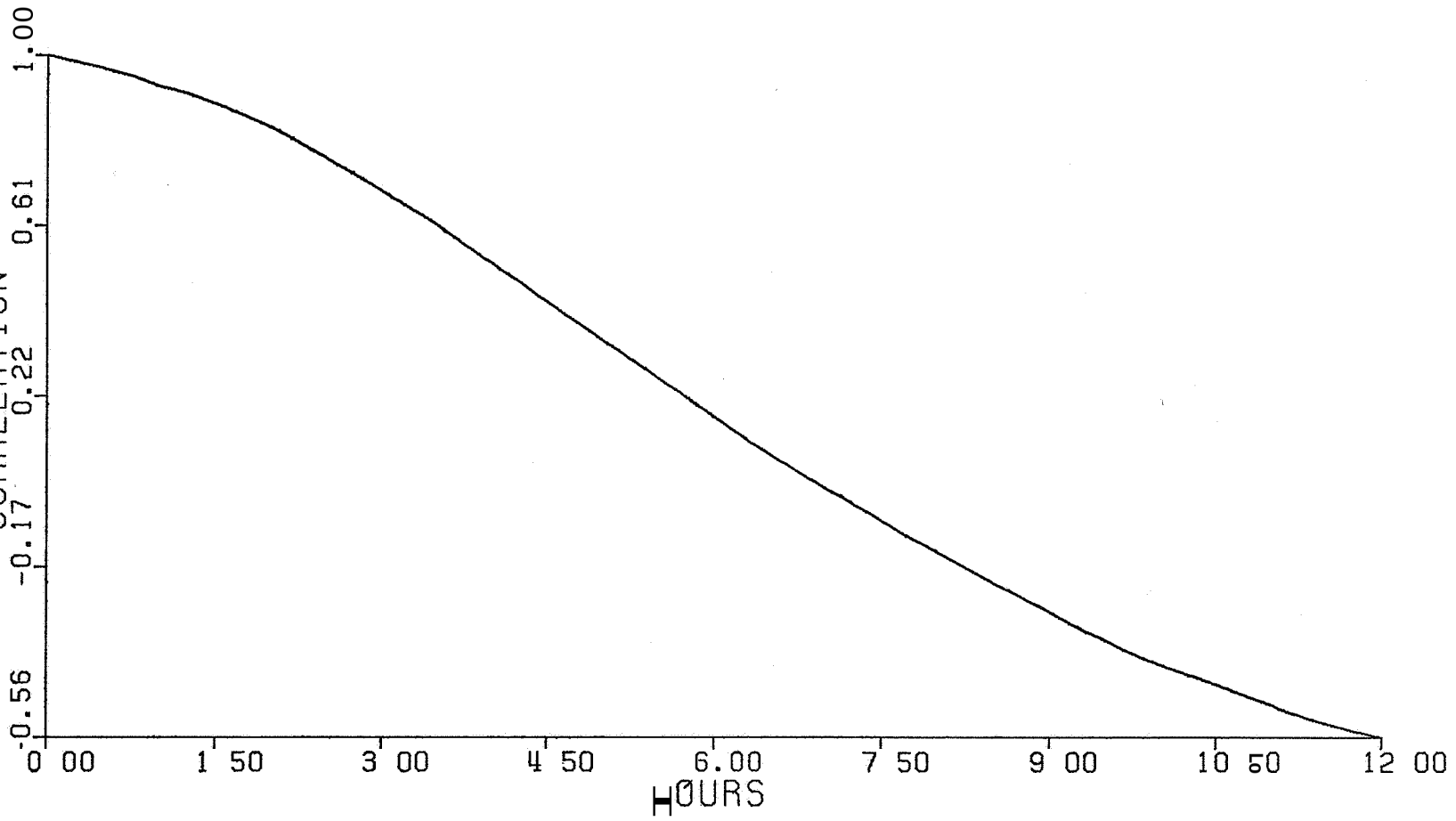

213853 21-OCT-83 EAST 7.50 / 7.09 KM

2.76 / 1.44 / 20.08 KM 4 OF 12 CONSENSUS 9 00 M/S

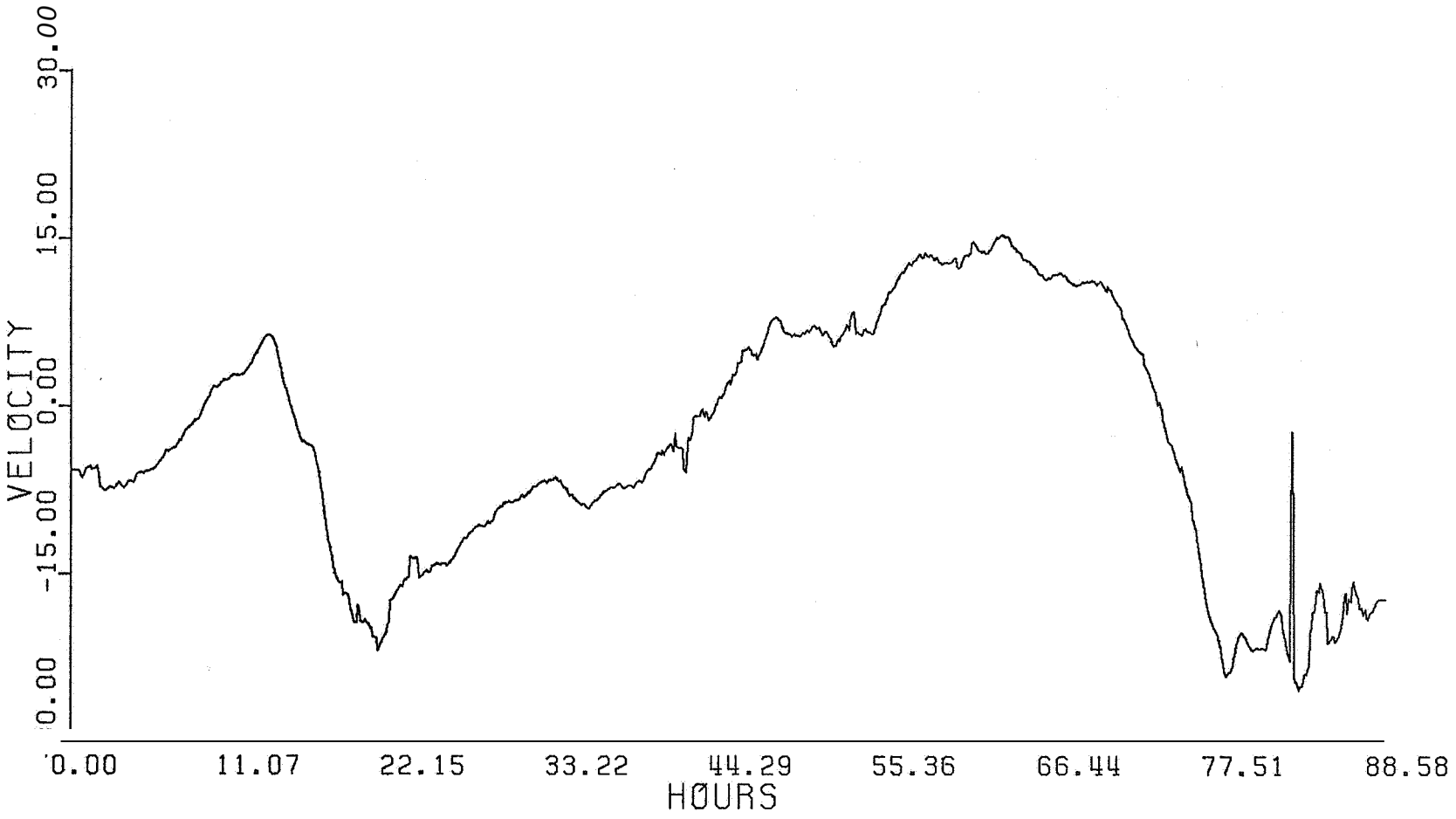

213853 21-OCT-83 NORTH 7.50 / 8.14 KM

2 34 / 1.45 / 19.76 KM 4 OF 12 CONSENSUS 9.00 M/S

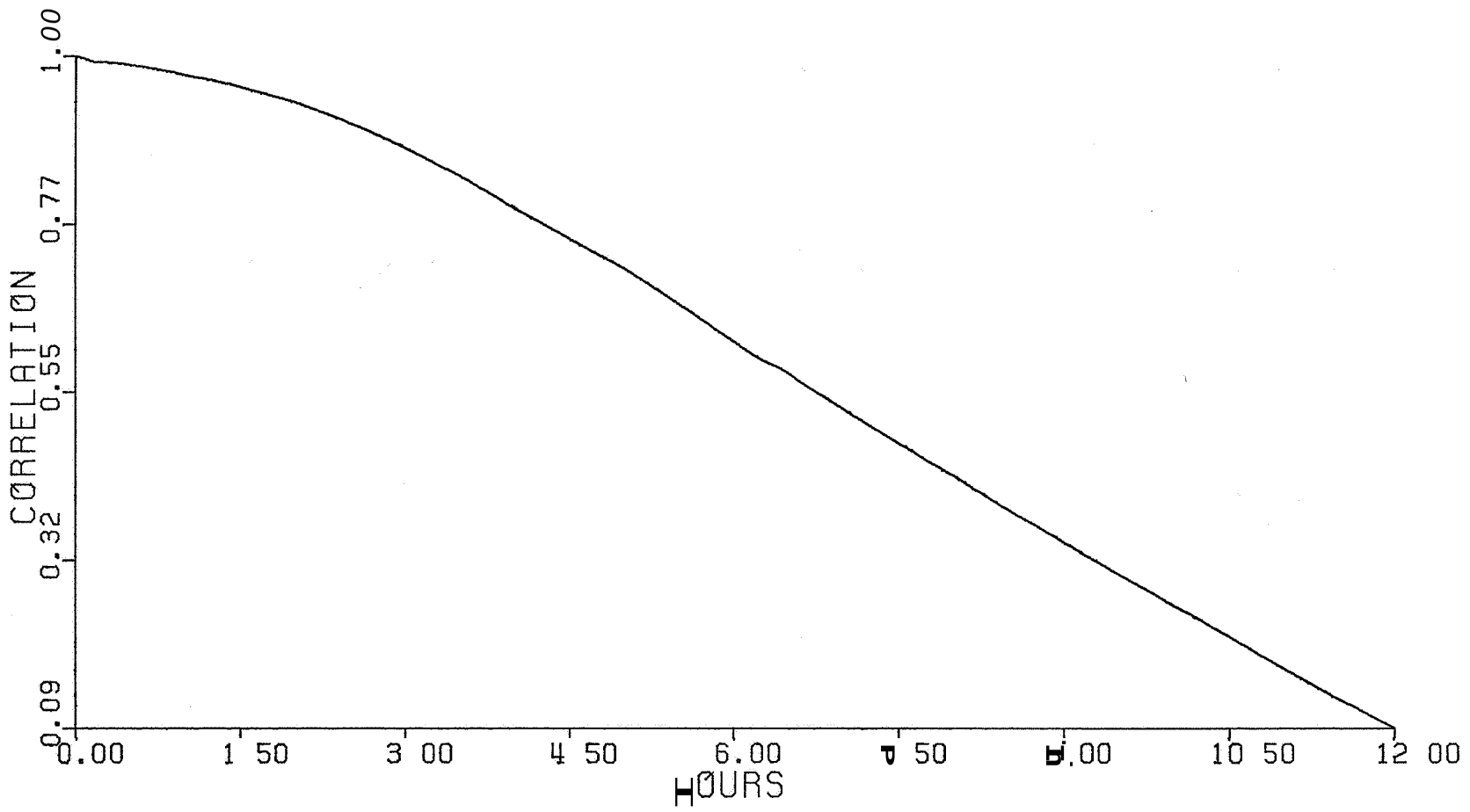

213853 21-OCT-83 NORTH 7.50 / 8.14 KM

2.34 / 1.45 / 19.76 KM 4 OF 12 CONSENSUS 9.00 M/S

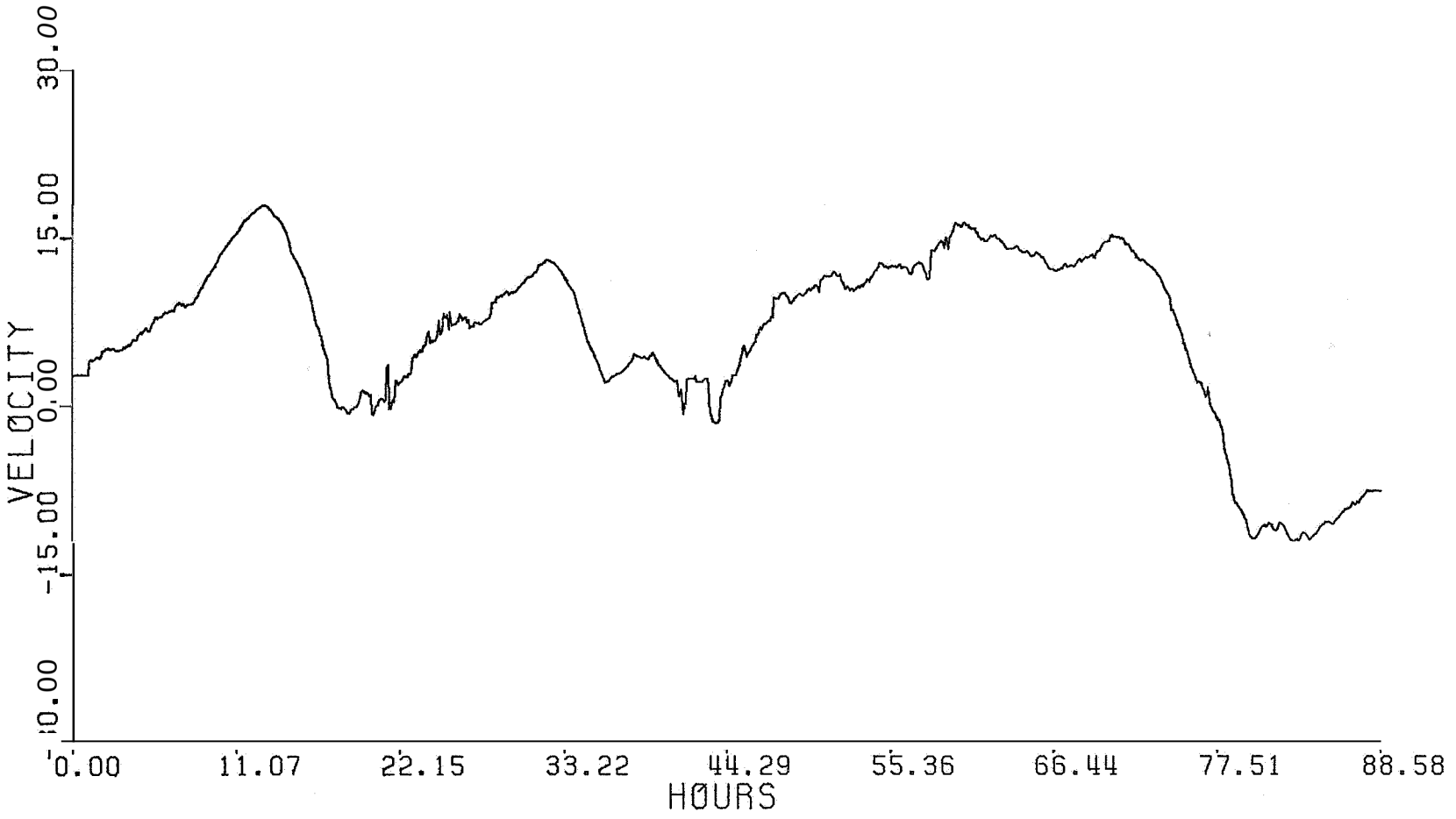

213853 21-OCT-83 EAST 8.00 / 8.53 KM

G-21

2.76 / 1.44 / 20.08 KM 8 OF 24 CONSENSUS 9.00 M/S

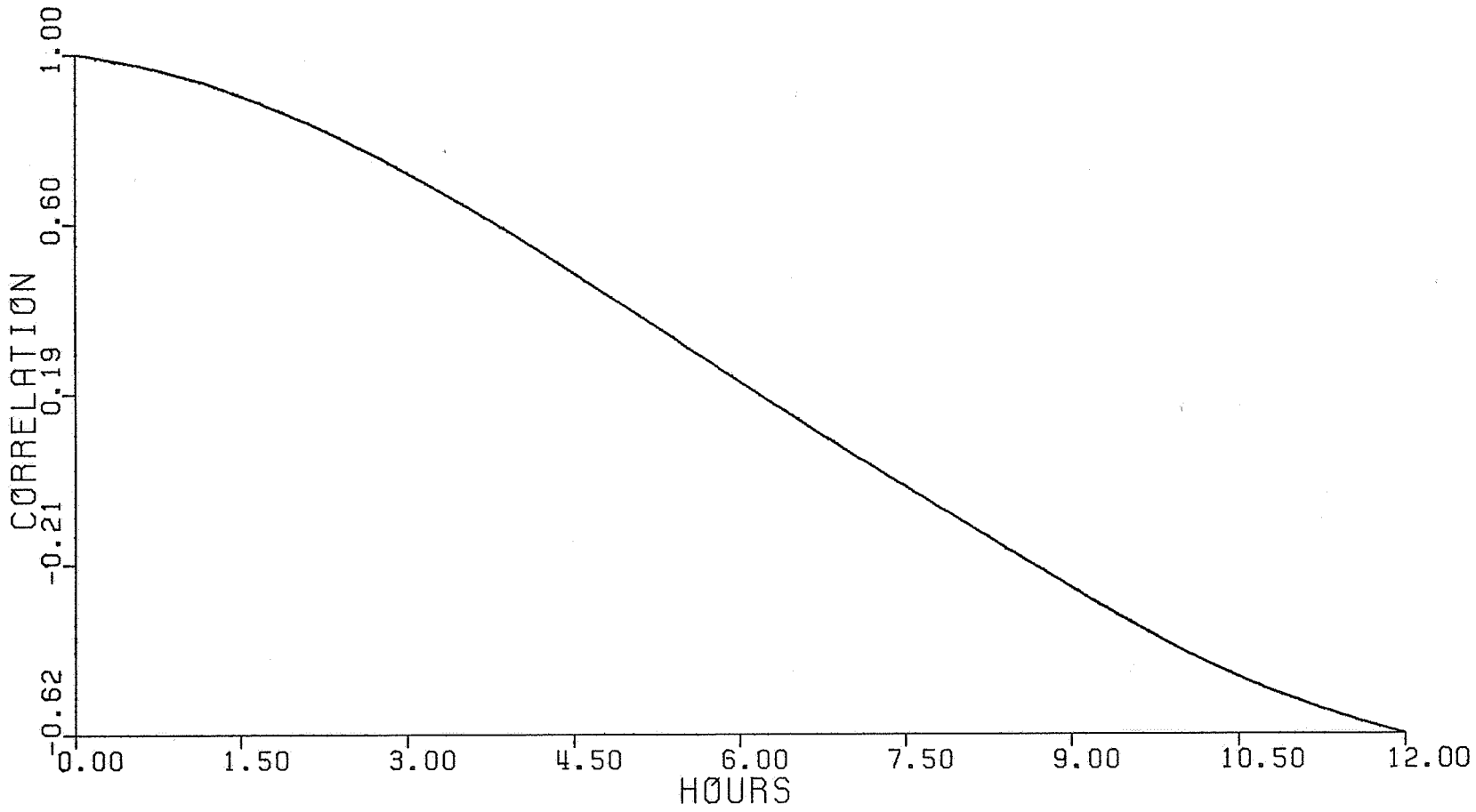

213853 21-OCT-83 EAST 8.00 / 8.53 KM

2.76 / 1.44 / 20.08 KM 8 OF 24 CONSENSUS 9.00 M/S

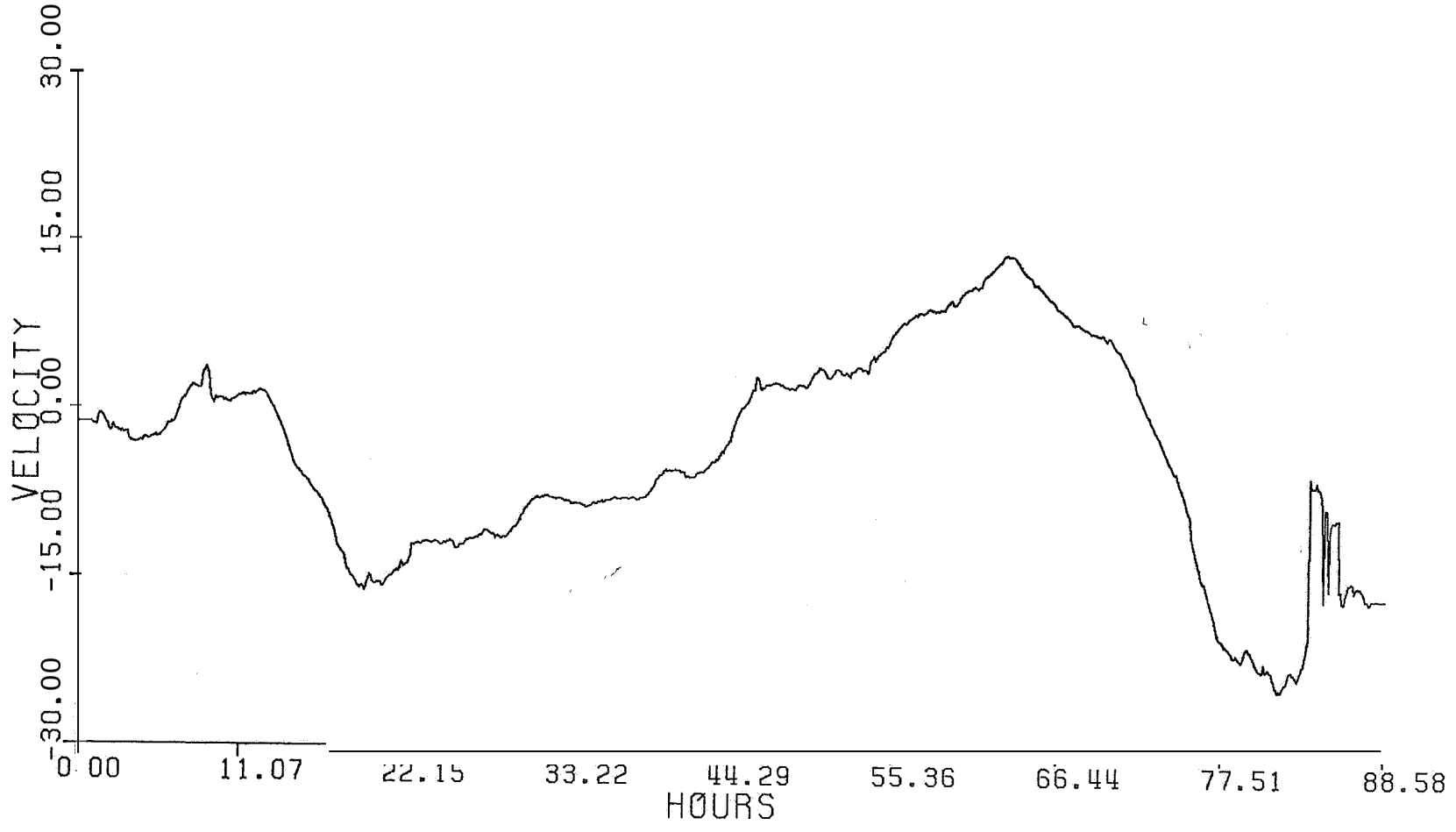

213853 21-OCT-83 NORTH 9.50 / 9.60 KM

2.34 / 1.45 / 19.76 KM 8 OF 24 CONSENSUS 9.00 M/S

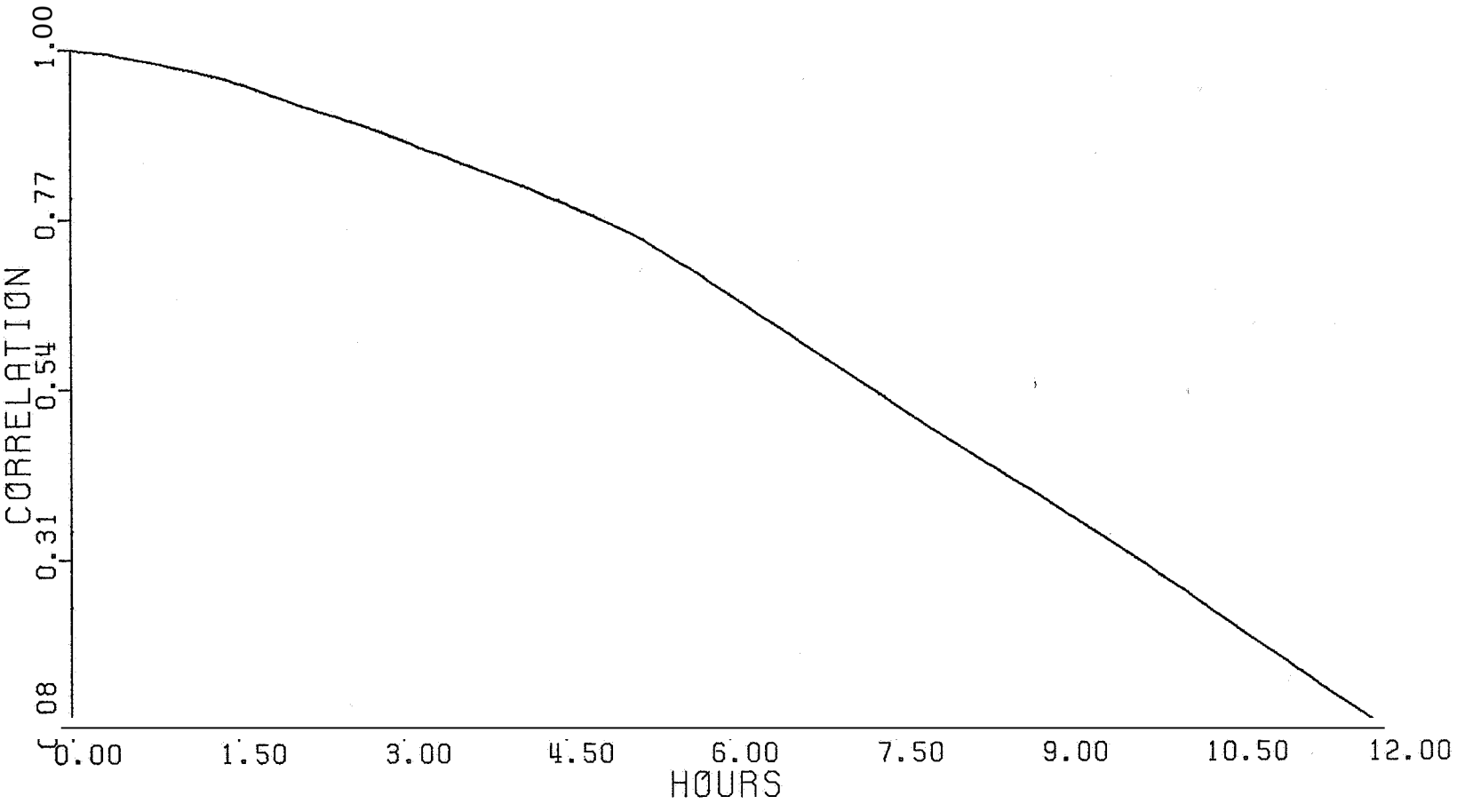

213853 21-0CT-83 N0RTH 9.50 / 9.60 KM

2.34 / 1.45 / 19.76 KM 8 0F 24 C0NSENSUS 9.00 M/S

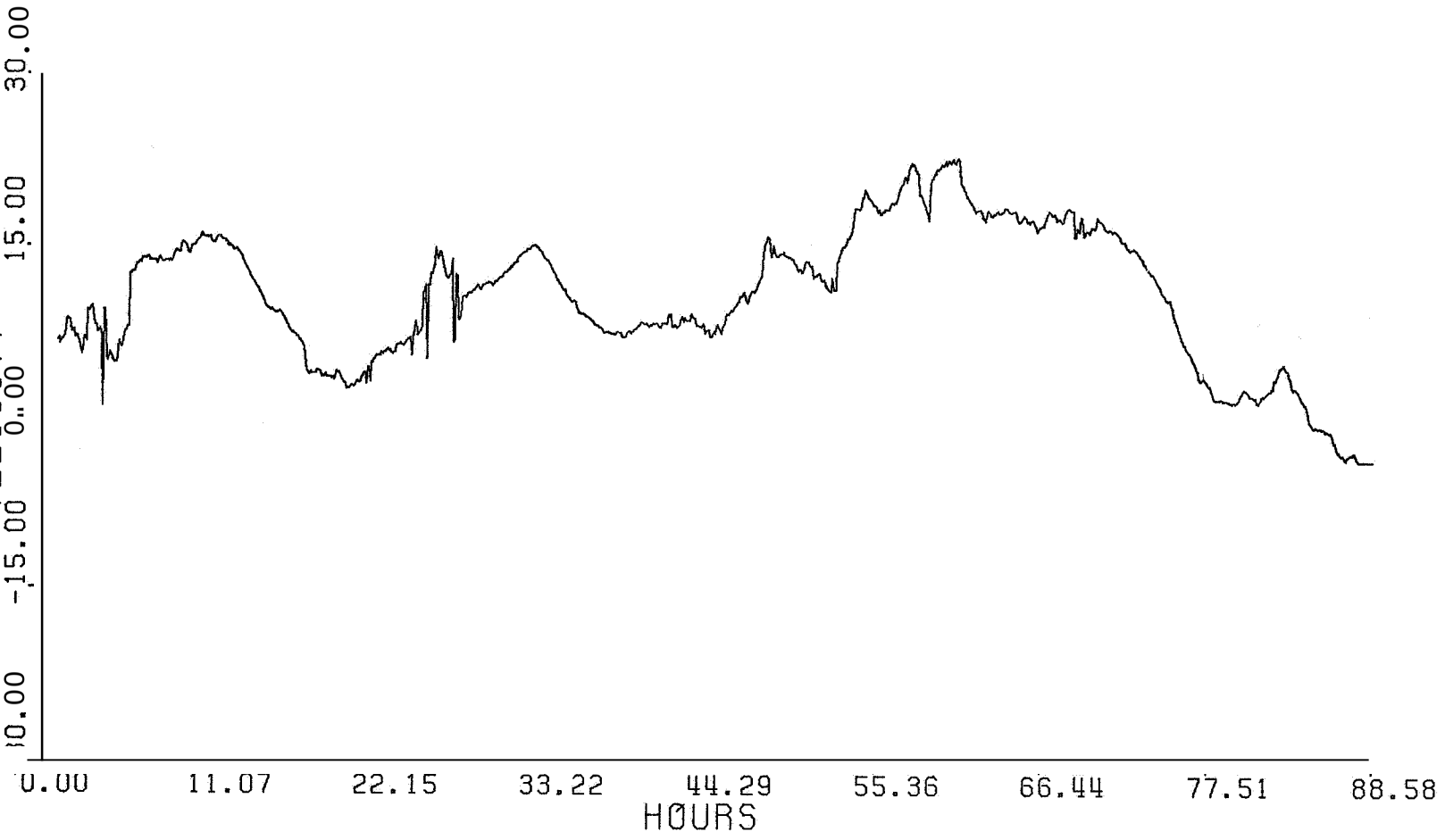

213853 21-OCT-83 EAST 9.50 / 9.98 KM

2.76 / 1.44 / 20.08 KM 8 OF 24 CONSENSUS 9.00 M/S

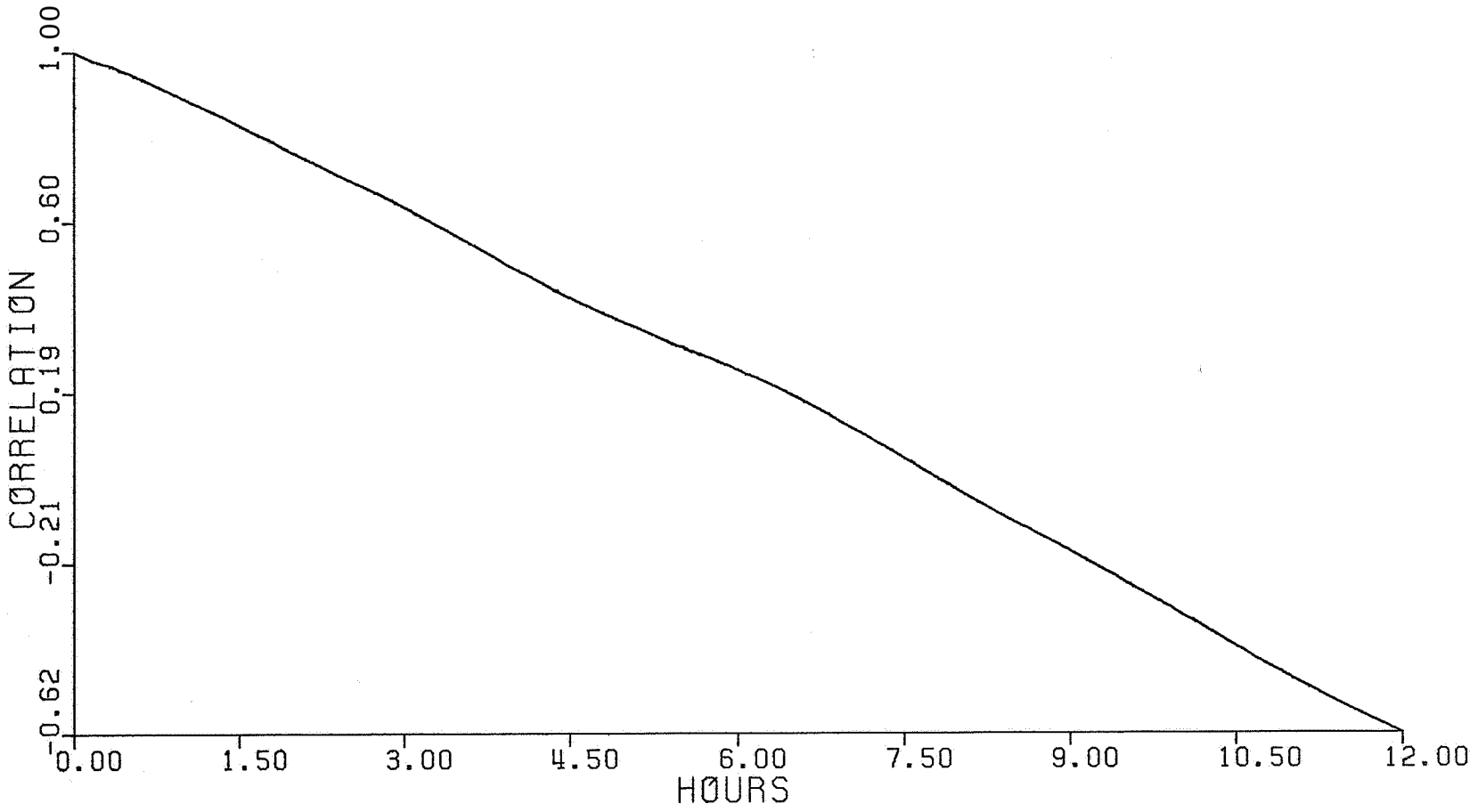

213853 21-OCT-83 EAST 9.50 / 9.98 KM

2.76 / 1.44 / 20.08 KM 8 OF 24 CONSENSUS 9.00 M/S

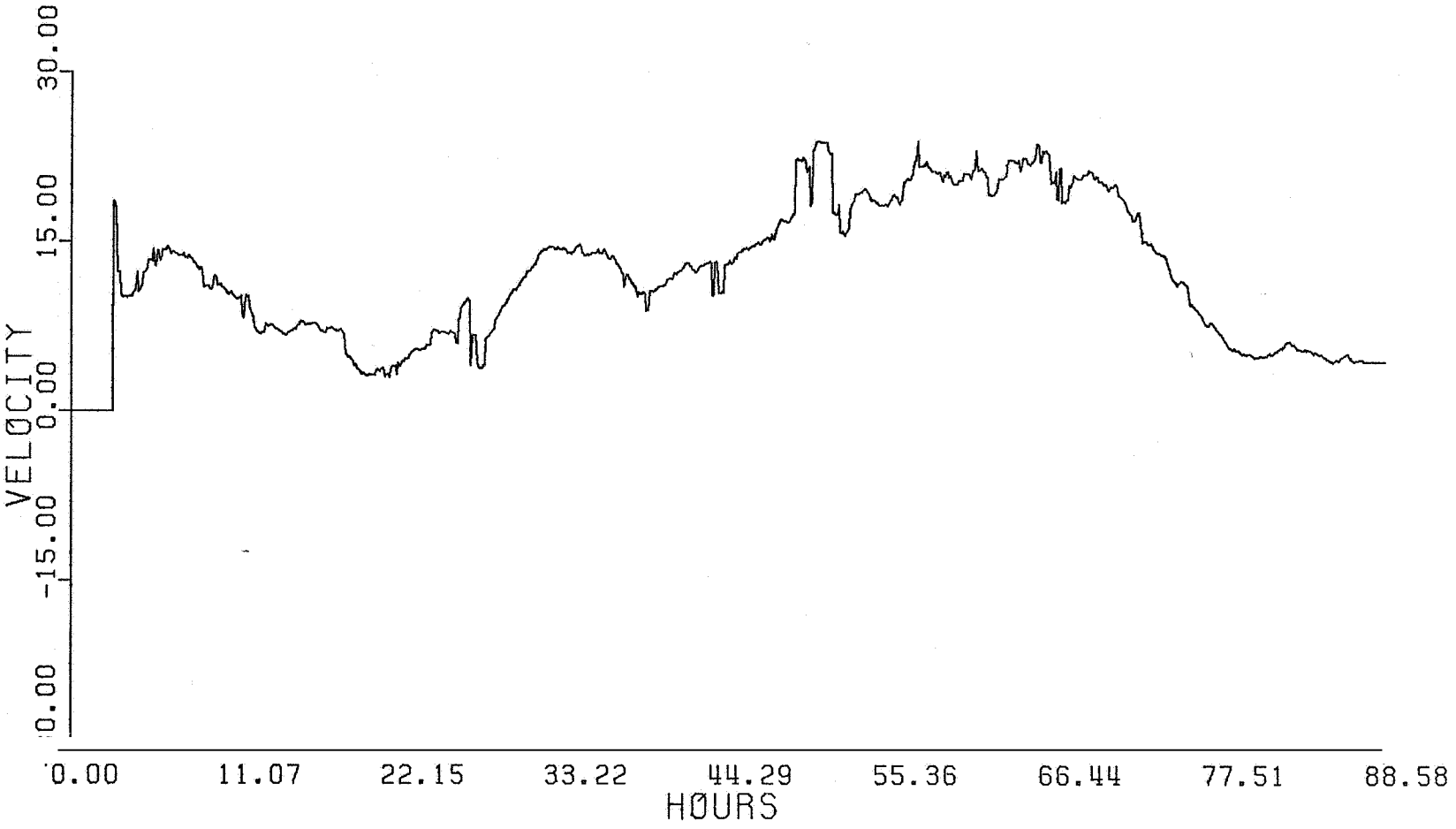

213853 21-OCT-83 EAST 11.00 / 11.42 KM

G-27

2.76 / 1.44 / 20.08 KM 12 OF 36 CONSENSUS 9.00 M/S

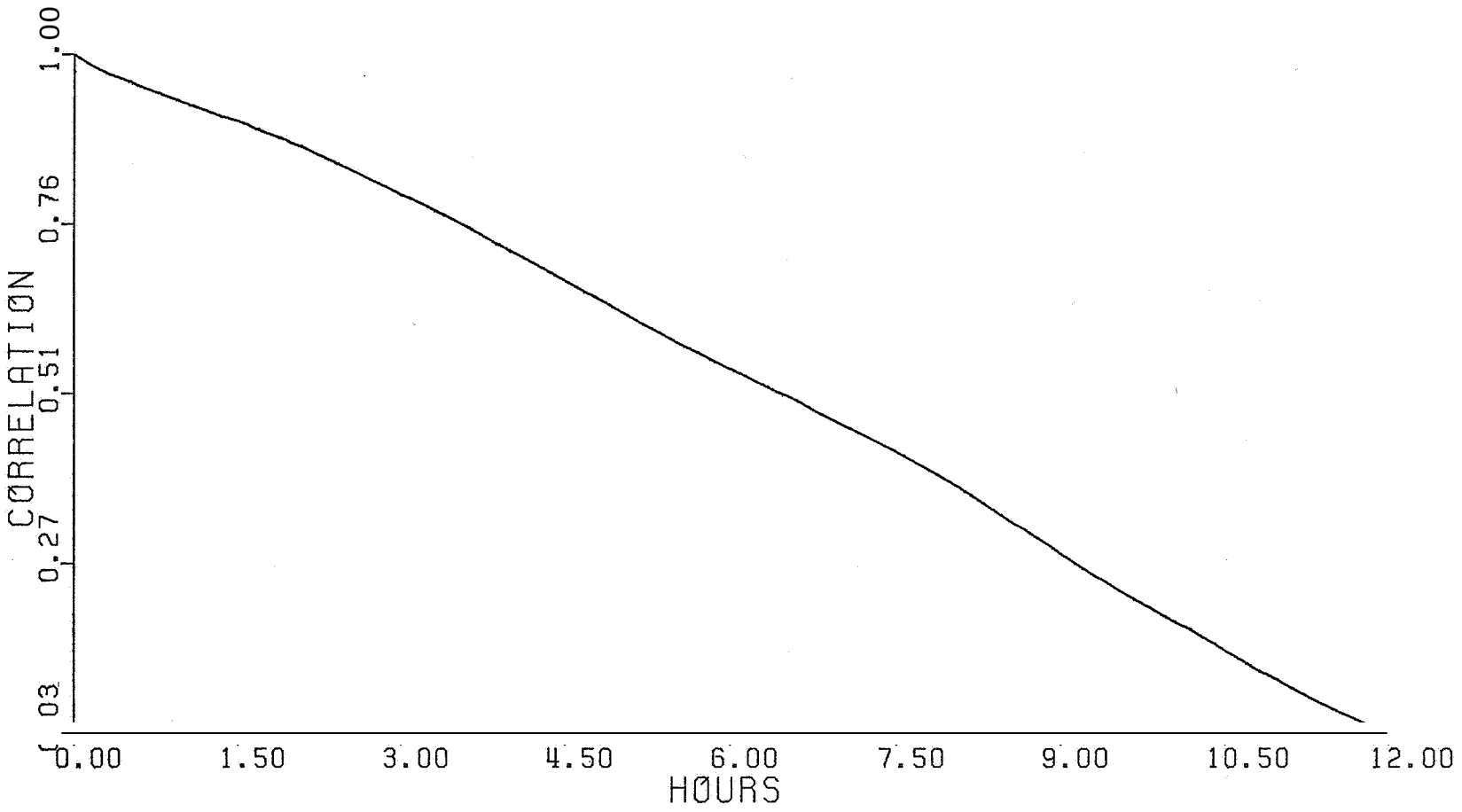

213853 21-OCT-83 EAST 11.00 / 11.42 KM

G-28

2.76 / 1.44 / 20.08 KM 12 OF 36 CONSENSUS 9.00 M/S

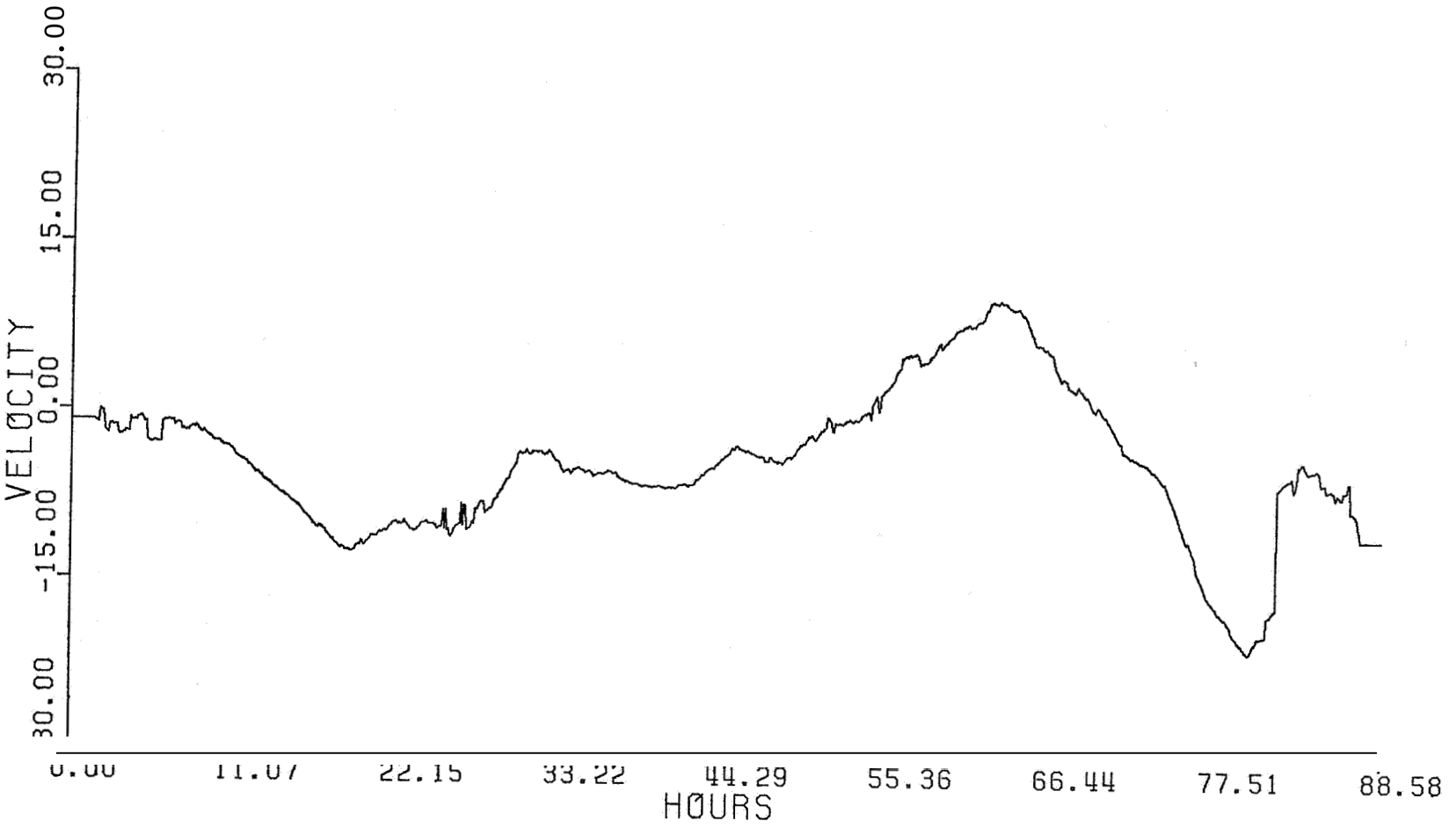

213853 21-OCT-83 NORTH 11.00 / 11.05 KM

2.34 / 1.45 / 19.76 KM 12 OF 36 CONSENSUS 9.00 M/S

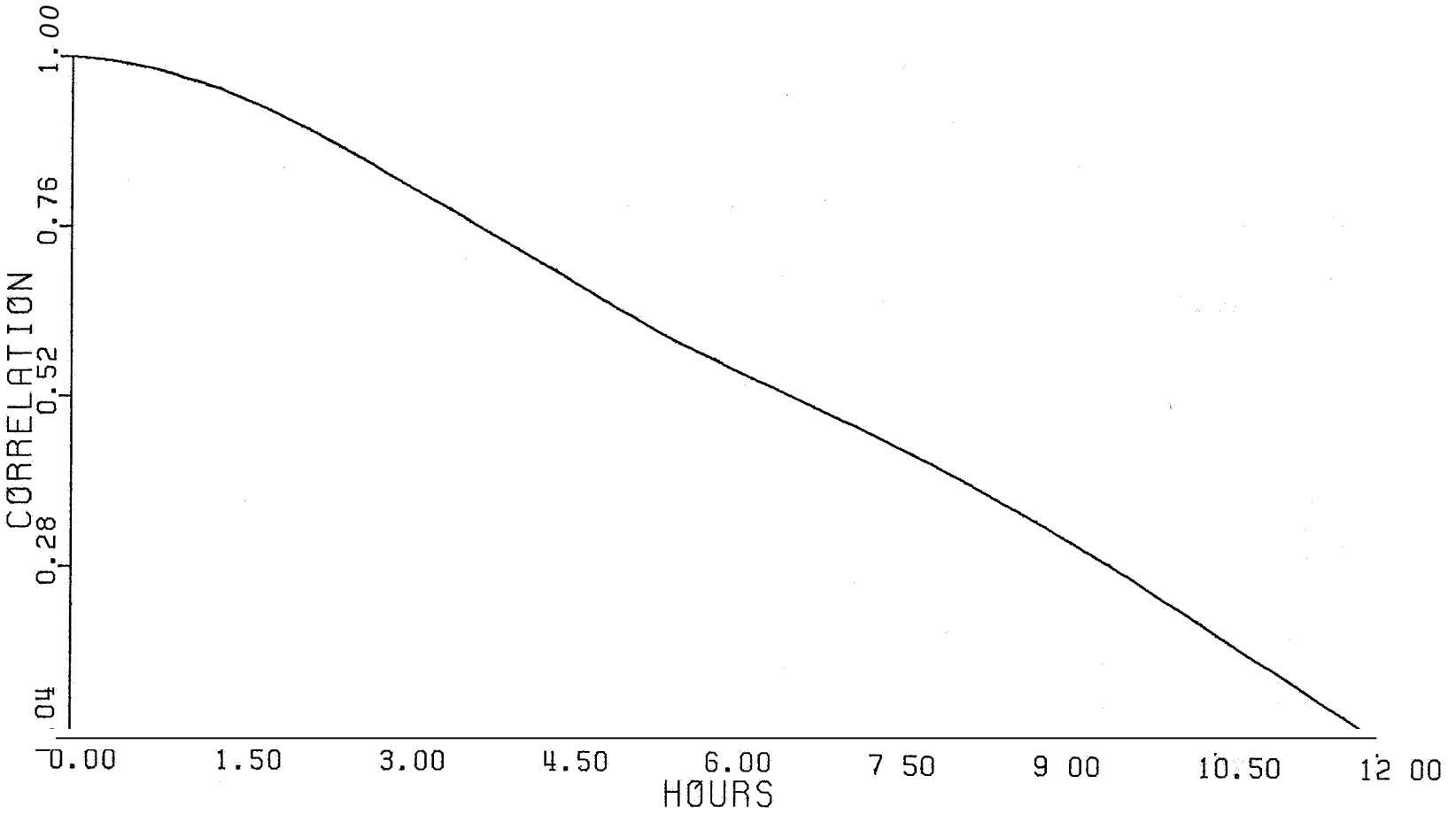

213853 21-OCT-83 NORTH 11.00 / 11.05 KM

2.34 / 1.45 / 19.76 KM 12 OF 36 CONSENSUS 9 00 M/S

1. REPORT NO.	2. GOVERNMENT ACCESSION NO.	3. RECIPIENT'S CATALOG NO.
NASA CR-3861		

4. TITLE AND SUBTITLE	5. REPORT DATE
A Feasibility Study on the Use of Wind Profilers To Support Space Shuttle Launches	December 1984
	6. PERFORMING ORGANIZATION CODE

7. AUTHOR(S)	8. PERFORMING ORGANIZATION REPORT #
R. B. Chadwich, A. S. Frisch, and R. G. Strauch	

9. PERFORMING ORGANIZATION NAME AND ADDRESS	10. WORK UNIT, NO.
NOAA/ERL/Wave Propagation Laboratory Boulder, Colorado 80303	M-472
	11. CONTRACT OR GRANT NO. P.O. H-77152B

12. SPONSORING AGENCY NAME AND ADDRESS	13. TYPE OF REPORT & PERIOD COVERED
National Aeronautics and Space Administration Washington, D. C. 20546	Contractor Report
	14. SPONSORING AGENCY CODE ED41/MSFC

15. SUPPLEMENTARY NOTES

Contract Monitor: John Kaufman, Atmospheric Sciences Division, Systems Dynamics Laboratory, Marshall Space Flight Center, Alabama

16. ABSTRACT

This report describes the feasibility of using a clear-air radar wind Profiler to support Space Shuttle launches by measuring prelaunch winds aloft at the Kennedy Space Center, Florida and the Vandenburg Air Force Base, California. These winds are currently measured by Jimspheres (special balloons) tracked with a high-resolution radar. This technique provides a single high resolution (about 25 meter altitude increment with 1.0 ms^{-1} or less vector error) wind profile from the surface to about 18 km. Two operational disadvantages of the Jimsphere/radar tracking system are that it takes about 1.0 hour to measure a wind profile to the required altitude and that the wind profile applies only to the path of the ascending Jimsphere balloon. This difference in location may be up to 70 km, during very high winds, from the actual trajectory of the Space Shuttle in the maximum inflight dynamic pressure region. The radar wind Profiler automatically and nearly continuously measures the motion of natural tracers of the atmosphere almost directly over the radar site. The accuracy and resolution of the radar wind Ptofiler is a function of the integration time and the resolution (altitude increment) used to obtain the wind profile measurements. Currently, radar wind Profiler systems operate at significantly less altitude resolution (about 400 meters or less) than does the Jimsphere/radar tnacking system and integrate over 30 minutes or longer for a wind profile measurement. The radar wind Profiler feasibility report describes the potential for achieving altitude resolution and accuracy approaching the Jimsphere/radar tracking system capabilities with respect to frequency-cost trade offs and assumptions on bandwidth, frequency interference, and other system characteristics.

17. KEY WORDS	18. DISTRIBUTION STATEMENT
Winds aloft Remote sensing of winds Clear air radar applications Space Shuttle wind loads High resolution wind profiles	Unclassified - Unlimited Subject Category: 47

19. SECURITY CLASSIF. (of this report)	20. SECURITY CLASSIF. (of this page)	21. NO. OF PAGES	22. PRICE
Unclassified	Unclassified	109	A06

For sale by National Technical Information Service, Springfield, Virginia 22161 NASA-Langley, 1984